OBSERVING BRANE INFLATION IN THE SKY

A Dissertation

Presented to the Faculty of the Graduate School

of Cornell University

in Partial Fulfillment of the Requirements for the Degree of

Doctor of Philosophy

by

Jiajun Xu

May 2010

OBSERVING BRANE INFLATION IN THE SKY

Jiajun Xu, Ph.D.

Cornell University 2010

Brane inflation is a natural cosmic inflation scenario from string theory. Explicitly constructed brane inflation models enable us to probe string theory using cosmological data. This is an exciting area where observations make contact with fundamental physics at or around the string scale.

In this work, I review the basic setup of warped brane inflation models, discuss how novel kinetic term, the Dirac-Born-Infeld (DBI) action, naturally arises and what inflaton potential string theory gives us. Depending on the magnitude of the inflaton mass relative to the Hubble scales, there are three different scenarios: the slow-roll scenario, the Ultraviolet DBI scenario, and the Infrared DBI scenario. I will review each scenario in detail, and discuss their predictions on the cosmic microwave background (CMB) sky. Some predictions, such as primordial non-Gaussianities, are so distinctive, that if detected in the foreseeable future, will reveal the nature of cosmic inflation in great detail. In fact, as we will show, current observational bounds on non-Gaussianity is already powerful enough to rule out Ultraviolet DBI inflation in the relativistic regime. Some predictions have very stringy natures. Such as the stringy phase transition during the early stage of Infrared DBI inflation that leads to significant running of the spectral index, and the sharp features in the warp factor as a gravity dual of Sieberg duality cascade. All these observable features opens the door for cosmological observations to test the nature of the theory. In this work, we will present cosmological data analysis which constrain specific brane inflation models in great detail.

Aside from the observational prospects, we will also discuss the conceptual issue

of eternal inflation in brane inflation scenarios. It is generically believed that eternal inflation is unavoidable in field theory inflation models; however, string theory offers new insights. As we will show, a bound on the inflaton field range from the size of the compactified manifold forbids stochastic eternal inflation in the slow-roll scenario. Eternal inflation in the DBI scenarios are also not generic, either due to the relativistic motion of the brane or due to the stringy phase transition at the tip of the throat.

The last chapter of the work discuss our recent efforts in building inflation models on the string landscape. It is now widely accepted that string theory allows an enormous number of vacua. In the early universe, if the inflaton field is mobile in the landscape, the resulting cosmic inflation picture is quite different from usual points of view. Here we expect a multi-dimensional inflaton potential with random features. Such randomness in the potential causes the inflaton to undergo Brownian-like motion; the detours always increase the number of e-folds, ameliorating the fine tuning of a flat potential in slow-roll model building. Meanwhile, detours lead to fluctuations in the primordial power spectrum, which could show up in the CMB power spectrum. If we are fortunate, the PLANCK satellite will be able to reveal some of these features for us.

We will conclude this work with summaries and remarks on future research.

BIOGRAPHICAL SKETCH

Prior to obtaining his Ph.D. degree in theoretical physics in May 2010, Jiajun Xu has been a graduate student in the high energy theory group of Laboratory of Elementary Particle Physics, Cornell University from 2004 to 2010. In the meantime, he worked as teaching assistant in several introductory physics courses in the Department of Physics, Cornell University. Jiajun was an undergraduate in Tsinghua University, Beijing, China, where he obtained the B.S. degree with honors in 2004.

Born in Shanghai, the most modern city in P.R. China, Jiajun has been curious about the nature since a little child. In high school, he was actively involved in many science contests and those little prizes he won gradually built up his ambition to be a physicist. Jiajun's genuine interest in theoretical physics started when reading "A Brief History of Time" by Steven Hawking and "Fearful Symmetry" by A. Zee while he was an undergraduate. When continuing his graduate study at Cornell University, Jiajun became intrigued in string cosmology, and worked primary with his advisor S.H.-Henry Tye on the observable features of brane inflation models.

Other than his adventure in the early universe, Jiajun spent a lot of his spare time in travelling, photography, cooking and volleyball.

Dedicated to my parents

ACKNOWLEDGEMENTS

First of all, I am indebted to my advisor, Professor S.H.-Henry Tye, for many years of invaluable guidance and support. Henry's enthusiasm, wisdom, and insights have impacted me in every aspect of my research. He has not only taught me a great deal of physics but also showed me the art of identifying, approaching and tackling problems. Especially, I thank Henry for his encouragements and support during my difficult times. It is my great honor to have had Henry as a mentor. Second, I thank Professor Rachel Bean for collaboration in a series of papers that contribute to this work, and for being a great resource for my cosmology research in the past years. Among other faculty members in the theory group, I thank Professor Liam McAllister for discussions in string theory; Professor Csaba Csaki and Professor Maxim Perelstein for teaching me field theory; and Professor Jim Alexander for support and encouragements as my committee member.

I have benefited greatly from current and former Cornell postdocs and graduate students. I thank Xingang Chen for the fruitful collaborations in the past years; I thank Hassan Firouzjahi, Girma Hailu, Louis Leblond, Enrico Pajer, Sarah Shandera, Benjamin Shlaer, Dan Wohns, Gang Xu, Yang Zhang, for valuable and stimulating discussions. Outside Cornell, I thank Robert Brandenberger, Jim Cline, Alan Guth, Eiichiro Komatsu, Eugene Lim, Hiranya Peiris, Gary Shiu and Bret Underwood, for discussions.

I am grateful to the Physics Department and the Laboratory of Elementary Particle Physics of Cornell University for financial support. Part of my research has been supported by the National Science Foundation under grant PHY-0355005.

Finally, I thank my parents ZhenKang Xu and Ying Pan for their support throughout my entire education and life. I thank Jiahong Zhang, whose love and support have made the past years valuable life experience for me. I thank all my friends for the wonderful memories at Cornell.

TABLE OF CONTENTS

LIST OF FIGURES

LIST OF TABLES

CHAPTER 1

INTRODUCTION

The last decade of the twentieth century has been an era where precise cosmological observations reveal the nature of our universe in great details. It is generally believed that our universe was hot and dense in the primordial era; the energy in the radiation drives the expansion of the universe; and the temperature of the universe gradually cools down as the universe expands. This is the Big-Bang scenario, which is strongly supported by the detection of cosmic microwave background radiation, the relics from the early hot universe. The abundances of light elements also strongly indicate that the universe was hot while these elements were formed. However, standard Big-Bang theory cannot explain why our universe is so flat, so homogeneous and so isotropic. These questions can be answered if the universe before the Big-Bang went through a period of accelerated expansion, *cosmic inflation* [1], after which the universe is dynamically made flat, homogeneous and isotropic. Meanwhile, inflation also provides the quantum origin of structures in our universe, by seeding the initial inhomogeneities that later grow into galaxies and clusters. Albeit the success of cosmic inflation in solving cosmological problems, the theoretical underpinning of inflation is still not clear more than twenty years after its invention. Cosmological observations suggests that cosmic inflaton happens at an energy scale not too far below the Planck scale, where the quantum gravity effect is large. Therefore, superstring theory, as a complete framework to treat quantum gravity, becomes an ideal theoretical tool to study the inflationary era. Meanwhile, cosmological observation could provide the experimental probe of superstring theory. If we are fortunate, some stringy features may show up in a distinctive fashion on the sky,

providing the smoking-gun signatures of superstring theory.

1.1 Brane Inflation from String Theory

The standard Big-Bang cosmology is fantastically successful at explaining the thermal history of the observed universe. However, there remain key conceptual puzzles if we inspect the standard Big-Bang theory closely.

Observations of the cosmic microwave background (CMB) suggests the existence of temperature correlations over distances on the sky that corresponded to super-horizon scales at the time the CMB was released (last scattering). In fact, standard Big-Bang theory predicts that causally connected regions on the last scattering surface correspond to only an angular separation of 1° on the sky. The fact that CMB temperature is nearly the same to one part in 10^5 in all directions [2, 3] leads to the *Horizon Problem*: if two points were never in causal contact before last scattering, there is no way to establish thermal equilibrium between them.

CMB observations also suggest that our universe is extremely flat today; the curvature density fraction (relative to the critical density) $\Omega_{\rm k} \sim \mathscr{O}(0.01)$ [4]. However, the curvature density decreases as we go back in time. $\Omega_{\rm k} \sim 0.01$ today implies that $\Omega_{\rm k} \sim 10^{-60}$ at the begging of radiation domination; or $\Omega_{\rm k} \sim 10^{-20}$ at the epoch of Big-Bang Nucleosynthesis (BBN). In order to have the correct value of $\Omega_{\rm k}$ today, standard Big-Bang theory requires us to fine tune $\Omega_{\rm k}$ at early times to be extremely close to zero. This is the *Flatness Problem*.

The inflationary epoch [1] solves the flatness and horizon problem in a beautiful way. During inflaton, the Hubble scale is almost constant, so that

$$\Omega_{\rm k} = \Omega - 1 = \frac{k}{a^2 H^2} \propto \frac{1}{a^2} \ .$$

To set the initial value of $(\Omega - 1)$ at the beginning of the radiation-dominated phase to

$\sim 10^{-60}$, we require that during inflation

$$\frac{|\Omega - 1|_{t_f}}{|\Omega - 1|_{t_i}} = \left(\frac{a_i}{a_f}\right)^2 = e^{-2N}. \tag{1.1}$$

Taking $|\Omega - 1|_{t_i}$ of order unity, it is enough to require that $N \approx 60$. If the early universe went through a period of accelerated expansion for at least 60 e-folds, i.e., the scale factor grows by at least a factor of e^{60}, we will be able to drive $\Omega_{\rm k}$ sufficiently close to zero that we still observe it near zero today.

Furthermore, during inflation, the physical wavelength grows faster than the horizon; fluctuations are hence stretched outside the horizon during inflation and re-enter the horizon at late times. Super-horizon scales on the last scattering surface were in fact inside horizon before inflation. Therefore, the uniformity of CMB temperature can be explained by causal micro-physics. In addition to solving the horizon and flatness problems, inflation also helps to remove all the dangerous defects, especially magnetic monopoles, from phase transitions in the early universe; these monopoles, if present today, will close our universe. A bonus we get from inflation is that quantum fluctuations during inflation provide seeds for large scale structure formation, linking cosmological observations today to physics in the primordial universe.

Cosmological observations have yielded striking evidence for an inflationary epoch in the early universe. However, to date, there is still no compelling theoretical underpinning for inflation. In the field theory context, the most studied realization of cosmic inflation is the slow-roll scenario [5, 6], in which inflation is driven by a scalar field slowly rolling down a flat potential. Because the potential is extremely flat, enough inflation can be achieved to solve the horizon problem. Furthermore, the spectrum of primordial quantum fluctuation is nearly scale invariant and Gaussian. Slow-roll inflationary scenarios confront cosmological observations via two observables [2, 4] ,

1. The amplitude of the density perturbation or temperature fluctuations in the cosmic microwave background (CMB) as measured by COBE $\delta_H \sim 10^{-5}$ and WMAP

$A_S \sim 10^{-9}$ (The two different normalization is related by $A_s = 25\delta_H^2/4$.)

2. The spectral index of the scalar power spectrum $n_S \approx 0.96$ ($n_S = 1$ for exactly scale invariant power spectrum)

In addition, there are three observational upper bounds [4]:

1. The level of primordial gravitational waves, as measured by the tensor to scalar ratio $r \lesssim 0.22$
2. The scale dependence (running) of the scalar spectral index $|\mathrm{d}n_S/\mathrm{d}\ln k| \lesssim 0.1$
3. The non-Gaussian component in primordial density perturbations, as measured by the non-linear parameter $f_{\mathrm{NL}} \lesssim \mathscr{O}(100)$

Typical predictions of r, $\mathrm{d}n_S/\mathrm{d}\ln k$ and f_{NL} may very well be far too small to be detected at current stage. Since the COBE normalization is typically satisfied by changing the energy scale of cosmic inflation, so far, the deviation of n_S from unity is the only parameter that discriminates among slow-roll inflationary models. It is not surprising, therefore, that present data allows a large degeneracy of models. The status is expected to change dramatically in the near future. With the launch of the PLANCK satellite and many ground based observations, we will be able to put unprecedented constraints on $\mathrm{d}n_S/\mathrm{d}\ln k$, f_{NL} and r, offering great opportunities to test the nature of cosmic inflation scenarios.

If superstring theory is correct, it must provide an inflationary scenario for the early universe. Furthermore, it should provide a precise and restrictive framework for inflationary model building while at the same time, predict distinctive signatures that, if observed, can be used to support superstring theory. It is along this direction that this work attempts to address. Here we would like to discuss the possibility of stringy features that may show up in a distinctive fashion in the CMB. If the proposal is realized

in nature, the hope to link superstring theory and cosmological observations may become amazingly realistic, substantially strengthening the test of inflation as well as the specific string theory realization of inflation.

Imagine our universe is described by a brane world solution in Type IIB string theory. In this scenario, six of the nine spatial dimensions are dynamically compactified to a finite size. There are $D3$-branes (and probably $D5$- and $D7$-branes as well) that span our observable universe. Standard model particles are the lightest open string modes which must end on branes. The $D3$-branes are point-like in the six-dimensional compactified manifold known as the bulk. Closed strings can be everywhere, with the graviton being the lightest mode.

Based on the brane world scenario, it has become clear that the brane inflationary scenario is quite natural in string theory [7]. In the early universe, it is easy to imagine additional $D3$-$\bar{D}3$ brane pairs around. Here, the inflaton is simply the position of a mobile brane in the compactified bulk [8, 9], and the inflaton potential comes from the brane tensions and interactions and various back reaction effects from moduli stabilization. In flux compactification in Type IIB string theory, where all closed string moduli are dynamically stabilized, warped geometry appears naturally in the compactified bulk as warped throats [10, 11]. In the simple but realistic scenarios, inflation takes place as $D3$-branes move up or down a warped throat [12, 13, 14]. Fluctuations that are present before inflation, such as defects, radiation or matter, will be inflated away. Inflation typically ends when the $D3$-branes reach the bottom of a throat and annihilate the $\bar{D}3$-branes sitting there. The energy released heats up the universe and starts the hot big bang.

To make the picture more precise, let us start with the 10-dimensional metric for the throat region of the compactified bulk,

$$\mathrm{d}s^2 = h^2(r)(-\mathrm{d}t^2 + a(t)^2\mathrm{d}\mathbf{x}^2) + h^{-2}(r)\tilde{g}_{mn}\mathrm{d}y^m\mathrm{d}y^n \tag{1.2}$$

Here the cosmic scale factor $a(t)$ is that of an expanding homogeneous isotropic uni-

verse spanned by the 3-dimensions $\mathbf{x}$, and y^m's are the coordinates along the compact dimensions in the throat region. We can usually separate y^m into radial and angular coordinates,

$$\tilde{g}_{mn}\mathrm{d}y^m\mathrm{d}y^n = \mathrm{d}r^2 + \mathrm{d}\Sigma_{X_5}^2 \ .$$

The warp factor $h(r)$ and the metric on the extra dimensions $\tilde{g}_{mn}$ are inputs to the model. Warped spaces are natural in string theory models and are useful for flattening potentials and for generating a hierarchy of scales with the UV at the top (edge) of the throat and the IR scale at the warped bottom (around $r \sim r_A$). The best known example suitable for brane inflation is the $\mathscr{N} = 1$ supersymmetric Klebanov-Strassler (K-S) throat in type IIB string theory on approximate $AdS_5 \times T^{1,1}$ background [15]. For most practical purposes, especially away from the tip of the throat, we can approximately use the AdS warp factor

$$h(r) \approx \frac{r}{R} \ , \quad R^4 \equiv 4\pi g_s \alpha'^2 N_A / v \tag{1.3}$$

Here R sets the AdS radius scale. N_A is the total number of background (F_5) charge that generates the warped geometry. In the K-S throat, the warping is sourced by M units of F_3 flux and $-K$ units of H_3 flux. We have $N_A = KM$. v is the volume ratio of X_5 to 5-sphere ($\mathrm{Vol}(S^5) = \pi^3$). $v = 16/27$ for the K-S throat. We sketch the throat in Fig.1.1.

String theory suggests not only the metric for this model, but also the appropriate action for the $D3$-brane, the Dirac-Born-Infeld (DBI) action [16, 17, 18]. The bosonic part of the DBI action is given by

$$S_{D3} = -T_3 \int \mathrm{d}^4\xi \ e^{-\Phi} \ \sqrt{\det|G_{ab} + B_{ab} + 2\pi\alpha' F_{ab}|} \pm \mu_3 \int \left[\sum_{p=0}^{4} C_p\right] \wedge Tr\left[e^{2\pi\alpha' F + B}\right]$$

where the quantities inside the determinant have been pulled back onto the brane and the $\pm$ is for a brane/anti-brane. In particular, note that the pulled back metric (G_{ab}) will contain the warp factor. Here Φ is the dilaton field, whose expectation value sets the string coupling constant $g_s \equiv e^{\langle\Phi\rangle}$. B_{ab} is the anti-symmetric tensor and F_{ab} is the world

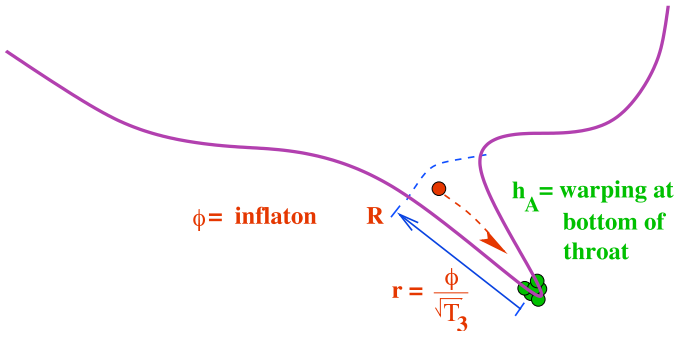

Figure 1.1: A cartoon of the throat in the compact extra dimensions. There may in general be warped throats of a variety of sizes attached to the bulk space. R sets the scale of the throat, while h_A is the warping at the bottom. The $D3$-brane moves down the throat, attracted by a $\bar{D}3$-brane (or a stack of them) sitting at the bottom. The inflaton ϕ is related to the brane position r.

volume gauge field. The topological Chern-Simons term contains couplings between the brane and R-R fields (p-forms) C_p, with p even for type IIB theory. The brane charge μ_3 is normalized such that $\mu_3 = g_s T_3$. We use variable ξ and indices $\{a,b\}$ for coordinates and quantities on the brane.

We now look at a simplified form of DBI action, which has constant dilaton, vanishing pullbacks B_{ab} and F_{ab}, and only C_4 non-zero ($D3$-branes are charged under the 4-form RR field C_4). The $D3$-brane alone in this background is supersymmetric. In addition, the supergravity equations require that components of C_4 on the brane be $h^4(r)/g_s$ [10]. We have aligned the $D3$-brane coordinates with the four dimensional space-time coordinates so that the world volume determinant becomes

$$S_{D3} = -T_3 \int \mathrm{d}^4x\, a^3(t) h^4(r) \left(\sqrt{1 + h^{-4}(r) \tilde{g}_{mn} \partial_\mu y^m \partial^\mu y^n} - 1 \right) . \tag{1.4}$$

If we only consider the radial motion of the brane, we have the further simplified single field action

$$S_{D3} = -\int \mathrm{d}^4x\, a^3(t) T(\phi) \left(\sqrt{1 + T^{-1}(\phi) \partial_\mu \phi \partial^\mu \phi} - 1 \right) \tag{1.5}$$

in which we have defined the inflaton field ϕ and warped tension $T(\phi)$

$$\phi \equiv \sqrt{T_3}\, r \ , \quad T(\phi) \equiv T_3\, h^4(\phi) \ . \tag{1.6}$$

We also have the useful relation

$$T(\phi) = \frac{\phi^4}{\lambda} \ , \quad \lambda \equiv T_3 R^4 = \frac{N_A}{2\pi^2\, v} \ . \tag{1.7}$$

If we expand the DBI action (1.5) to leading order in $\tilde{g}_{mn}\partial_\mu y^m \partial^\mu y^n / h^4$, we get the action of a canonical scalar field.

$$S_{D3} = -\frac{1}{2}\int \mathrm{d}^4x\, a^3(t)\partial_\mu\phi\partial^\mu\phi$$

Having derived the action for a single $D3$-brane, we now turn to the potential terms in the action. The inflaton potential can in principle be computed from a detailed knowledge of the string theory background (the flux compactification) and is of the form

$$V(\phi) = V_F + V_{\text{uplift}} + V_{D\bar{D}} + V_{\text{BR}} \ , \tag{1.8}$$

The term V_F is the contribution from closed string moduli stabilization, and is usually negative leading to the AdS vauca. In order to realize inflation, we need to uplift the vacuum energy to positive value and this is usually done by adding a $\bar{D}3$-brane to introduce a positive contribution V_{uplift} to the total vacuum energy [11]. The interaction term $V_{D\bar{D}}$ comes from the attraction between the mobile $D3$-brane and a $\bar{D}3$-brane sitting naturally at the bottom (small r end) of the throat. V_{BR} represents all the back reactions from moduli stabilization, which originates from the complications in describing open string moduli on the close string background. The complete computation of V_{BR} is challenging, and is not within the scope of this work. We will discuss effective parametrization of such an effect later.

Combining all the contributions, we can write

$$V(\phi) = 2T_3 h_A^4\left(1 - \frac{1}{N_A}\frac{r_A^4}{r^4}\right) + V_{\text{BR}} = V_0\left(1 - \frac{V_0}{4\pi^2 v}\frac{1}{\phi^4}\right) + V_{\text{BR}} \tag{1.9}$$

The $1/\phi^4$ term can be most simply understood as the analog of the Coulomb interaction in the six dimensions transverse to the branes. In the warped geometries considered here, one brane can be treated as a probe moving in the compact space with a metric perturbed by the other brane [12]. This explains the factor of $1/N_A$, since the perturbation due to a single extra brane should be suppressed by the number of background branes. Note that the singularity of the Coulomb term is never reached. When the branes are within the string scale distance, the Coulomb potential is curtailed due to the exchange of the infinite tower of closed string modes, as well as the emergence of a tachyon mode, whose rolling signifies the collision and annihilation of the $D3$-$\bar{D}3$ brane pair.

We now illustrate how the back reaction term $V_{\rm BR}$ comes into play. Let us look at the complex Kähler modulus (the overall size) of the Calabi-Yau manifold

$$\rho \equiv \sigma + i\chi \ ,$$

where σ is related to the warped four cycle volume of the Calabi-Yau manifold, and χ is the associated axion. The Kähler potential is given by

$$\mathscr{K} = -3\ln(\rho+\bar{\rho}) \ . \tag{1.10}$$

Following the scheme in Ref.[11], suppose the Kähler modulus is stabilized at the value σ_0, which results in a negative vacuum energy, adding a $\bar{D}3$-brane will contribute

$$V_{\rm uplift} = \frac{2T_3 h_A^4}{(2\sigma_0)^2} \tag{1.11}$$

and lift the vacuum to de-Sitter.

Now we introduce a mobile $D3$-brane in the warped throat. The position of the mobile $D3$-brane in the six compact dimensions are labeled by three complex coordinates z_i ($i=1,2,3$). With the $D3$-brane in the throat, the Kähler potential is shifted

$$\mathscr{K} \to -3\ln\left[\rho+\bar{\rho}-c\,k(z_i,\bar{z}_i)\right] \ , \quad k(z_i,\bar{z}_i) = r^2 \ , \quad c = \frac{\sigma_0}{3}\frac{T_3}{M_{\rm Pl}^2} \ . \tag{1.12}$$

$k(z_i, \bar{z}_i)$ is the Kähler potential for the Calabi-Yau manifold. The normalization constant c is determined in Ref.[19],

For any fixed brane location z_i, the Kähler modulus acquires a stabilized value $\rho^*(z_i)$. As the brane moves in the throat, it introduces a perturbation in the warp factor, which sources a change in the warped four-cycle volume. The location ρ^* of the instantaneous minimum changes. We will take the adiabatic approximation [19] that ρ moves to remain in the instantaneous minimum. Effectively, we need to shift the stabilized value of Kähler modulus,

$$2\sigma_0 \to 2\sigma_0 - a\,k(z_i, \bar{z}_i) = 2\sigma_0 - c\,r^2 \ . \tag{1.13}$$

Now the uplifting term becomes

$$V_{\rm uplift} = \frac{2T_3 h_A^4}{(2\sigma_0 - c\,r^2)^2} \approx \frac{2T_3 h_A^4}{(2\sigma_0)^2}\left(1 + \frac{1}{3}\frac{\phi^2}{M_{\rm Pl}^2}\right) \ . \tag{1.14}$$

The shift in Kähler modulus introduces explicitly a mass term for the inflaton field. Generically, the Hubble scale is related to the warped brane tension

$$3M_{\rm Pl}^2 H^2 = \frac{2T_3 h_A^4}{(2\sigma_0)^2} \ ,$$

the inflaton potential becomes

$$V(\phi) = 3M_{\rm Pl}^2 H^2 + H^2\phi^2 \ .$$

As is well known, this potential is too steep for slow-roll inflation. The resulting slow-roll parameter

$$\eta_{\rm SR} \equiv M_{\rm Pl}^2 \frac{V_{\phi\phi}}{V} \approx \frac{2}{3} \ ,$$

while we generically expect $\eta_{\rm SR} \sim 0.01$ for slow-roll inflation to be viable. The 1% fine tuning of $\eta_{\rm SR}$ is generic in most super-gravity inflation models; it re-emerges in our scenario through moduli stabilization. In realistic cases, one also has to consider the ϕ dependence in the super-potential, and calculating the back reaction term becomes a

long and cumbersome task [20, 19]. Because of these difficulties, in this work we take the pragmatic approach of parametrizing the back reaction effects into a parameter β, and write the inflaton potential as

$$V(\phi) = \frac{1}{2}\,\beta\, H^2\phi^2 + V_0\left(1 - \frac{V_0}{4\pi^2 v}\frac{1}{\phi^4}\right)\,. \tag{1.15}$$

The inflaton dynamics and resulting cosmological predictions are very sensitive to the value of β. For slow-roll inflation to be viable, we need $\beta \sim 0.01$. If $\beta \sim 1$, one gets an entirely new scenario, the Dirac-Born-Infeld inflation [13], which has distinctive observable features such as large primordial non-Gaussian perturbations. Since the value of β is dictated by the details of compactification, CMB data could reveal to us the structures of the compactified manifold, a very exciting aspect we will discuss in detail in the following chapters.

CHAPTER 2

BRANE INFLATION IN THE WARPED THROAT

2.1 The Homogeneous Background Solutions

In this chapter, we first discuss the dynamics of the classical inflaton field, i.e. the radial motion of the $D3$-brane in the warped throat, dictated by the non-linear DBI action. We then classify the inflaton dynamics into four different scenarios, depending on the inflaton mass parameter β: the slow-roll scenario, the ultra-relativistic and intermediate UV-DBI scenario, and the IR-DBI scenario. Details on each scenario will be covered later in their respective chapters.

We first look at the homogeneous background solution for the inflaton field. Since the DBI action is highly non-linear, we will adopt the k-inflation formalism [21, 22] to write the full Einstein-Hilbert action in the form

$$S = \frac{1}{2}\int \mathrm{d}^4x\sqrt{-g}\left[M_{\rm Pl}^2 R + 2P(X,\phi)\right] \ , \tag{2.1}$$

where

$$X \equiv \frac{1}{2}g^{\mu\nu}\partial_\mu\phi\,\partial_\nu\phi \ .$$

For brane inflation in the warped throat, we have from Eq.(1.5)

$$P(X,\phi) = -T(\phi)\left(\sqrt{1-\frac{2X}{T(\phi)}}-1\right) - V(\phi) \ . \tag{2.2}$$

To reproduce the canonical scalar field action, we can take the limit $X \ll T(\phi)$.

The energy momentum tensor is given by,

$$\begin{aligned} T_{\mu\nu} &= \frac{-2}{\sqrt{-g}}\frac{\delta S}{\delta g^{\mu\nu}} \\ &= P(X,\phi)\,g_{\mu\nu} + P_X\partial_\mu\phi\,\partial_\nu\phi \ , \end{aligned} \tag{2.3}$$

where $P_X \equiv \partial P/\partial X$. Comparing with the stress tensor of perfect fluid $T_{\mu\nu} = pg_{\mu\nu} + (\rho + p)u_\mu u_\nu$, we have

$$p = P(X,\phi) \ , \quad \rho = 2Xp_X - p \ . \tag{2.4}$$

A useful parameter is the sound speed c_s, which gives the propagation speed of perturbations within the horizon,

$$c_s^2 \equiv \frac{p_X}{\rho_X} = \frac{p_X}{p_X + 2Xp_{XX}} \ . \tag{2.5}$$

For the DBI action in particular,

$$c_s = \sqrt{1 - \frac{\dot\phi^2}{T(\phi)}} \ ,$$

is related to the Lorentz factor

$$\gamma \equiv \frac{1}{\sqrt{1 - \dot\phi^2/T(\phi)}} = \frac{1}{c_s} \ .$$

In terms of γ, the DBI energy density and pressure now becomes

$$\rho = T(\phi)(\gamma - 1) + V(\phi) \ , \quad p = T(\phi)(1 - \gamma^{-1}) - V \ . \tag{2.6}$$

In the non-relativistic limit $X \ll T(\phi)$, canonical scalar field is recovered from the DBI action, so that

$$\rho = \frac{1}{2}\dot\phi^2 + V(\phi) \ , \quad p = \frac{1}{2}\dot\phi^2 - V(\phi) \ , \quad c_s \approx 1 \ . \tag{2.7}$$

The homogeneous background equation of motion for DBI inflation takes the form

$$\ddot\phi - \frac{3T_\phi}{2T}\dot\phi^2 + T_\phi + \frac{3H}{\gamma^2}\dot\phi + \left(V_\phi - T_\phi\right)\frac{1}{\gamma^3} = 0 \tag{2.8}$$

where a subscript ϕ denotes derivative with respect to ϕ.

Using the continuity equation and the Friedmann equation

$$3H^2M_{\rm Pl}^2 = \rho \ , \quad \dot\rho = 3H(\rho + p) \ . \tag{2.9}$$

we get the Hamilton-Jacobi equations for $\dot{\phi}$ and γ,

$$\dot{\phi} = -\frac{2M_{\rm Pl}^2}{\gamma(\phi)} H_\phi \ , \tag{2.10}$$

$$\gamma(\phi) = \sqrt{1+4M_{\rm Pl}^4 H_\phi^2/T(\phi)} \ . \tag{2.11}$$

We now introduce a few frequently used inflationary parameters

$$\varepsilon \equiv -\frac{\dot{H}}{H^2} \ , \quad \eta \equiv \frac{\dot{\varepsilon}}{H\varepsilon} \ , \quad s \equiv \frac{\dot{c}_s}{Hc_s} \ . \tag{2.12}$$

The usual slow roll parameters defined using the scalar potential can be related easily

$$\varepsilon_{SR} \equiv \frac{M_{\rm Pl}^2}{2}\left(\frac{V_\phi}{V}\right)^2 = \varepsilon \ , \quad \eta_{SR} \equiv M_{\rm Pl}^2 \frac{V_{\phi\phi}}{V} = -\frac{1}{2}\eta + 2\varepsilon \ . \tag{2.13}$$

As usual,

$$\frac{\ddot{a}}{a} = H^2(1-\varepsilon) \ ,$$

so inflation happens when $\varepsilon < 1$.

The amount of inflation is usually measures in terms of e-folds N_e,

$$N_e = \int H {\rm d}t = \int \frac{H}{\dot{\phi}} {\rm d}\phi = \frac{1}{2M_{\rm Pl}^2} \int \frac{\gamma H}{H_\phi} {\rm d}\phi \ . \tag{2.14}$$

We note here that a relativistic brane ($\gamma \gg 1$) greatly enhanced the number of e-folds. Intuitively, the DBI action resembles the action of a relativistic particle with speed limit set by the warped tension $T(\phi)$. As the brane moves towards the strong warping end of the throat, $T(\phi)$ decreases and therefore put a strong upper bound on the velocity of the brane. The inflaton has to move slow due to the speed limit, greatly enhancing the number of e-folds generated even if the scalar potential is steep. This is the main reason why DBI effect may help solve the η problem discussed in Chapter 1.1.

As we have seen earlier, the inflaton potential is of the form

$$V(\phi) = \frac{1}{2}\beta H^2 \phi^2 + V_0 + V_{D\bar{D}} + \dots \ . \tag{2.15}$$

Overall, there are four scenarios depending on the value of β, three for a $D3$-brane moving down a throat and one for a $D3$-brane coming out of a throat. We will use "UV-DBI" for the scenario when the brane moves into the throat and generates most of the inflationary e-folds at the ultra-violet end of the throat. Similarly, we use "IR-DBI" for the scenario with the brane moving out of the throat and generating inflationary e-folds at the infrared end. The IR-DBI scenario requires an run-away potential with $\beta < 0$.

1. $\beta \ll 1$, $\gamma \simeq 1$, the *slow-roll* case. The $m^2 = 0$ case is studied in Ref.[12] and the more general small m^2 case is studied in Ref.[23, 24], where it was found that $\beta < 0.05$; that is, the range $0.05 \lesssim \beta \lesssim 0.2$ is ruled out. One can adjust the parameter β to fit the power spectrum index; for small β, $n_S \sim 0.98 + \beta$, the tensor to scalar ratio $\log(r) \sim -8.8 + 60\beta$, and the cosmic string tension $\log(G\mu) \sim -9.4 + 30\beta$. The non-Gaussianity and tensor mode produced are both negligible. Since it is a slow-roll model, the running of spectral index is small. This scenario is very hard to be distinguished from field theory models.

2. $\beta \sim 1$, the *intermediate UV-DBI scenario*. Typically $\gamma \simeq 1$ during inflation, but increases to a large value towards the end of inflation. This scenario is not easily studied analytically and is more suited to numerical integration. The intermediate regime offers the best hope of a large tensor mode that has a tensor power index n_t different from that predicted by the slow-roll scenario [25]. However, we will find in Chapter 2.3 that the tensor to scalar ratio r is strongly constrained by a field range bound from compactification, and therefore turns out negligibly small.

3. $\beta \gg 1$, the *ultra-relativistic UV-DBI scenario*, where $\gamma \gg 1$ throughout. This region typically has large distinctive non-Gaussianity [26, 22]. The non-Gaussianity parameter $f_{NL} \sim -0.32\,\gamma^2$ increases towards the end of inflation, leading to more non-Gaussian perturbations on small scales than on large scales. In fact, the amount of non-Gaussianity produced is too large to fall within the current ob-

servational bound, so that this scenario is not much favored by data now [27].

4. $\beta < 0$, the *IR-DBI scenario*, where $\gamma \gg 1$ during the initial stage of inflation, when the brane is deep in the IR end of the throat, and $\gamma \sim 1$ when the brane exits from the UV end into the bulk. This scenario is realized in a multi-throat compactification [14, 28] which we will discuss in detail in Chapter 2.4. The IR-DBI scenario also predicts large non-Gaussianity $(-0.32\,\gamma^2)$ with the same shape as in the UV model. The difference is the running. Since γ decrease during inflation, it will lead to more non-Gaussianities on larger scales than on small scales in the CMB sky. The power spectrum index undergoes an interesting phase transition, from red-tilted $(n_S - 1 \approx -4/N_e)$ at small scales to blue-tilted $(n_S - 1 \sim 4/N_e)$ at large scales [28, 29]. If such a transition falls into the observable range of WMAP/PLANCK, it predicts a large negative $\mathrm{d}n_S/\mathrm{d}\ln k$. Details about the IR-DBI scenario will be presented in Chapter 2.4.

2.2 The Primordial Perturbations in General

Before we discuss different scenarios of brane inflation, we would like to review the cosmological observables that link cosmic inflaton models to observations in general. The most common observables are the amplitude of scalar perturbations A_S, the scalar spectral index n_S, the running of the scalar spectral index $\mathrm{d}n_S/\mathrm{d}\ln k$, the tensor to scalar ration r, the tensor spectral index n_T and the primordial non-Gaussianity parameter f_{NL}. We will discuss them one by one in this chapter.

2.2.1 The Scalar Perturbations

During inflation, the inflaton field can be decomposed into its homogeneous rolling background $\phi(t)$ and the fluctuations $\delta\phi$,

$$\phi(\mathbf{x},t) = \phi(t) + \delta\phi(\mathbf{x},t) \ ,$$

where $\delta\phi$ owes its origin to quantum fluctuations.

Through Einstein's equation, the inflaton perturbation sources the metric fluctuation, which, in the Newtonian gauge, can be written as

$$\mathrm{d}s^2 = -(1-2\Phi)\,\mathrm{d}t^2 + a(t)^2(1+2\Phi)\,\mathrm{d}\mathbf{x}^2 \tag{2.16}$$

with Φ the curvature perturbation, and Newtonian potential is $-\Phi$ in this gauge.

The curvature perturbation on a constant energy density slice is given by the linear combination

$$\zeta(\mathbf{x},t) = \Phi(\mathbf{x},t) - \frac{H}{\dot{\rho}}\delta\rho(\mathbf{x},t) \ . \tag{2.17}$$

This variable is gauge invariant and therefore corresponds to a physical observable. Furthermore, ζ is conserved once it exits the horizon during inflation, providing the link between primordial physics and the temperature fluctuation in the cosmic microwave background radiation.

Another useful gauge invariant variable is the comoving curvature perturbation $\mathscr{R}$,

$$\mathscr{R}(\mathbf{x},t) = -\Phi(\mathbf{x},t) + \frac{H}{\dot{\phi}}\delta\phi(\mathbf{x},t) \tag{2.18}$$

On super-horizon scales, one can show that ζ and $\mathscr{R}$ differ only by a minus sign

$$\zeta = -\mathscr{R} \ . \tag{2.19}$$

We will use ζ exclusively in the following discussions.

The evolution of perturbation ζ is dictated by the quadratic terms in the perturbed Einstein-Hilbert action [22],

$$S_2 = \int \mathrm{d}\tau \mathrm{d}^3x \, \frac{a^2\varepsilon}{c_s^2}\left[\zeta'^2 - c_s^2\,(\partial\zeta)^2\right] \tag{2.20}$$

where τ is the conformal time $\mathrm{d}t = a\mathrm{d}\tau$. This action can be put into canonical form by introducing the Sasaki-Mukhanov variable $v(\tau,\mathbf{x})$,

$$v \equiv z\zeta \ , \quad z \equiv \frac{a}{c_s}\sqrt{2\varepsilon}\,M_{\rm Pl} \ . \tag{2.21}$$

In terms of v, the action becomes that of a free canonical scalar field

$$S_2 = \frac{1}{2}\int \mathrm{d}\tau \mathrm{d}^3x \, \left[v'^2 - c_s^2(\partial v)^2 + \frac{z''}{z}v^2\right] \ , \tag{2.22}$$

The equation of motion is

$$v_k'' + \left(c_s^2k^2 - \frac{z''}{z}\right)v_k = 0 \ , \tag{2.23}$$

where v_k is the Fourier mode of $v(\tau,\mathbf{x})$

$$v(\tau,\mathbf{x}) = \int \frac{\mathrm{d}\mathbf{k}^3}{(2\pi)^3}\, \mathrm{e}^{i\mathbf{k}\cdot\mathbf{x}} \, \left[v_k(\tau,\mathbf{k})a(\mathbf{k}) + v_k^*(\tau,-\mathbf{k})a^\dagger(-\mathbf{k})\right]$$

Using the inflationary parameters defined in Eq.(2.12), we can expand z''/z,

$$\frac{z''}{z} = 2a^2H^2\left(1 - \frac{\varepsilon}{2} + \frac{3\eta}{4} - \frac{3s}{2} - \frac{\varepsilon\eta}{4} + \frac{\varepsilon s}{2} + \frac{\eta^2}{8} - \frac{\eta s}{2} + \frac{s^2}{2} + \frac{\dot{\eta}}{4H} - \frac{\dot{s}}{2H}\right) \ . \tag{2.24}$$

In most simple cases, when not only ε, η, s, but also their time variations on Hubble scale, remain much smaller than 1,

$$\frac{z''}{z} \approx a^2 H^2 \left(2-\varepsilon+\frac{3\eta}{2}-3s\right) , \tag{2.25}$$

To solve Eq.(2.23), we perform a change of variable to $y \equiv c_s k/(aH)$, and rewrite Eq.(2.23) as

$$(1-2\varepsilon-2s)\frac{\mathrm{d}^2 v_k}{\mathrm{d}y^2} - \frac{s}{y}\frac{\mathrm{d}v_k}{\mathrm{d}y} + \left[1-\frac{1}{y^2}\left(2-\varepsilon+\frac{3\eta}{2}-3s\right)\right] v_k = 0 , \tag{2.26}$$

with its solution given by

$$\begin{aligned} v_k &= y^{(1+s)/2}\left[C_1 H_\nu^{(1)}((1+\varepsilon+s)y) + C_2 H_\nu^{(2)}((1+\varepsilon+s)y)\right] , \\ \nu &= \frac{3}{2}+\varepsilon+\frac{\eta}{2}+\frac{s}{2} . \end{aligned} \tag{2.27}$$

For modes outside of horizon ($y \to 0$) and deep inside horizon ($y \gg 1$), the Hankel function asymptotes

$$\begin{aligned} H_\nu^{(1,2)}(y\to 0) &\sim \pm i\sqrt{\frac{2}{\pi}}\frac{\Gamma(\nu)}{\Gamma(\frac{3}{2})}2^{\nu-3/2}y^{-\nu} , \\ H_\nu^{(1,2)}(y\gg 1) &\sim \sqrt{\frac{2}{\pi y}}\exp\left[\pm i\left(y-\frac{\nu\pi}{2}-\frac{\pi}{4}\right)\right] , \end{aligned}$$

with "+" sign for $H_\nu^{(1)}$ and "−" sign for $H_\nu^{(2)}$.

On the other hand, the solution for modes deep inside the horizon (corresponding to the Bunch-Davies vacuum) can be obtained under the adiabatic approximation,

$$\begin{aligned} v_k &\approx \frac{1}{\sqrt{2c_s k}}\exp\left[-i\int c_s k\,\mathrm{d}\tau\right] \\ &= \frac{1}{\sqrt{2c_s k}}\exp\left[iy(1+\varepsilon+s)\right] , \quad (y\gg 1) , \end{aligned} \tag{2.28}$$

where we have used $\mathrm{d}y = -c_s k(1-\varepsilon-s)\mathrm{d}\tau$.

Matching Eq.(2.27) and Eq.(2.28) in the $y \gg 1$ limit, we determine that

$$C_2 = 0 , \quad C_1 = \frac{\sqrt{\pi}\,y^{-s/2}}{2\sqrt{c_s k}}\sqrt{1+\varepsilon+s}\;e^{i(\pi\nu/2+\pi/4)} .$$

When the perturbation mode exits the horizon, we take the asymptotic limit $y \to 0$,

$$\left|\frac{v_k}{z}\right|_{y\to 0} = \frac{H}{2\sqrt{c_s\varepsilon}\,M_{\rm Pl}}\frac{y^{3/2-\nu}}{k^{3/2}}(1+\varepsilon+s)^{1/2-\nu}\,\frac{\Gamma(\nu)}{\Gamma(\frac{3}{2})}\,2^{\nu-3/2} \tag{2.29}$$

Now the primordial power spectrum is defined by

$$\langle\zeta(\mathbf{k})\zeta(\mathbf{k}')\rangle = \frac{2\pi^2}{k^3}P_\zeta(k)(2\pi)^3\delta(\mathbf{k}-\mathbf{k}') \tag{2.30}$$

from which we get

$$\begin{aligned} P_\zeta(k) &= \frac{k^3}{2\pi^2}\left|\frac{v_k}{z}\right|^2_{y\to 0} \\ &\approx \frac{H^2}{8\pi^2 M_{\rm Pl}^2 c_s\varepsilon}\,(1-2(\mathscr{C}+1)\varepsilon-(2+\mathscr{C})s-\mathscr{C}\eta)\left(\frac{c_s k}{aH}\right)^{3-2\nu} . \end{aligned} \tag{2.31}$$

Here $\mathscr{C} = \gamma - \ln 2 - 2 \approx -0.73$, with $\gamma = 0.577\ldots$ the Euler constant.

The power spectrum is usually parametrized by the power law

$$P_\zeta(k) = A_S\left(\frac{k}{k_0}\right)^{n_S-1} ,$$

comparing with the result Eq.(2.31), we have

$$A_S = \frac{H^2}{8\pi^2 M_{\rm Pl}^2 c_s\varepsilon}\,(1-2(\mathscr{C}+1)\varepsilon-(2+\mathscr{C})s-\mathscr{C}\eta) , \tag{2.32}$$

$$n_S - 1 \equiv \frac{{\rm d}\ln P_\zeta}{{\rm d}\ln k} \approx -2\varepsilon-\eta-s+\mathscr{O}(\varepsilon^2) \tag{2.33}$$

We have used the relations $k = aH/c_s$ at horizon crossing, so that

$$\frac{{\rm d}\ln k}{{\rm d}N_e} = 1-\varepsilon-s , \tag{2.34}$$

$$\frac{\rm d}{{\rm d}\ln k} = \frac{{\rm d}N_e}{{\rm d}\ln k}\frac{\rm d}{{\rm d}N_e} \approx (1+\varepsilon+s)\frac{\rm d}{{\rm d}N_e} . \tag{2.35}$$

The running of the spectral index

$$\frac{{\rm d}n_s}{{\rm d}\ln k} \approx -2\eta - \frac{\dot\eta}{H\eta} - \frac{\dot s}{Hs} + \mathscr{O}(\varepsilon^2) . \tag{2.36}$$

Current observations of WMAP5+BAO+SN [4] gives $A_S = (2.445 \pm 0.096)\times 10^{-9}$, $n_S = 0.960 \pm 0.013$ at $k = 0.002\,{\rm Mpc}^{-1}$. The running of the spectral index is not significant, the current data from WMAP5+ACBAR08 [4] imply ${\rm d}n_S/{\rm d}\ln k = -0.035^{+0.024}_{-0.025}$ at $k = 0.002\,{\rm Mpc}^{-1}$.

2.2.2 The Tensor Perturbations

In addition to scalar perturbations, metric perturbations also contains symmetric traceless tensor degrees of freedom h_{ij} in the form

$$\mathrm{d}s^2 = -\mathrm{d}t^2 + a^2(t)(\delta_{ij} + h_{ij})\mathrm{d}x^i \mathrm{d}x^j \ , \quad \partial^i h_{ij} = 0 \ , \quad h^i_i = 0 \ .$$

Unlike scalar perturbations, tensor perturbations are gauge invariant by themselves at linear order. The quadratic action for tensor mode is

$$S_{T2} = \frac{M_{\rm Pl}^2}{8} \int \mathrm{d}\tau \mathrm{d}^3x \, a^2 \, \partial_\mu h_{ij} \, \partial^\mu h^{ij} \ , \tag{2.37}$$

by changing to the variable

$$v_\lambda \equiv \frac{M_{\rm Pl}}{2} a h_{ij} \mathbf{e}^{ij}_\lambda \ , \quad \mathbf{e}^\lambda_{ij} \mathbf{e}^{ij}_{\lambda'} = \delta^\lambda_{\lambda'} \ ,$$

where $\mathbf{e}^\lambda_{ij}$ ($\lambda = \pm$) labels the polarization state, we get a canonical action

$$S_{T2} = \frac{1}{2} \int \mathrm{d}\tau \mathrm{d}^3x \, \left[v'^2_\lambda - (\partial v_\lambda)^2 + \frac{a''}{a} v^2_\lambda \right] \ . \tag{2.38}$$

The tensor mode equation of motion reads

$$v''_\lambda(\mathbf{k}, \tau) + \left(k^2 - \frac{a''}{a} \right) v_\lambda(\mathbf{k}, \tau) = 0 \ . \tag{2.39}$$

It can be easily solved to give

$$\left| \frac{v_\lambda}{a} \right| = \frac{H}{\sqrt{2k^3}} \frac{\Gamma(\nu)}{\Gamma(\frac{3}{2})} 2^{\nu - 3/2} (1+\varepsilon)^{1/2-\nu} \left(\frac{k}{aH} \right)^{-\varepsilon} \ , \quad \nu \approx \frac{3}{2} + \varepsilon \tag{2.40}$$

which leads to the tensor power spectrum

$$P_h(k) = \frac{k^3}{2\pi^2} \sum_\lambda \frac{4}{M_{\rm Pl}^2} \left| \frac{v_\lambda}{a} \right|^2 = \frac{2}{\pi^2} \frac{H^2}{M_{\rm Pl}^2} \left[1 - 2(1+\mathscr{C})\varepsilon \right] \left(\frac{k}{aH} \right)^{-2\varepsilon} \ . \tag{2.41}$$

Similar to the scalar power spectrum, the tensor power spectrum is parametrized by

$$P_h = A_T \left(\frac{k}{k_0} \right)^{n_T} \ . \tag{2.42}$$

Therefore, we have

$$A_T = \frac{2}{\pi^2}\frac{H^2}{M_{\rm Pl}^2}\left[1-2(1+\mathscr{C})\varepsilon\right] , \tag{2.43}$$

$$n_T \equiv \frac{{\rm d}\ln P_h}{{\rm d}\ln k} = \frac{-2\varepsilon}{1-\varepsilon-s} . \tag{2.44}$$

A useful parameter relevant for observation is the tensor to scalar ratio r,

$$r \equiv \frac{A_T}{A_S} \approx 16\,\varepsilon c_s . \tag{2.45}$$

The current observation bound on the tensor scalar ratio is $r \lesssim 0.22$ (95% C.L.) from a combined analysis of WMAP5+BAO+SN data [4]. Note that there is a parameter degeneracy between n_S and r. Since tensor perturbations decays on sub-horizon scales, a large tensor contribution implies a relatively blue-tilted scalar power spectrum.

Measurement of the tensor to scalar ratio can pin down the energy scale of inflation. Using Eq.(2.32) and Eq.(2.45), we can write

$$A_S = \frac{2}{\pi^2}\frac{H^2}{M_{\rm Pl}^2}\frac{1}{r} \quad \Rightarrow \quad \frac{H}{M_{\rm Pl}} = \pi\sqrt{\frac{A_S r}{2}}$$

Therefore the current bound $A_S \sim 10^{-9}$, $r \lesssim 0.22$ gives

$$\frac{H}{M_{\rm Pl}} \lesssim 10^{-5} . \tag{2.46}$$

The Hubble scale during inflation is $\lesssim 10^{13}\,{\rm GeV}$.

Note that for slow-roll inflation $c_s = 1$, we have the consistency relation

$$n_T = -\frac{r}{8}\left(\frac{1}{1-\varepsilon}\right) , \tag{2.47}$$

while for the DBI scenario, we have

$$n_T = -\frac{r}{8}\left(\frac{\gamma}{1-\varepsilon-s}\right) . \tag{2.48}$$

With $c_s < 1$ in the DBI case, the slope of the $n_T - r$ relation is a factor of γ larger than in the slow-roll case. This suggests a key way to distinguish slow-roll inflation from the DBI scenario.

2.2.3 Primordial non-Gaussianities

So far, we have been discussing the two-point correlation functions of the primordial perturbations, which is the most well know observable based on current observations. In the near future, with the launch of PLANCK, we expect to test higher order (3-pt, 4-pt) correlation functions for the primordial perturbations, which will provide a much more powerful discriminator on inflationary models.

The temperature anisotropies in the CMB sky are related to the curvature perturbation $\Phi(x)$ in the matter domination era, which can be expanded to non-linear order,

$$\Phi(x) = \Phi_{\rm L}(x) + f_{\rm NL}\left[\Phi_{\rm L}^2(x) - \left\langle \Phi_{\rm L}^2(x)\right\rangle\right] \ .$$

Φ in the matter dominated era is related to the primordial perturbation through

$$\Phi = \frac{3}{5}\zeta \ ,$$

so we have

$$\zeta = \zeta_{\rm L} + \frac{3}{5} f_{\rm NL}\left[\zeta_{\rm L}^2 - \left\langle \zeta_{\rm L}^2\right\rangle\right] . \tag{2.49}$$

The sign convention for $f_{\rm NL}$ used here follows Komatsu & Spergel [30] and differs from Maldecena's convention [31] by a minus sign.

Since $\Delta T/T \sim -\Phi/3$, a positive $f_{\rm NL}$ will make the temperature fluctuation negatively skewed, one will see more cold spots on the temperature map. This is a physical effect, independent of conventions.

In Fourier space,

$$\zeta_{\rm L}(\mathbf{x}) = \int \frac{d^3\mathbf{k}}{(2\pi)^3}\,\zeta_{\rm L}(\mathbf{k})\, e^{i\mathbf{k}\cdot\mathbf{x}} \ ,$$

so that

$$\begin{aligned}
\zeta(\mathbf{k}) &= \zeta_{\rm L}(\mathbf{k}) + \frac{3}{5} f_{\rm NL}\zeta_{\rm NL}(\mathbf{k}) , \\
\zeta_{\rm NL}(\mathbf{k}) &\equiv \int \frac{d^3\mathbf{q}}{(2\pi)^3}\zeta_{\rm L}(\mathbf{q}+\mathbf{k})\zeta_{\rm L}(-\mathbf{q}) - (2\pi)^3\delta(\mathbf{k})\left\langle \zeta_{\rm L}^2(\mathbf{x})\right\rangle
\end{aligned}$$

A non-vanishing component in the 3-pt correlation function will be

$$\langle\zeta(\mathbf{k}_1)\zeta(\mathbf{k}_2)\zeta(\mathbf{k}_3)\rangle = \frac{3}{5} f_{\rm NL}\left[\langle\zeta_{\rm NL}(\mathbf{k}_1)\zeta_{\rm L}(\mathbf{k}_2)\zeta_{\rm L}(\mathbf{k}_3)\rangle + perm.\right] .$$

After some rearrangement, we get

$$\langle\zeta(\mathbf{k}_1)\zeta(\mathbf{k}_2)\zeta(\mathbf{k}_3)\rangle = (2\pi)^7 \left(\frac{3}{10} f_{\rm NL}\right)\left(\frac{P_\zeta(k_2)}{k_2^3}\frac{P_\zeta(k_3)}{k_3^3} + perm.\right)\delta(\sum \mathbf{k}_i) \qquad (2.50)$$

From the theoretical side, computing the correlation function $\langle\zeta^3\rangle$ usually gives $f_{\rm NL}$ as a function of the three momentum, i.e., $f_{\rm NL}(k_1,k_2,k_3)$. So the value of $f_{\rm NL}$ depends on the shape of the momentum triangle. In the limit that one of the momentum goes to zero, say $k_1 \to 0$, one gets a squeezed triangle. We define the local form $f_{\rm NL}$,

$$f_{\rm NL}^{\rm local} \equiv \lim_{k_1\to 0} f_{\rm NL}(k_1,k_2,k_3) . \qquad (2.51)$$

Another commonly use shape is the equilateral triangle with $k_1 = k_2 = k_3$, we define the equilateral non-linear parameter

$$f_{\rm NL}^{\rm equil} \equiv f_{\rm NL}(k_1,k_2,k_3)\Big|_{k_1=k_2=k_3} . \qquad (2.52)$$

The current observational bound from WMAP5 is $-9 < f_{\rm NL}^{\rm local} < 111$ (95% C.L.) and $-151 < f_{\rm NL}^{\rm equil} < 253$ (95% C.L.) [4]. In the near future, the PLANCK satellite is expected to constrain $f_{\rm NL}^{\rm local} \lesssim 6$ (95% C.L.) [32]. And Large-Scale Structure (LSS) measurements can achieve $f_{\rm NL}^{\rm local} \lesssim 7$, $f_{\rm NL}^{\rm equil} \lesssim 90$ (95% C.L.) [33].

To evaluate the 3-pt function, one needs to expand the action to cubic terms [31, 22], which to leading order is

$$\begin{aligned} S_3 &= \int {\rm d}\tau {\rm d}^3x \left\{ -a\left(\Sigma(1-c_s^{-2})+2\lambda\right)\frac{\zeta'^3}{H^3} + \frac{a^2\varepsilon}{c_s^4}(\varepsilon-3+3c_s^2)\zeta\zeta'^2 \right. \\ &+ \left. \frac{a^2\varepsilon}{c_s^2}(\varepsilon-2s+1-c_s^2)\zeta(\partial\zeta)^2 - 2a\frac{\varepsilon}{c_s^2}\zeta'(\partial\zeta)(\partial\chi)+\ldots \right\} , \qquad (2.53) \end{aligned}$$

where the variables λ, Σ and χ are defined by

$$\lambda \equiv X^2 P_{XX} + \frac{2}{3} X^3 P_{XXX} \ , \tag{2.54}$$

$$\Sigma \equiv X P_X + 2X^2 P_{XX} \ , \tag{2.55}$$

$$\partial^2 \chi = a \frac{\varepsilon}{c_s^2} \zeta' \ . \tag{2.56}$$

The standard method to compute $\langle \zeta^3 \rangle$ is the In-In formalism [31], where we treat the quadratic action (2.22) as the free Lagrangian, and the cubic actions (2.53) as *perturbative* interactions.

$$\langle \zeta(\tau, \mathbf{k}_1) \zeta(\tau, \mathbf{k}_2) \zeta(\tau, \mathbf{k}_3) \rangle = -i \int_{\tau_0}^{\tau} \mathrm{d}\tau' \langle [\zeta(\tau, \mathbf{k}_1) \zeta(\tau, \mathbf{k}_2) \zeta(\tau, \mathbf{k}_3), H_{\rm int}(\tau')] \rangle \ , \tag{2.57}$$

Slow-roll inflation based on canonical single scalar field produce $f_{\rm NL} \sim \mathscr{O}(\varepsilon, \eta)$ [31], and non-linear gravitational corrections after inflation contribute $f_{\rm NL} \sim \mathscr{O}(1)$. Detection of primordial non-Gaussianity at the level $f_{\rm NL} \gg 1$ certainly rules out most canonical single field slow-roll models.

Scalar field with a non-canonical kinetic term generally produce large non-Gaussianity of the equilateral shape [22]. The result can be summarized as

$$f_{\rm NL}^{\rm equil} = -\frac{35}{108} \left(c_s^{-2} - 1 \right) + \frac{5}{81} \left(c_s^{-2} - 1 - \frac{2\lambda}{\Sigma} \right) \ . \tag{2.58}$$

We note that the DBI action (2.2), in particular, gives

$$\frac{2\lambda}{\Sigma} = c_s^{-2} - 1 \ , \tag{2.59}$$

so that the second term in Eq.(2.58) is zero. Therefore for DBI inflation

$$f_{\rm NL}^{\rm equil} = -\frac{35}{108} \left(c_s^{-2} - 1 \right) \approx -\frac{1}{3} c_s^{-2} \ . \tag{2.60}$$

2.3 The Ultraviolet Dirac-Born-Infeld Scenario

In this chapter, we study the UV-DBI scenario in detail [34]. We will see that the observational bound on primordial non-Gaussianity and the theoretical bound on the inflaton field range from string compactification put a tight constraint on the model, ruling out the ultra-relativistic regime. Detailed comparison with cosmological observations will be discussed.

2.3.1 Impact of Warp Factor: The Klebanov-Strassler Throat

The power spectrum index is sensitive to the deformation of the throat once we are away from the slow-roll region, and as such the precise shape of the throat, i.e., the warped geometry and the deformation can be measured using observations [35]. For this reason we discuss the warped throat in some detail here.

Consider two different approximate ways to incorporate the deformation of the warped conifold, namely the *AdS* and the *mass gap* cases for which the warped D3-brane tension is given by:

$$T_{\rm AdS}(\phi) = \frac{\phi^4}{\lambda}, \quad \phi \geq \phi_A \ , \tag{2.61}$$

$$T_{\rm mg}(\phi) = \frac{(\phi^2+b^2)^2}{\lambda}, \quad \phi \geq 0 \tag{2.62}$$

We expect $\phi_A \simeq b$, so away from the bottom of the throat, for large ϕ, we expect little difference in physics. However, in Ref.[25], we find $n_S - 1$ is slightly positive ($\sim \varepsilon^2/\gamma$) while in the second case, Ref.[36] finds that the spectrum has a red tilt. This difference appears in the DBI region. We expect a small (hopefully observable) effect of the warp factor in the large mass region. (The warp factor drops out in the slow-roll region.) This means n_S and its running will tell us about the shape of the throat, an exciting prospect. Note that the location and size of the 4-cycles in the bulk (partially) measures

the inflaton mass [20]. So we really can learn a lot about the compactification geometry from the CMB.

Now we have to consider the geometry of the throat more carefully. Although there is a wide class of possible geometries, we only know the full metric of the Klebanov-Strassler (K-S) throat. So let us consider this case. Consider the 10-dimensional metric (1.2),

$$\begin{aligned} \mathrm{d}s^2 &= h^2(r)(-\mathrm{d}t^2 + a^2(t)\mathrm{d}\mathbf{x}^2) + h^{-2}(r)(\mathrm{d}r^2 + r^2\mathrm{d}\Sigma_{T_{11}}^2) \\ &= h^2(\tau)(-\mathrm{d}t^2 + a^2(t)\mathrm{d}\mathbf{x}^2) + h^{-2}(\tau)\left(\frac{\varepsilon^{4/3}}{6K^2(\tau)}\mathrm{d}\tau^2 + \dots\right) \end{aligned} \tag{2.63}$$

(here, ε is the deformation parameter, not the inflationary parameter) where

$$K(\tau) = \frac{(\sinh(2\tau) - 2\tau)^{1/3}}{2^{1/3}\sinh\tau} \tag{2.64}$$

Unless we want to study the iso-curvature density perturbations, we shall ignore the shape encoded in $\mathrm{d}\Sigma_{T_{11}}^2$. The warp factor $h(\tau)$ is given by the following integral expression [15]

$$h^{-4}(\tau) = 2^{2/3}(g_s M\alpha')^2\varepsilon^{-8/3}I(\tau), \tag{2.65}$$

$$I(\tau) \equiv \int_\tau^\infty dx \frac{x\coth x - 1}{\sinh^2 x}(\sinh(2x) - 2x)^{1/3}. \tag{2.66}$$

where M is a parameter characterizing the background flux. Both $K(\tau)$ and $I(\tau)$ are well-behaved functions of τ:

$$\begin{aligned} &K(\tau\to 0) \to (2/3)^{1/3}(1 + \frac{\tau^2}{30} + ...), \quad K(\tau\to\infty) \to 2^{1/3}e^{-\tau/3} \\ &I(\tau\to 0) \to a_0 + \mathscr{O}(\tau^2), \quad I(\tau\to\infty) \to 3.2^{-1/3}\left(\tau - \frac{1}{4}\right)e^{-4\tau/3} \end{aligned} \tag{2.67}$$

where $a_0 \sim 0.71805$. Here we take $\varepsilon^{2/3}$ to have dimension of length. So we have

$$\begin{aligned} h(r) &= h(\tau) \\ \mathrm{d}r &= \frac{\varepsilon^{2/3}}{\sqrt{6}K(\tau)}\mathrm{d}\tau \end{aligned} \tag{2.68}$$

Integrating this equation gives the relation between τ and the throat radial coordinate r,

$$r - r_0 = \frac{1}{2^{5/6}3^{1/6}}\varepsilon^{2/3}\tau\left(1+\frac{\tau^2}{18}+...\right) \tag{2.69}$$

From the explicit expressions in terms of τ, we can obtain $h(r)$ or $T(\phi)$. For large τ, its relation to the radial coordinate r is given by

$$r^2 \simeq \frac{3}{2^{5/3}}\varepsilon^{4/3}e^{2\tau/3} \tag{2.70}$$

In the limit $\varepsilon \to 0$, finite r implies $\tau \to \infty$, so the metric of the compact dimensions is

$$ds_6^2 \to \mathrm{d}r^2 + r^2\mathrm{d}\Sigma_{T_{11}}^2 \tag{2.71}$$

which is simply the conifold metric. At $\tau = 0$, we have $h_A = h(r_0) = r_0/R$ and

$$h^2(r_0) = h^2(\tau=0) = \frac{c_0}{g_sM}\frac{\varepsilon^{4/3}}{\alpha'} = \exp\left(-\frac{4\pi K}{3g_sM}\right) \tag{2.72}$$

where $c_0 = 1/(2^{1/3}\sqrt{a_0})$, so

$$r_0^2 = \frac{c_0}{g_sM}\left(\frac{\varepsilon^{4/3}}{\alpha'}\right)R^2 \tag{2.73}$$

where R is given in Eq.(1.3). $N_A = KM$, with K and M the H_3 and F_3 flux numbers.

The edge of the throat is glued smoothly to the bulk of the generalized Calabi-Yau manifold. The bulk of the Calabi-Yau manifold is defined to have no significant warping, so that the warp factor in the bulk is essentially of order unity. Suppose τ_c is the point where the throat is glued to the bulk. We may estimate τ_c using (2.69):

$$\begin{aligned} R - r_0 &\approx \frac{\varepsilon^{2/3}}{\sqrt{6}}\int_0^{\tau_c}\frac{1}{K(\tau)}\mathrm{d}\tau \approx \frac{\varepsilon^{2/3}}{\sqrt{6}}\int_0^{\tau_c}\frac{1}{2^{1/3}e^{-\tau/3}}d\tau \\ e^{\tau_c/3} &\approx (R-r_0)\varepsilon^{-2/3}\frac{2^{1/3}\sqrt{6}}{3}+1 \end{aligned} \tag{2.74}$$

as long as $\tau_c \gg 1$, which is true for reasonable parameter values. This expression agrees well with the numerical value for which $h(\tau_c) = 1$.

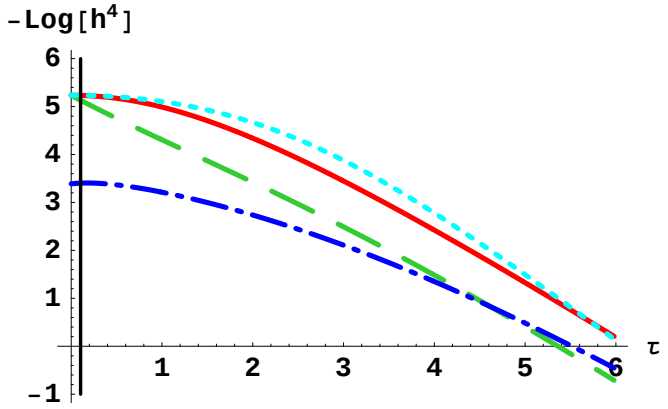

Figure 2.1: Comparison of the various warp factor expressions. The solid (red) line is the full warped deformed conifold expression. The long dashed (green) line is the AdS warp factor. The dot-dashed (dark blue) is the log-corrected expression, and the short-dashed (light blue) is the mass-gap. For this plot $N_A = 10^6$, $M = 4000$. The vertical black line indicates τ_E, where the tachyon develops and inflation ends.

The relation between τ_c, ε and l_s is important to impose the constraint that the throat must fit inside the bulk. The physical size of the throat is given by

$$l = 6^{-1/2}\,\varepsilon^{2/3}\int_0^{\tau_c} \mathrm{d}\tau\,\frac{h^{1/4}(\tau)}{K(\tau)} \sim \sqrt{g_s M}\,l_s\,\tau_c \tag{2.75}$$

We must require that $l < V_6^{1/6}$, where V_6 is the volume of the compactification.

Which approximate warp factor is closer to the actual solution depends on details of how the throat is cut-off. To illustrate this point, we show numerical examples of the various expressions for the warp factor in Figures 2.1 and 2.2. Note that when $M > \sqrt{N_A}$, the mass-gap formula is much more accurate than the AdS expression. In particular, the AdS warp factor indicates a throat that is much too short (the point where the throat connects to the bulk is when $h(\tau_c) = 1$). However, when $M < \sqrt{N_A}$, the mass-gap expression is actually too flat and the AdS expression is more accurate. This is especially true for small N_A, where the slope of the full solution changes considerably in one warped string length. For completeness, we also plot the log-corrected solution (see [15]), although we do not use it in our analysis since it deviates strongly from the

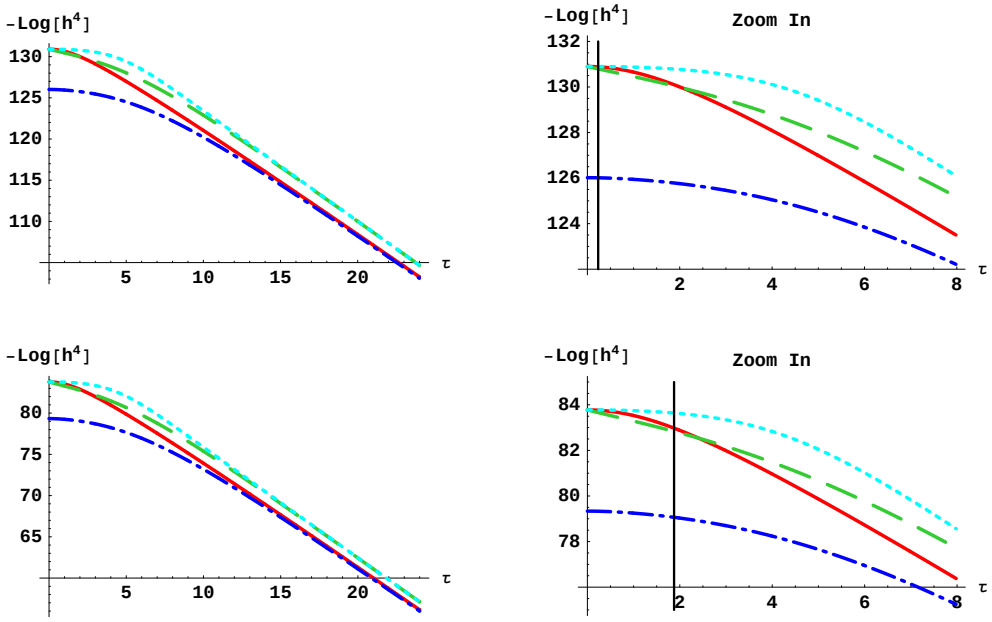

Figure 2.2: As in Figure 2.1 showing warp factors for (top panels) $N_A = 10^6$, $M = 800$ and (bottom panels) $N_A = 10^2$, $M = 10$. The right hand panels show a zoomed in region. The vertical black line indicates τ_E, where the tachyon develops and inflation ends.

actual K-S solution at small τ.

One can understand these results by examining the initial slopes of the various expressions, accounting for the change of coordinates between r and τ in the small τ limit. The important constant in the AdS and mass-gap expressions is $r_0/\varepsilon^{2/3} \sim (\sqrt{N_A}/M)^{1/2}$. If this constant is large, the slope of the mass-gap expression decreases and that warp factor flattens out, while the AdS expression is less negative. If the constant is small, the AdS case has a very large negative slope initially, while the mass-gap case has a stronger τ dependence.

2.3.2 The Ultra-Relativistic and Intermediate Regime

In the large γ case, the inflaton mass m is relatively big and one may neglect the other two terms in the potential (1.15). Let us take the AdS warp factor, $T(\phi) = \phi^4/\lambda$. In

the ultra-relativistic regime ($\gamma \gg 1$), the inflaton speed is essentially close to the speed limit, we therefore have

$$\dot{\phi} = \sqrt{T(\phi)} = \frac{\phi^2}{\sqrt{\lambda}} \ , \tag{2.76}$$

From Eq.(4.34) and Eq.(4.35), we further have

$$\gamma(\phi) = 2M_{\rm Pl}^2 H_\phi \frac{\sqrt{\lambda}}{\phi^2} \ , \tag{2.77}$$

$$\dot{\phi} = \frac{-2M_{\rm Pl}^2 H_\phi}{\gamma(\phi)} \ . \tag{2.78}$$

The set of equations can be solved by

$$H(\phi) = c\,\phi \ , \quad c \approx \frac{m}{\sqrt{6}M_{\rm Pl}} \ , \tag{2.79}$$

from which we find a useful relation

$$\varepsilon = -\frac{\dot{H}}{H^2} = -\frac{H_\phi \dot{\phi}}{H^2} = \frac{2}{\gamma}\left(\frac{M_{\rm Pl}}{\phi}\right)^2 \tag{2.80}$$

One also note that ε is a constant for ultra-relativistic motion of the brane

$$\varepsilon = \frac{1}{c\sqrt{\lambda}} \ . \tag{2.81}$$

In string theory, the reduced Planck mass $M_{\rm Pl}$ is related to the (warped) volume V_6 of the 6-dimensional bulk via

$$M_{\rm Pl}^2 \sim g_s^{-2} m_s^{-8} V_6 \ , \tag{2.82}$$

Since the throat is glued to the bulk, its size R is restricted,

$$R^6 \lesssim V_6 \ . \tag{2.83}$$

The position of the $D3$-brane cannot be physically larger than the largest dimension of the compactified bulk. Therefore, we have

$$\sqrt{T_3} R \lesssim \sqrt{T_3} V_6^{1/6} \ . \tag{2.84}$$

Using the relation $R^4 \sim g_s N_A m_s^{-4}$ and $T_3 \sim g_s^{-1} m_s^{-4}$, we get a tight constraint,

$$\frac{\sqrt{T_3} R}{M_{\rm Pl}} \lesssim \frac{1}{\sqrt{N_A}} \,. \tag{2.85}$$

A more rigorous analysis has been done by Baumann and McAllister [27] for the K-S throat, where they find

$$\frac{\phi}{M_{\rm Pl}} < \sqrt{\frac{4}{N_A}} \,. \tag{2.86}$$

Now using the bound (2.86) together with the relation (2.80), we see that

$$N_A \lesssim \frac{2\varepsilon}{c_s} \approx -\frac{3}{8} f_{\rm NL}^{\rm equil}\, r \,. \tag{2.87}$$

We have used the relation $r = 16 c_s \varepsilon$ and $f_{\rm NL}^{\rm equil} \approx -c_s^{-2}/3$. Now using the current observational bounds $r \leq 0.22$, $-151 < f_{\rm NL}^{\rm equil} < 253$, we have

$$N_A \leq 13 \,. \tag{2.88}$$

So current observational bounds on tensor mode and non-Gaussianity severely constrains the amount of five-form flux for ultra-relativistic UV-DBI inflation with quadratic potential.

We now look at the constraints from the primordial power spectrum. Using Eq.(2.77) and $H = c\,\phi$, we get

$$c = \frac{\gamma}{2M_{\rm Pl}^2} \frac{\phi^2}{\sqrt{\lambda}} \,. \tag{2.89}$$

Using $\lambda = N/(2\pi^2 v)$, we have

$$\frac{H^2}{M_{\rm Pl}^2} = \frac{4\pi^2 c_s v}{N_A \varepsilon^2} \,, \tag{2.90}$$

Therefore, the primordial power spectrum

$$P_\zeta = \frac{H^2}{8\pi^2 M_{\rm Pl}^2 \varepsilon\, c_s} = \frac{v}{2N_A \varepsilon^4} = \frac{2^{15}}{9} \frac{-v}{N_A\, r^4 (f_{\rm NL}^{\rm equil})^2} \sim 10^{-9} \,. \tag{2.91}$$

Plugging the current bound on r and $f_{\rm NL}$, we get

$$N_A \gtrsim 10^{11}\, v \,. \tag{2.92}$$

In most cases, $v \sim 1$, so the bound (2.88) and (2.92) are apparently incompatible. To keep the amplitude of primordial perturbations small, we need a huge amount of F_5 flux, which will make the field range $\phi/M_{\rm Pl}$ extremely small. Since the vacuum energy for inflation is provided by the quadratic term in the potential, we need a big mass parameter to provide sufficient amount of inflation; this is the origin of the over-production of non-Gaussianity. As we shall see, consistent with this discussion, when combined with data, imposing the bulk volume bound (2.86) would rule out the region of the parameter space with large γ (and large non-Gaussianity).

While we have analytic solutions for the ultra-relativistic regime, the intermediate regime with $\beta \sim 1$ is much harder to solve and we will need to numerically solve the set of Hamilton-Jacobi equations

$$
\begin{aligned}
3M_{\rm Pl}^2 H^2 &= V(\phi) + T(\phi)(\gamma - 1) \,, && (2.93)\\
\dot{\phi} &= -\frac{2M_{\rm Pl}^2}{\gamma(\phi)} H_\phi \,, && (2.94)\\
\gamma(\phi) &= \sqrt{1 + 4M_{\rm Pl}^4 H_\phi^2 / T(\phi)} \,. && (2.95)
\end{aligned}
$$

Here $V(\phi)$ takes the full form in Eq.(1.15)

$$
V(\phi) = \frac{1}{2}\beta H^2 \phi^2 + V_0 \left(1 - \frac{V_0}{4\pi^2 v}\frac{1}{\phi^4}\right) \,, \tag{2.96}
$$

The constant term V_0 may become comparable to the ϕ^2 terms and cannot be neglected.

To numerically integrate Eq.(2.93) through Eq.(2.95), one needs to specify initial conditions ϕ_i and γ_i. We choose $\phi_i = \sqrt{T_3}R$, the edge of the throat, and choose $\gamma_i \approx 1$. It is much more convenient to use e-fold as time, so we may rewrite Eq.(2.94) as

$$
\frac{{\rm d}\phi}{{\rm d}N_e} = -\frac{2M_{\rm Pl}^2}{\gamma(\phi)}\frac{H_\phi}{H} \,. \tag{2.97}
$$

For the DBI scenario, ε is suppressed by $1/\gamma$ and almost never grow larger than 1 at the end of inflation. In fact, in the DBI scenario, inflation ends by $D\bar{D}$ annihilation,

which happens when the proper distance between $D\bar{D}$ pairs is at the string scale $\sqrt{\alpha'}$. Using the metric (1.2), the proper distance between the branes is

$$\int ds = \int \frac{dr}{h(r)}. \tag{2.98}$$

For the AdS warp factor (2.61),

$$\phi_E = \phi_A \exp\left(\sqrt{\alpha'}/R\right) \tag{2.99}$$

For the mass-gap warp factor (2.62) ,

$$\phi_E = b \sinh\left(\sqrt{\alpha'}/R\right) \ . \tag{2.100}$$

The result of our numerical integration is $H(N_e)$, $H_\phi(N_e)$, $\gamma(N_e)$ and $\phi(N_e)$. We then calculate the observables such as $P_\zeta(N_e)$. To relate N_e to today's observable scale k, we need the horizon crossing relation $c_s k = aH$, which gives

$$N_e = 65 - \ln\frac{k}{0.002\,\mathrm{Mpc}^{-1}} + \ln\frac{H\,c_s^{-1}}{T_{\mathrm{reheat}}} \ . \tag{2.101}$$

In our calculating, we assume 100% efficiency in converting the inflaton energy into radiation at the end of inflation.

Having $P_\zeta(k)$ at hand, we can use cosmological data to constrain the model. This will be the topic of the next chapter.

2.3.3 The Phase Diagram for UV-DBI Inflation

In this chapter, we draw the phase diagram of UV-DBI inflation in terms of two parameters: the inflaton position ϕ and the inflaton mass m. We use this diagram to show the condition under which slow-roll, intermediate and relativistic dynamics happen.

Consider the potential (ignoring the Coulomb term)

$$V(\phi) = V_0 + \frac{1}{2}m^2\phi^2 + \dots \ , \tag{2.102}$$

where $V_0 = 2n_A h_A^4 T_3$ are provided by n_A antibranes at the end of the A throat, which eventually get annihilated by the same number of branes.

If the flatness of the potential $V(\phi)$ satisfies the slow-roll conditions, the branes can slowly roll non-relativistically and the kinetic term of the brane DBI action reduces to the minimal non-relativistic form. To indicate this condition in the phase diagram, we draw a curve of

$$\eta_{\rm SR} \equiv M_{\rm Pl}^2 \frac{V_{\phi\phi}}{V} = 1$$

which is

$$\phi^2 = 2M_{\rm Pl}^2 - \frac{2V_0}{m^2} \,, \tag{2.103}$$

where we neglected the Coulomb potential term for simplicity. Eq. (2.103) corresponds to the solid line stretching from the lower-left (at $m = \sqrt{V_0}/M_{\rm Pl}$) to upper-right (at $\phi = \sqrt{2}M_{\rm Pl}$) in Fig. 2.3. Inclusion of the Coulomb term will cause a slight deformation at the lower-left corner of this curve and will not affect our conclusion. The shaded region above and to the left of this curve has $\eta_{\rm SR} < 1$, and corresponds to the slow-roll inflation phase; here the condition $\varepsilon_{\rm SR} < 1$ is always weaker. The lower-left shaded region is the small-field slow-roll region where the potential is dominated by the constant V_0. As ϕ increases toward the upper part of the shaded region, it corresponds to large-field slow-roll inflation where the potential is dominated by $m^2\phi^2$ term. Note that in this region ϕ is trans-Planckian, $\phi > \sqrt{2}M_{\rm Pl}$.

Outside of this slow-roll region, naively the inflaton will roll down the potential very fast and make inflation impossible. However because of the presence of the warped space, the velocity of the inflaton is bounded by the warped speed of light and therefore cannot be arbitrarily increased. Based on Eq.(2.81), if

$$m \gg M_{\rm Pl}/\sqrt{\lambda_A} \,, \tag{2.104}$$

we will have DBI inflation [13], in which the full form the DBI kinetic term has to

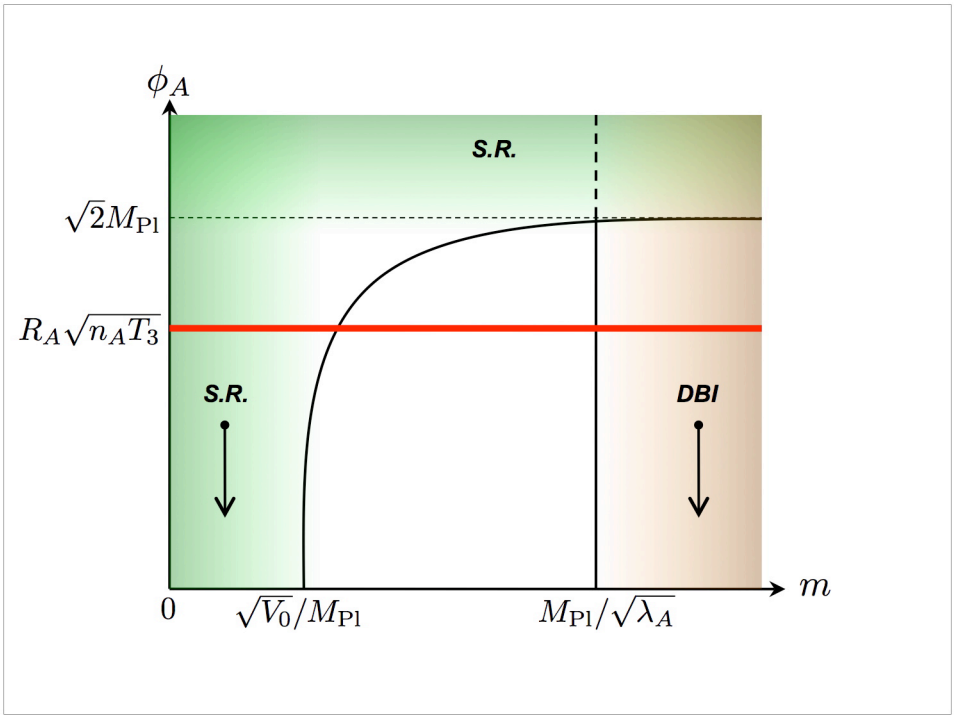

Figure 2.3: The inflation phase diagram for UV models. The shaded regions correspond to parameter space that can give rise to inflation. The darker the region is, the larger e-folds it can provide. "S.R." stands for slow-roll inflation; "DBI" stands for DBI inflation. The arrows indicate the starting point and rolling direction of the inflaton. In brane inflation, inflatons have to stay below the horizontal solid line (at $\phi_A = R_A\sqrt{n_A T_3}$); the two vertical lines (at $m = \sqrt{V_0}/M_{\rm Pl}$ and $m = M_{\rm Pl}/\sqrt{\lambda_A}$) are widely separated. The curve stretching from $m = \sqrt{V_0}/M_{\rm Pl}$ to $\phi_A = \sqrt{2}M_{\rm Pl}$ corresponds to $\eta_V = \beta/3 = 1$. See text for discussion.

be taken into account. We indicate this condition by the solid vertical line (at $m = M_{\rm Pl}/\sqrt{\lambda_A}$) in Fig. 2.3 and the DBI inflation phase by the shaded region to the right.

There are two possible regions where these two phases merge onto each other: when the inflaton in the DBI phase starts from a Planckian value (the upper-right corner of Fig. 2.3), the inflation can go continuously from slow-roll to DBI; when $\sqrt{V_0}/M_{\rm Pl} \sim M_{\rm Pl}/\sqrt{\lambda_A}$ so the two vertical lines in Fig. 2.3 become very close to each other or even switch places, the inflaton around this border will trigger an inflationary phase that lies

in-between the slow-roll and DBI regimes. These are the "intermediate regions".

However, so far we have been discussing an effective field theory description where one is allowed to independently choose the throat charge N_A, fundamental string mass m_s and the inflaton field range ϕ. In a realistic string compactification, the inflaton brane separation is restricted by

$$\phi \lesssim R_A \sqrt{n_A T_3} \ , \quad \text{or} \quad \phi \lesssim L \sqrt{n_A T_3} \ , \tag{2.105}$$

for n_A branes moving in the throat or the bulk respectively. Here L is the size of the bulk in a certain dimension. For our phase diagram, the geometric constraints (2.82) and (2.83) imply

$$\frac{\sqrt{V_0}}{M_{\rm Pl}} \Big/ \frac{M_{\rm Pl}}{\sqrt{\lambda_A}} \lesssim \frac{n_A h_A^2}{N_A} \ll 1 \ , \tag{2.106}$$

and

$$\frac{R_A \sqrt{n_A T_3}}{M_{\rm Pl}} \lesssim \frac{\sqrt{n_A}}{\sqrt{N_A}} \ll 1 \ . \tag{2.107}$$

Thus the two vertical solid lines (at $m = \sqrt{V_0}/M_{\rm Pl}$ and $m = M_{\rm Pl}/\sqrt{\lambda_A}$ respectively) in Fig. 2.3 should be widely separated; the inflaton can only move below the horizontal solid line (at $\phi = R_A \sqrt{n_A T_3}$) which is well below $\phi = \sqrt{2} M_{\rm Pl}$. This excludes the large field models where $\phi \gtrsim M_{\rm Pl}$, and opens up a wide region in the middle of the parameter space where there is no inflation. This is also why the tensor mode in brane inflation is unobservable [27]. Consistent with this discussion, in the next chapter, we will see that the parameter space for the intermediate regime becomes tiny once we impose the bulk volume bound. In Chapter 3.2, we will see that it also exclude the stochastic eternal inflation in slow-roll scenario [37].

2.3.4 Comparison with Cosmological Observations

In the previous chapter we outlined how the initial spectrum of scalar and tensor perturbations arising from brane inflation can be characterized in terms of six parameters: the

inflaton mass m, background charge N_A, minimum warping $h_A = h(\phi_A)$, the volume ratio parameter v in (1.3), string length $\sqrt{\alpha'}$, and the string coupling g_s. To compare with observations we consider the predicted spectrum normalization, A_S, scalar and tensor spectral indexes, n_S and n_T, and tensor to scalar ratio r, all evaluated at a near-horizon physical scale $k_{\rm pivot} = 0.002\,{\rm Mpc}^{-1}$.

For the following numerical analyses, unless otherwise stated, we fix the string coupling $g_s = 0.1$ and length $\alpha' M_{\rm Pl}^2 = 1000$. We investigate the constraints on the remaining four parameters $\{N_A,\ v,\ h_A,\ m^2\}$, and the slow-roll, intermediate and ultra-relativistic regimes outlined in chapter 2.1. We generate Monte Carlo selected brane inflation models, obtained using a flat prior on $\{\log N_A,\ \log v,\ \log m^2,\ A_S\}$ and finding h_A to give the required value of $A_S(k_{\rm pivot})$.

We compare the model parameters, for both the AdS and mass-gap geometries, to observational limits on the amplitude, spectral index, tensor-to-scalar ratio for the initial power spectra from the WMAP CMB data [38, 39, 40, 41], SDSS LRG matter power spectrum data[42] and SNLS supernovae [43]. We use the publicly available `cosmomc` code [44] to perform a Monte Carlo Markov Chain analysis for a ΛCDM cosmological scenario, assuming flat priors on the following set of cosmological parameters: the physical baryon and cold dark matter densities, $\omega_b = \Omega_b h^2$ and $\omega_c = \Omega_c h^2$ (where h is the reduced Hubble constant $h = H_0/100$), the ratio of the sound horizon to the angular diameter distance at decoupling, θ_s, and the optical depth to reionization, τ, as well as power spectrum parameters, $n_S(k_{\rm pivot})$, $\log\ A_S(k_{\rm pivot})$, and $r(k_{\rm pivot})$. As we discuss below, and in figures 2.5 and 2.6, in both the AdS and mass-gap scenarios, the running in the scalar spectral index is extremely small over observable scales, $|{\rm d}n_S/{\rm d}\ln k| < 4\times 10^{-3}$, and the vast majority models closely obey the consistency relation $n_T = -r/8$. We compare the Monte Carlo DBI models to compatible observational constraints obtained with ${\rm d}n_S/{\rm d}\ln k = 0$ and both with the consistency relation, and with

r and n_T allowed to be unrelated with $-0.02 < n_T < 0$. We consider purely adiabatic initial conditions and impose flat spatial curvature. The MCMC convergence diagnostics is done on seven chains though the Gelman and Rubin "variance of chain mean"/"mean of chain variances" R statistic for each parameter.

We also impose the following two consistency constraints:

1. *Sufficient e-folds and all e-folds in the throat:* Although there may be inflation from other sources (other branes or other parts of the $D3$ trajectory) we require that sufficient e-folds to solve the usual horizon problem take place in a single throat. One may in principle loosen this requirement, but a more detailed knowledge of the geometry in the bulk space would be needed. The required number of e-folds depends on the reheating temperature T_{RH} and inflation scale H_I through $N_e \approx 68.6 + \ln(H_I \gamma / T_{RH})$. This equation comes simply from the requirement that Ha at the beginning of inflation is at least as small as Ha today, where H is the Hubble parameter and a is the universe's expansion factor. In other words, the largest scale we observe today ($k_H \sim k_{\rm pivot}/10$) was once in causal contact. The expression is approximate because it assumes H is constant during inflation. In the appendix we discuss how to implement the condition more precisely. The requirement that enough inflation occurs in the throat can then be expressed as $\phi_H < \phi_{UV}$, where ϕ_{UV} is the scale where the throat is glued to the bulk. We use the condition $h(\phi_{UV}) = 1$. For simplicity we assume 100% efficient reheating, so that T_{RH} is set by the warped brane tension.

2. *A proportionally small throat:* In order to have the observable scales today correspond to the inflaton position inside the throat, we impose the bulk volume bound (2.86) in the form,

$$\frac{\phi_{\rm pivot} - \phi_A}{M_{\rm Pl}} < \sqrt{\frac{4}{N_A}} \tag{2.108}$$

where $\phi_{\rm pivot}$ is the value of ϕ corresponding to the physical pivot scale today, $k_{\rm pivot}$,

where the normalization to CMB data is applied.

For DBI inflation, the Lyth bound [45] still applies

$$\frac{1}{M_P}\frac{d\phi}{dN_e} = \frac{2M_P H'}{\gamma H} = \sqrt{\frac{r}{8}}\,. \tag{2.109}$$

Using the Lyth bound and considering that r may decrease rapidly during inflation, Ref.[27] concludes that in DBI inflation with a quadratic potential, the tensor/scalar ratio would be unobservable for $N_A > 10^6$. Meanwhile, it would badly violate the current bound on non-Gaussianity for $N_A \gtrsim 13$.

One may rewrite the Lyth bound (2.109) as

$$\begin{aligned} r_{\rm CMB} &\lesssim \frac{32}{N_A}\left(\frac{1}{N_{\rm eff}}\right)^2 \\ N_{\rm eff} &\equiv \int_0^{N_{\rm end}} {\rm d}N_e \left(\frac{r}{r_{\rm CMB}}\right)^{1/2} \end{aligned} \tag{2.110}$$

Note that this definition has number of e-folds N_e and $N_{\rm eff}$ increasing with time. From Eq.(2.45),

$$\frac{{\rm d}\ln r}{{\rm d}N_e} \approx \eta + s = -\left[(n_S - 1) + \frac{r}{8c_s}\right]\,. \tag{2.111}$$

This means that r decreases only when the scalar spectrum is blue to the sound speed is small, which is significantly constrained on observable scales. However, outside the observable window, c_s can decrease rapidly. Therefore, the intermediate regime has the best chance to predict large tensor mode.

In the most optimistic observable case and with $N_{\rm eff} \sim 1$, $r_{\rm CMB} \gtrsim 10^{-4}$ requires $N_A < 10^6$. One must then check whether the current bound on non-Gaussianity is violated. For our purpose, this constraint in the form of the bulk volume bound (2.108) turns out to be most useful. Note that this bound may be relaxed in some variations of the model that we discuss later.

We impose the first condition directly in the code, but implement the last as a consistency cut. Since other geometries (e.g., a squashed throat) or other choices for the

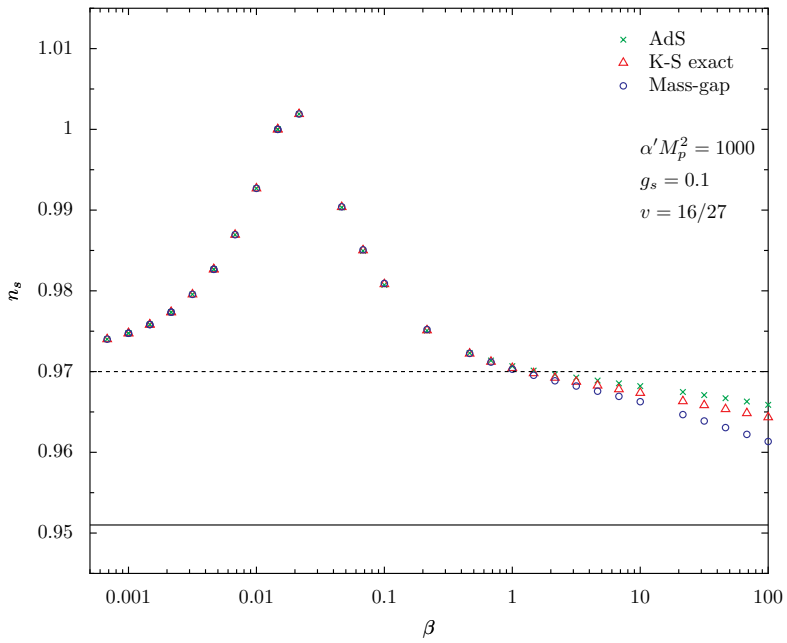

Figure 2.4: Comparison of n_S in different warped geometries.

inflaton may have a different dependence on N_A, it is interesting to examine the range of possible observables before and after imposing this constraint.

In Figure 2.4 we demonstrate the sensitivity of $n_S(k_{\text{pivot}})$ to different warped geometries, holding all parameters, except β, at typical values and varying β from slow-roll, $\beta \ll 1$, to ultra-relativistic, $\beta \gg 1$, regimes. We compare the AdS warp factor, the mass-gap warp factor and the exact Klebanov-Strassler warp factor. We see that in the slow-roll regime, since the warp factor does not come into play, different warped geometries give the same prediction on n_S. When $\beta > 1$ the model starts to deviate from slow-roll and the warp factor comes into play in the equation of motion, yielding different predictions on n_S. Typically, we find that the mass-gap geometry gives a more red-tilted spectrum than the AdS geometry and the exact K-S is in between the two.

In Figures 2.5 and 2.6 we demonstrate the wide variety of observational properties arising in DBI inflation. In addition to slow-roll behavior with red tilted, $n_S < 1$, and blue-tilted, $n_S > 1$, spectra, DBI inflation can also give rise to relativistic behavior

$\gamma > 1$, and intermediate models with large tensors, small running and a strong running-spectral tilt relation. The figures show key 2D parameter spaces for both observables and model parameters with Monte Carlo generated models which are consistent with the WMAP+SDSS+SN1a normalization $A_s = 2.3^{+1.5}_{-1.4} \times 10^{-9}$ at the 95% confidence level (C.L.). The red squares are within 1σ in the upper-left $r - n_S$ panel, the orange-yellow triangles are within 2σ, while the black crosses are outside 2σ. The nine panels from bottom left are:

1. $\log_{10} m^2 - \log_{10} v$ panel. Low masses, $m^2 \lesssim 10^{-12} M_{\rm Pl}^2$, produce slow-roll behavior $\gamma \sim 1$ with small tensors, $r < 0.05$, and obeying the usual consistency relation $r = -8 n_T$. Imposing a flat prior on $\log_{10} m^2$ and $\log_{10} v$, the majority of slow-roll models have a red-tilted spectrum. The normalization and e-folding constraints allow the orbifolding parameter, v, to extend over a large range of values, $\sim 10^{25}$ orders of magnitude. The intermediate and relativistic regimes are constrained in a small section of this space with very small orbifold factors $v \lesssim 10^{-17}$. As such, only the slow-roll regime is consistent with the Klebanov-Strassler Throat for which $v = 16/27$.

2. $\log_{10} m^2 - \log_{10} h_A$ panel. Two distinct regions, the slow-roll regime for $m^2 \lesssim 10^{-12} M_{\rm Pl}^2$ and a relativistic region with $m^2 \gtrsim 10^{-11} M_{\rm Pl}^2$ are carved out. The spread of h_A at small m^2 indicates the insensitivity of data to the warp factor of the throat. The requirement that there are sufficient e-foldings to include the physical scale $k_{\rm pivot}$ gives the lower bound on h_A for a given mass in the slow roll region, with the blue tilted slow-roll models lying close to this boundary. In the intermediate and relativistic regimes the normalization constraint translates into a thin region of allowed models. The relativistic models require a small warp factor at the bottom of the throat, $h_A \sim 10^{-1.5}$.

3. $\log_{10}(\phi_{\rm pivot} - \phi_A) - \log_{10} N_A$ panel. Conveniently demonstrates the bulk volume

bound (2.108). The relativistic models all have $(\phi_{\rm pivot} - \phi_A)/M_{\rm Pl} > \sqrt{4/N_A}$, as such, imposing the bound rules out all but the slow-roll regime.

4. $\mathrm{d}n_S/\mathrm{d}\ln k - n_S$ panel. For both the AdS and mass-gap geometries the bulk of the models satisfying the e-fold and normalization bounds have a very small negative or near zero running in the spectral tilt, $-0.001 < \mathrm{d}n_S/\mathrm{d}\ln k(k_{\rm pivot}) < 0$. The relativistic models, in particular, have extremely small running and $n_S \approx 1$ as discussed in regards to (2.33).

5. $\log_{10} m^2 - n_S$ panel. For $g_s = 0.1$ and $\alpha' M_{\rm Pl}^2 = 1000$ the slow-roll regime tends towards a common spectral tilt $n_S \approx 0.972$ as $m^2 \to 0$, which reproduces the spectral index in the slow-roll scenario [12].

6. $\log_{10} m^2 - r$ panel. Models with significant tensor contributions with $r > 0.05$ are purely generated in the intermediate regime with $m^2 \sim 10^{-11} M_{\rm Pl}^2$.

7. $n_S - r$ panel. Models with a noticeable deviation from the Harrison-Zeldovich spectrum ($n_S = 1$ and $r = 0$) are possible with $0.96 \lesssim n_S \lesssim 1.05$, including models with significant tensor contributions $0 < r \lesssim 0.15$. (2.33) and (2.45) lead to the relation $4(1 - n_S)/\gamma \sim r$. The AdS Monte Carlo models are able to have slightly higher tensors than the mass-gap geometry. The mass-gap, however, allows an interesting branch of models in the intermediate regime with large tensors and distinct n_S vs. r relation.

8. $n_T - r$ panel. Slow-roll and many intermediate tensor mode models are in good agreement with the $r = -8 n_T$ consistency relation. Significant deviations from this relation are seen in the relativistic models where the models have a significant tensor spectral tilt, but comparatively much smaller tensor amplitude given by $r \sim n_T/8\gamma$ in (2.48).

9. $\gamma - r$ panel. There is a the clear division of behavior between the large mass models, with intermediate models possessing large tensor modes but a comparatively

slowly rolling inflaton $\gamma \sim 1$, and relativistic scenarios with $\gamma > 1$ but vanishing tensor contributions in the limit $\gamma \gg 1$. For large γ, the Monte Carlo models are subject to additional constraints from CMB non-Gaussianity measurements, $\gamma < 31$.

In Figures 2.7 and 2.8 we compare the observational constraints from 3-year WMAP CMB + SDSS +HST GOODs data with the Monte Carlo results for DBI inflation for the AdS and mass-gap warp factor respectively without imposing a constraint on $\phi_{\rm pivot}$. The panels show the regions within 1σ (dark blue) and 2σ (pale blue) allowed by the data. The DBI models are marked red (yellow/orange) if they lie within 1σ (2σ) of the data in the key $n_S - r$ space. Black points are outside the 2σ region. It is clear that the data is constraining the parameter space of the model in a meaningful way.

One can see that in both cases the inflationary parameter space $\{N_A,\ v,\ h_A,\ m^2\}$ yields models wholly consistent with observations. For $g_s = 0.1$ and $\alpha' M_{\rm Pl}^2 = 1000$, the slow-roll, low mass, regime tends towards a common spectral index $n_S(k_{\rm pivot}) \approx 0.972$, consistent with observations at the 1σ level. An intermediate regime, for masses $m^2 \sim 10^{-11} M_{\rm Pl}^2$ and $N_A \sim 1$, with a significant tensor contribution, is also consistent at 1σ level. The relativistic ($\gamma \gg 1$) regime is consistent with data at the 95% C.L. For the AdS warp factor a handfull of Monte Carlo models, in agreement with the CMB and galaxy spectra at the 95% level, exceed the non-Gaussianity constraint from WMAP CMB on relativistic models, $\gamma < 31$.

In Figures 2.9 and 2.10 we show the allowed Monte Carlo models after additionally requiring that they also satisfy the bulk volume bound (2.108). This bound effectively constrains the tensor to scalar ratio, $r(k_{\rm pivot}) < 4 \times 10^{-3}$. In this case the slow-roll regime is allowed but the intermediate and relativistic regime do not satisfy the cut. In Figures 2.11 - 2.13 we investigate the intermediate regime more fully, for a variety of specific parameter values, and find that the bulk volume constraint disallows any of the

observationally consistent models to survive.

For the intermediate region, it is worth noting that the initial ϕ takes a rather large value. In this case, we expect that the truncation, keeping only the $m^2\phi^2$ term in the inflaton potential, may not be a good approximation. Let us, therefore, consider the impact of introducing a ϕ^4 term to the inflaton potential (1.8) :

$$V(\phi) \rightarrow V(\phi) + \mu V_0 \left(\frac{\phi}{M_{\rm Pl}}\right)^4 \tag{2.112}$$

We see in Figure 2.14 that turning on a ϕ^4 term tends to blue (red) tilt the power spectrum for small (intermediate) values of m^2.

In Figure 2.15, we show how the parameters and observables change with different values of μ. We find that as μ increases, h_A has to decrease in order to fit COBE normalization, meanwhile, n_S is driven to the red end and r increases. We also show in the figure that including the ϕ^4 term does not help to reduce the value of $\phi_{\rm pivot}$ but makes it even larger, consistent with the bound (2.109) as r increases with larger μ.

2.3.5 Summary of Results

We have discussed the cosmological predictions for DBI inflation, including the dependence of observed initial power spectra observables on the brane evolution and throat geometry. Three inflationary regimes are of interest, namely the slow-roll, intermediate relativistic and ultra-relativistic regimes, with rich properties including large tensor modes and non-Gaussianity.

After numerically integrating the background and perturbation equations we compare the predicted power spectrum properties to current cosmological CMB, galaxy and supernovae data. We find that the three regimes can fit the data well although the power spectrum normalization and e-fold constraints severely cut into the full multi-dimensional parameter space.

The small m^2 parameter region, which corresponds to a specific model within the usual slow-roll scenario, satisfies the cosmological data quite well predicting a spectral tilt around $n_s(k_{pivot}) \simeq 0.972$. Its predictions are in line with a typical inflationary scenario.

Before imposing the bulk volume bound (2.108), we find that the (relatively) large m^2 region, which corresponds to the DBI ultra-relativistic scenario, is compatible with the present data, in agreement with previous analyses. The potential of having a large non-Gaussianity [26, 35] with distinctive bi-spectrum [22] and trispectrum [46] is very encouraging to testing this very stringy scenario. However, imposing the bulk volume bound rules out most if not all of the large γ region. That the cosmological data strongly restricts the allowed parameter space and brane inflationary scenarios means that the scenario can be tested; this is very encouraging.

Interestingly, we find that the intermediate m^2 region, for which a numerical analysis is required, where the tensor mode can be large [25] and the $n_t - r$ relation deviates from the usual consistency relation, is also consistent with the data, when one neglects the bulk volume condition (2.108). When this condition is imposed, however, the region is ruled out in the simple scenario. There are a number of ways to vary the model to relax this bound or the constraint coming from this bound; however, in spite of this, we do not expect the ratio r to be much bigger than a few percent. Two possibilities discussed here are the multi-brane multi-throat scenario and the wrapped $D5$-brane scenario. If r is large enough to be measured, the deviation from the $r - n_t$ relation in the slow-roll case will be a fine signature for stringy physics.

The goal here is not only to find a stringy inflationary scenario that fits the data, but that such a scenario will also predict distinctive stringy signatures that may be detected and measured. Besides cosmic strings, searches for distinct string theory signatures in the slow-roll scenario continues. Recently, the proposal that the Seiberg duality cascade

in the KS throat may lead to observable signatures in the CMB power spectrum [47] is encouraging. Features in the warp factor or effects due to the fact that the inflaton is really a six-component field may source non-Gaussianity and slightly alter predictions for the power spectrum [48, 49].

Although the predicted tensor contribution of a few percent is beyond the capabilities of the WMAP satellite, this could well be in the detectable realm for the next generation of CMB instruments focusing on precision measurements of CMB BB polarization modes. Examples are, amongst others, the PLANCK, Clover, Spider, and BICEP projects, which hope to get $\Delta r \sim 0.01 - 0.05$. As such, the near future holds exciting prospects for better testing the rich properties of brane inflation.

Finally, it is worth mentioning that cosmic strings are generically produced toward the end of brane inflation. We find that the cosmic string tension μ roughly satisfies $10^{-14} < G\mu < 10^{-6}$; its particular value depends on the choice of m and λ. Roughly speaking, small allowed values of $G\mu$, $10^{-14} \lesssim G\mu \lesssim 10^{-10}$ are accompanied by a red tilt in the power spectrum, and in some cases by large non-Gaussianity.

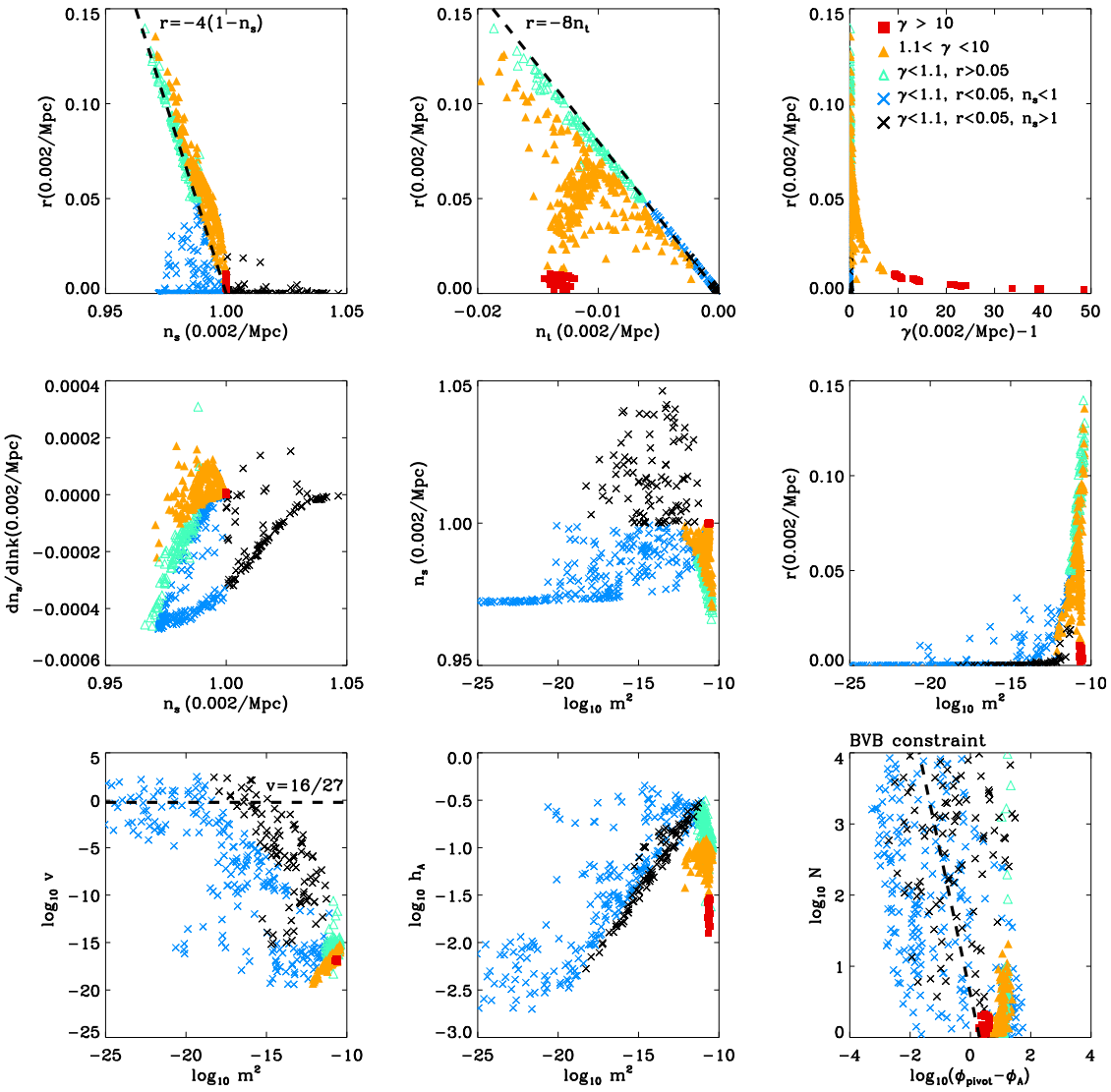

Figure 2.5: Taxonomy of the inflationary parameter space for the AdS warp geometry showing DBI inflationary models from a Monte Carlo simulation which satisfy the WMAP+SDSS+SN1a normalization constraint $A_s = 2.3^{+1.5}_{-1.4} \times 10^{-9}$ at 95% C.L.. The figure shows the wide variety of inflationary behavior arising from DBI inflation, including relativistic models ($1.1 < \gamma < 10$, filled yellow triangles and $\gamma > 10$ full red squares), large tensor modes (open green triangles), and blue and red-tilted slow-roll spectra (black and blue crosses, respectively). The taxonomy is presented in terms of relationships between the predicted spectrum observables (n_S, r, $\mathrm{d}n_S/\mathrm{d}\ln k$) and key model parameters (m^2, h_A, N_A, γ and $\phi_{\rm pivot}$). Note that the bottom right figure shows models in comparison to the bulk volume bound imposed by [27]. If the bound is imposed only slow-roll (low tensor, small running, non-relativistic models) with $\phi_{\rm pivot} - \phi_A < \sqrt{4/N_A}$ are allowed. See the main text for further discussion.

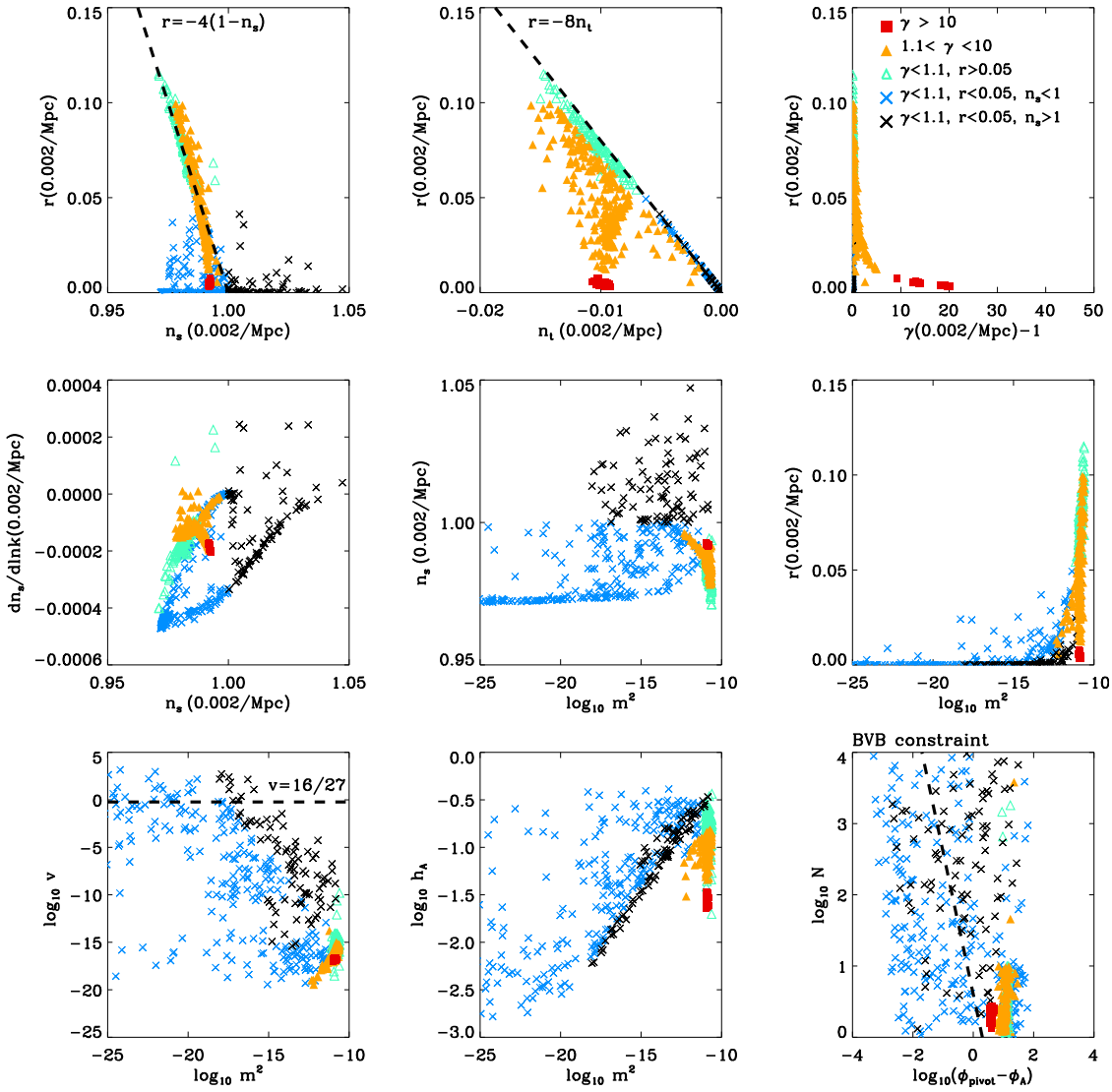

Figure 2.6: As in Figure 2.5 but for the mass-gap warp geometry.

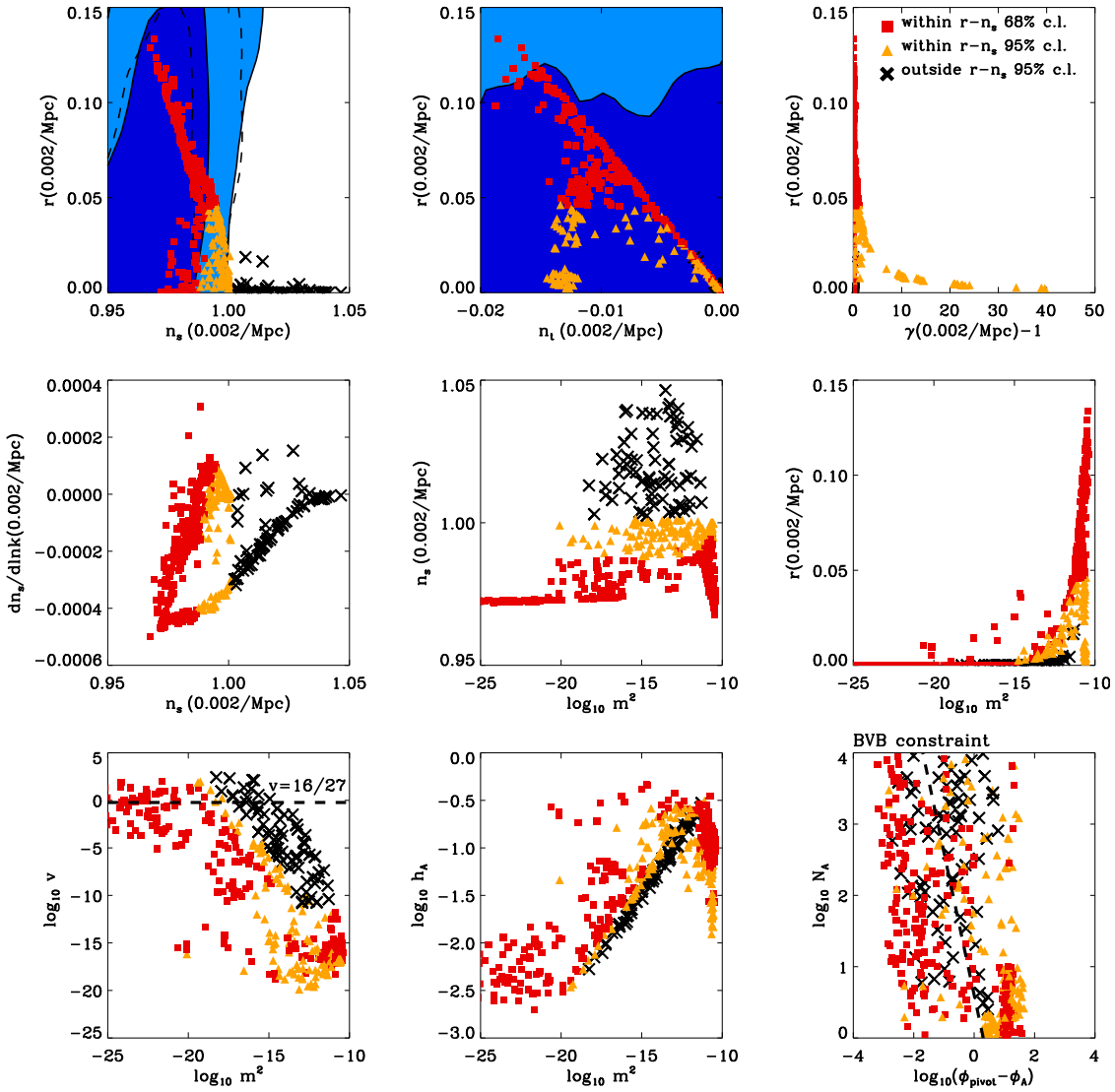

Figure 2.7: Inflation parameter space for the AdS geometry in comparison to cosmological observational constraints from 3-year WMAP data in combination with SDSS LRG power spectrum data and SNLS SN1a data. The top left figure (n_S vs r constraints) and top center figure (n_T vs r constraints) of each set show the observational constraints without imposing the $n_T = -r/8$ consistency relation, allowing $-0.02 < n_T < 0$, at the 68% (dark blue) and 95% (light blue) confidence level. Overlaid are DBI inflationary models from a Monte Carlo simulation which satisfy the WMAP normalization constraint $A_s = 2.3^{+1.5}_{-1.4} \times 10^{-9}$ at 95% C.L. and are in agreement with the $n_S - r$ WMAP+SDSS LRG+SN1a constraint within 68% (red square), 95% (yellow triangle) and outside 95% (black cross) confidence limits. The constraints with the consistency relation imposed (dashed contours in the top left plot) yield a very similar splitting of the DBI models by confidence level.

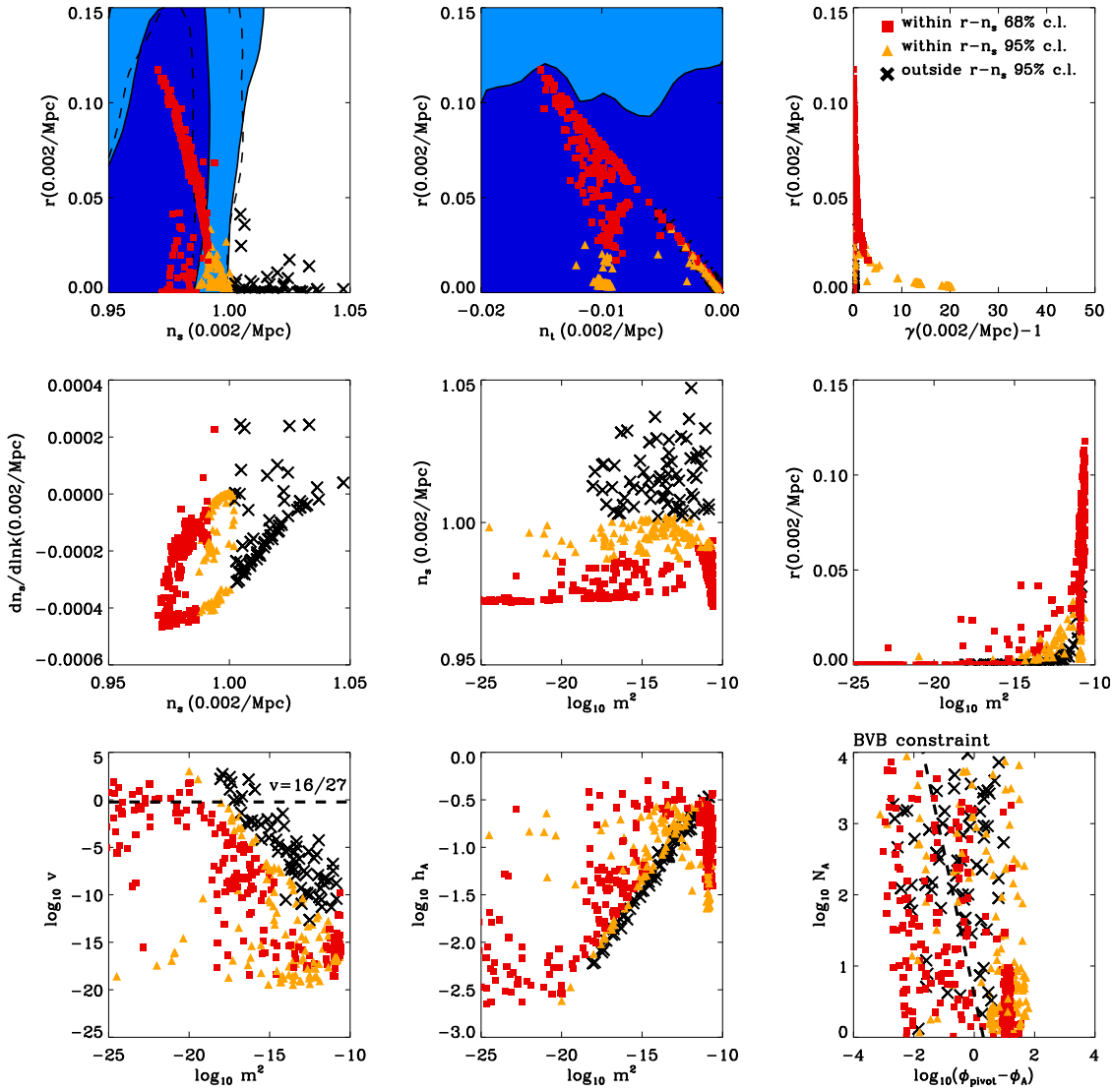

Figure 2.8: As in Figure 2.7 but for the mass-gap warp geometry.

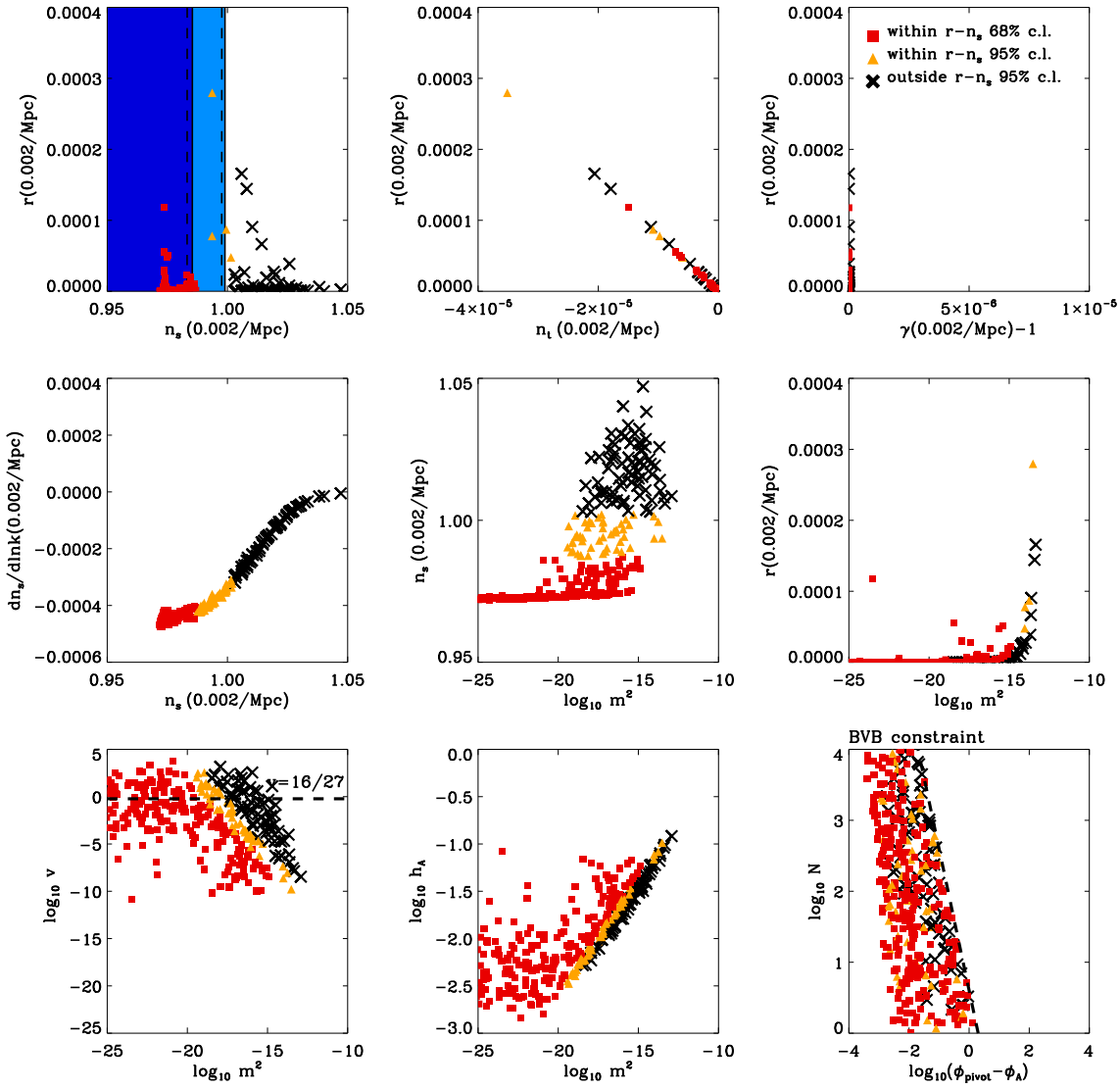

Figure 2.9: As in Figure 2.7 but imposing the bulk volume bound [27] of $\phi_{\text{pivot}} - \phi_A < \sqrt{4/N_A}$ for the AdS warp factor. Note that the tensor ratio and tensor tilt scales are reduced in comparison to Figure 2.7. The rescaled plots show that the, much more restricted, set of models are all in the slow-roll regime with $r < 0.003$ and $\gamma - 1 < 10^{-7}$ and satisfy the $n_T = -r/8$ consistency relation. The intermediate regime, while in strong agreement with observations, is incompatible with the bound.

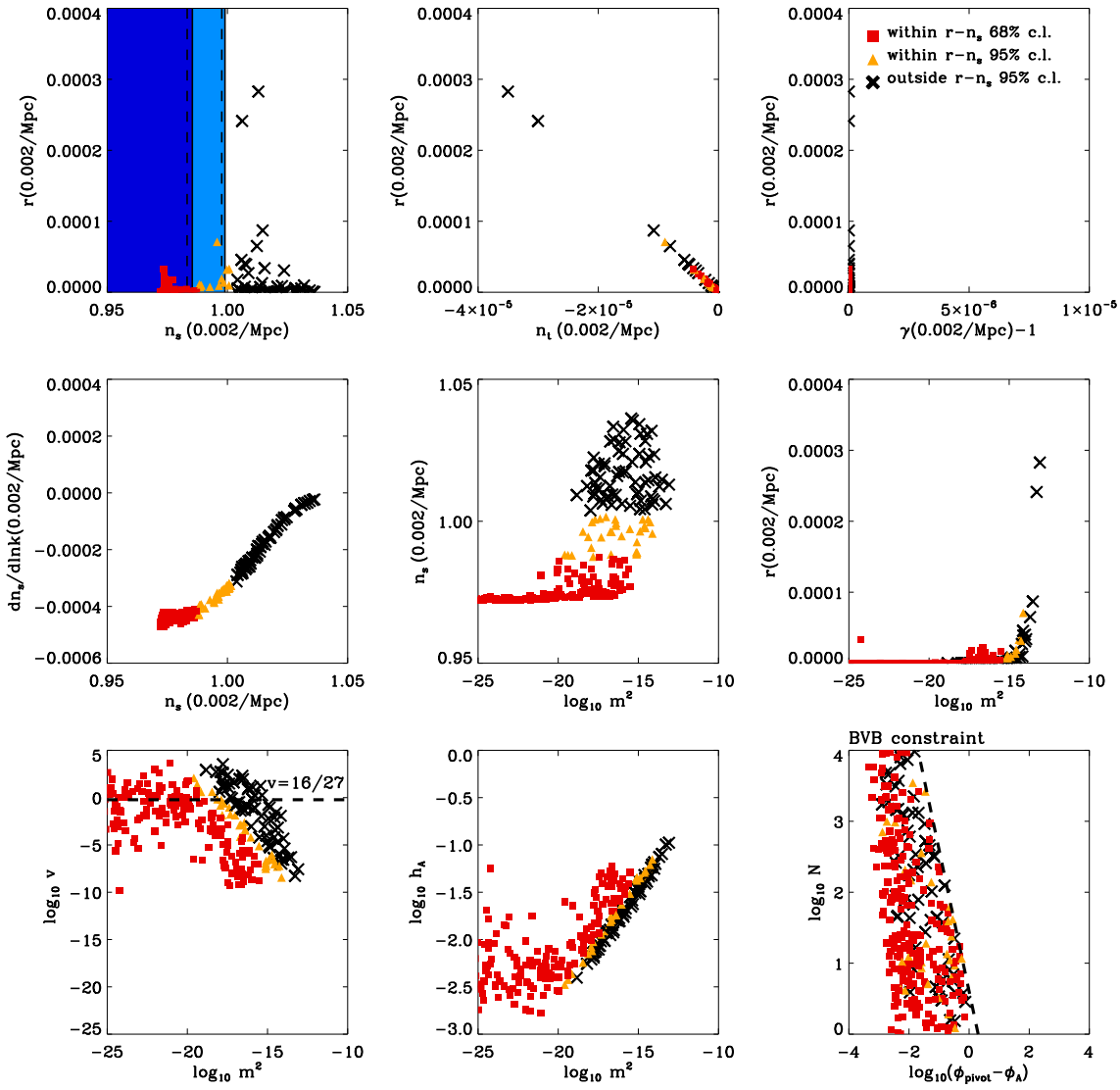

Figure 2.10: As in Figure 2.9 but imposing the bulk volume bound for the mass-gap geometry. Only slow-roll models remain consistent with the data at the 95% confidence level with $r < 0.001$ and $\gamma - 1 < 10^{-7}$ and satisfy the $n_T = -r/8$ consistency relation.

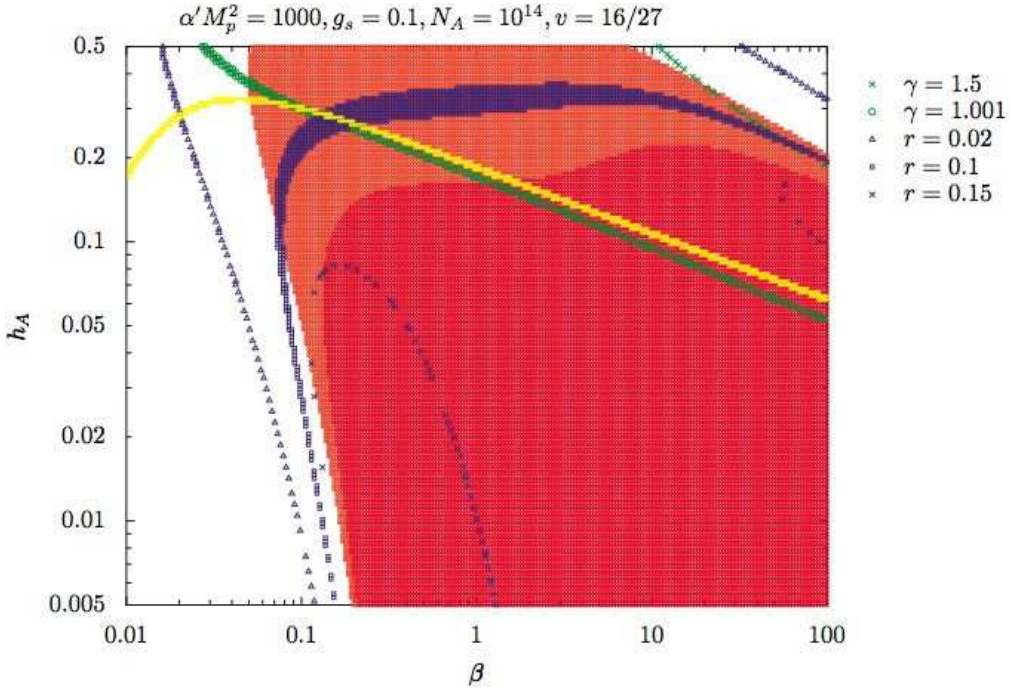

Figure 2.11: With $N_A = 10^{14}$, the figure shows the $\beta - h_A$ plane of parameter space for the AdS warp factor without orbifolding. The red region fits n_S within 2σ, and the yellow band is the constraint from COBE normalization. We find that we need N_A roughly 10^{14} to fit the WMAP data. The blue lines are contours of $r = 0.01, 0.1, 0.15$. The model yields significantly large tensor to scalar ratio. The green lines are contours of $\gamma = 1.001, 1.5$. All the models within the red region deviate from the slow-roll scenario, but γ at the pivot scale is not large enough to be in the ultra-relativistic regime. They all belong to the intermediate region. The tightest constraint here is actually the bulk volume bound (2.108), with $N_A \sim 10^{14}$: no points on this figure survive the bound.

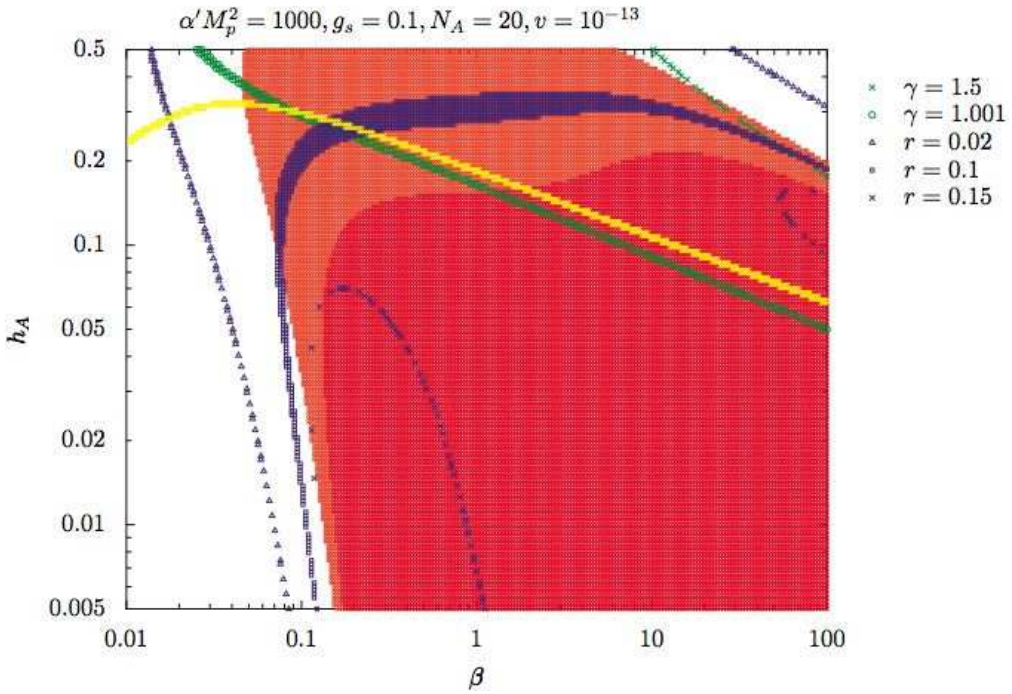

Figure 2.12: A similar graph as Figure 2.11 except that the volume of X_5 is decreased to $v = 10^{-13}$. We find models that fit WMAP data, and they come with much smaller N_A values than the case with $v \sim 1$. The graph shows a plane with $N_A = 20$. This figure is still in the intermediate region. However, even if N_A is decreased significantly, no model survives the bulk volume bound (2.108).

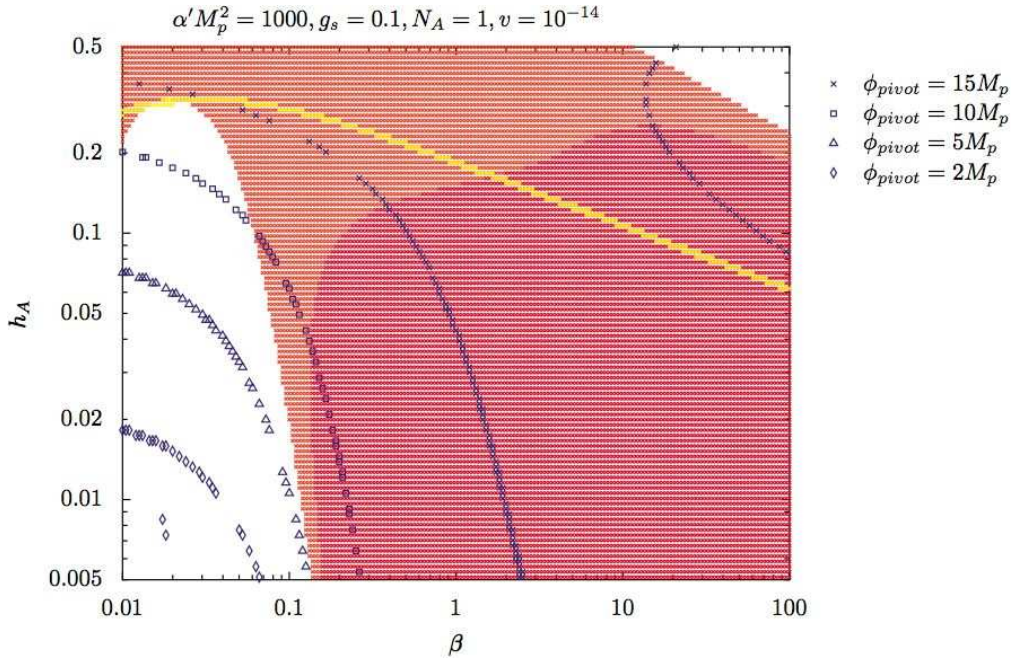

Figure 2.13: We now take the limit $N_A = 1$ and see if there are any models that fit the data and survive the bulk volume bound (2.108) at the same time. The blue lines are contours for different ϕ_{pivot} values. (Blue-tilt at small ϕ_{pivot}.) In the 2σ region of the n_S constraint, i.e. the red region, we see that $\phi_{\text{pivot}} > 10$, badly violating the bound on field range. The diamond points do show some points that survive the bound but they do not fit n_S well. The figure shows that the value of ϕ_{pivot} decreases in the upper-right and lower-left corner, so for $\beta > 10^2$ and $\beta < 10^{-2}$, the chance to get small ϕ_{pivot} is much larger, and these two regions are the slow-roll region and the DBI region.

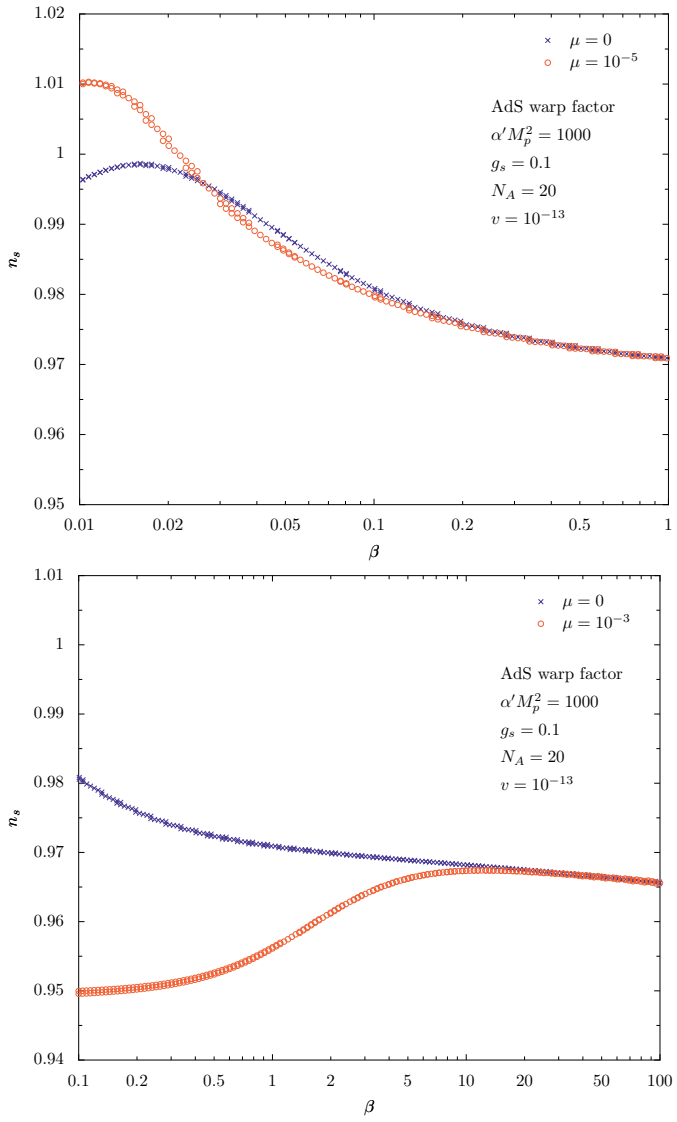

Figure 2.14: These two figures show the prediction of n_S if the inflaton potential is perturbed by a $\mu\phi^4$ term. In the slow-roll regime ($\beta < 0.1$), a $\mu\phi^4$ term will drive the n_S to the blue end and is not favored by data. But in the intermediate regime ($\beta > 0.1$), adding a $\mu\phi^4$ term in the potential drives n_S to the red end and improves the model's agreement with data.

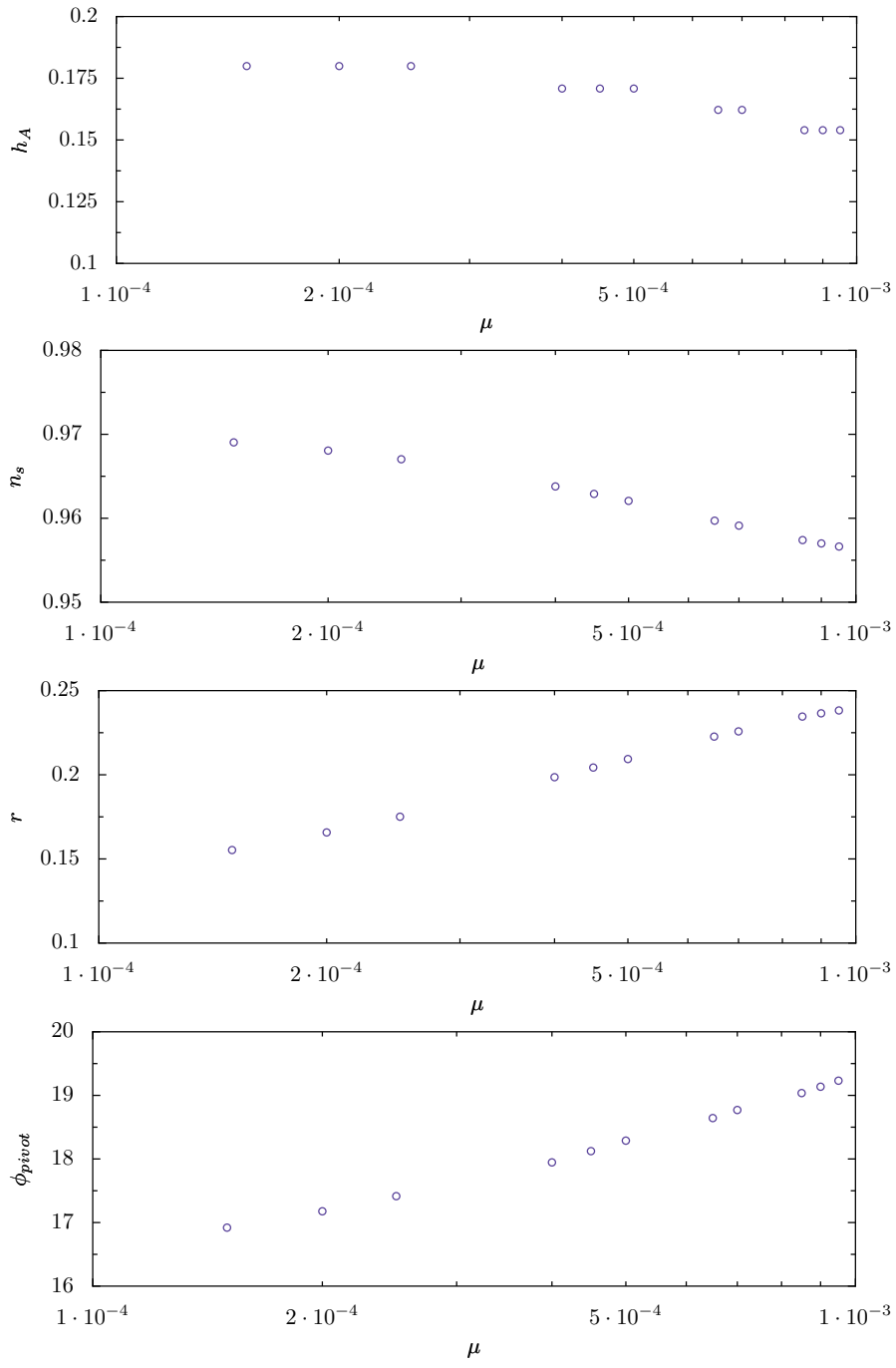

Figure 2.15: For $\beta = 1$, these figures show the dependence of $\{h_A, n_S, r, \phi_{\text{pivot}}\}$ on the $\mu\phi^4$ term. The other parameters are fixed to be $N_A = 20$, $v = 10^{-13}$, $g_s = 0.1$, $\alpha' M_{\text{Pl}}^2 = 1000$.

2.4 The Infrared Dirac-Born-Infeld Scenario

2.4.1 A Multi-throat Scenario

In the IR models, branes are started from the IR side of a throat (denoted as the B-throat) and roll toward the UV side under the moduli potential

$$V(\phi) = V_0 - \frac{1}{2}m^2\phi^2 \ . \tag{2.113}$$

The origin of ϕ is at the tip of the throat, which can be realized for example if the tip of the throat is an orbifold fixed point. The Coulomb attraction from antibranes in other throats is neglected here unless m^2/H^2 is very small.

The IR model can arise in the following scenario [14] (illustrated in Fig. 2.16): At the beginning, anti-branes are naturally attracted to and settle down at the end of various throats induced by fluxes. However they are semi-stable at most, and will eventually annihilate against some fluxes [50]. The end products are n_B $D3$-branes. As mentioned, unlike antibranes, branes experience no potential if the extra dimensions are not compactly stabilized. But for realistic inflation models in string compactification, their moduli space is lifted. If the mass term is tachyonic as in (2.113) for a B-throat, these liberated branes will roll out. The inflationary energy V_0 is provided by longer-living antibranes in other throats (denoted as the A-throats) or in the bulk. Shorter A-throats give more dominant contributions to V_0. These antibranes eventually get annihilated by some of the inflaton branes. The annihilation products will naturally heat low mass-scale sectors in case of tunnelling reheating [51], such as branes residing in very long throats or in a large bulk.

We now study the phase diagram for IR-DBI inflation. In the absence of the warped space, the $|\eta_{\rm SR}| = 1$ line is

$$\phi^2 = -2M_{\rm Pl}^2 + \frac{2V_0}{m^2} \ , \tag{2.114}$$

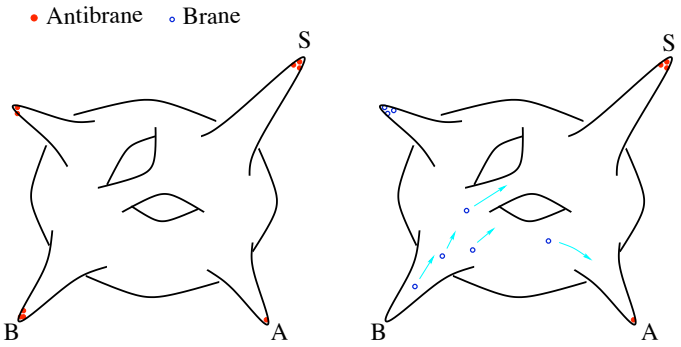

Figure 2.16: Multi-throat brane inflation scenario. In the left figure, antibranes are settled down in throats. In the right figure, in some throats antibranes annihilate fluxes and generate branes. For a throat with tachyonic brane moduli, branes fall out and settle down somewhere else, triggering either IR or UV models of brane inflation.

which corresponds to the vertical line (at $m = \sqrt{V_0}/M_{\rm Pl}$) in Fig. 2.17. Slow-roll inflation occurs when $|\eta_{\rm SR}| < 1$ which is the region to the left of this line.

In the presence of the warped space, DBI inflation can be triggered even if the slow-roll condition is not satisfied. Ref. [14, 28] show that, for $\beta \equiv m^2/H^2 \sim |\eta_{\rm SR}| \gtrsim 1$, DBI inflation happens if

$$\phi < HR_B^2\sqrt{n_B T_3}\ . \tag{2.115}$$

Here, an important difference from the UV model condition (2.104) is that, because the inflationary energy V_0 is provided by antibranes in other throats instead of the moduli potential itself, the shape of the potential that can achieve inflation becomes rather flexible. Of the special interest is the generic case $m^2 \sim H^2$. Even for $\beta < 1$ when slow-roll inflation is possible, the speed-limit provided by the warped space cannot be neglected if the inflatons are started from the region [28]

$$\phi < \beta HR_B^2\sqrt{n_B T_3}\ . \tag{2.116}$$

This implies that the DBI and slow-roll phases can be smoothly connected by an intermediate region in this corner of the parameter space. Overall, the DBI inflation

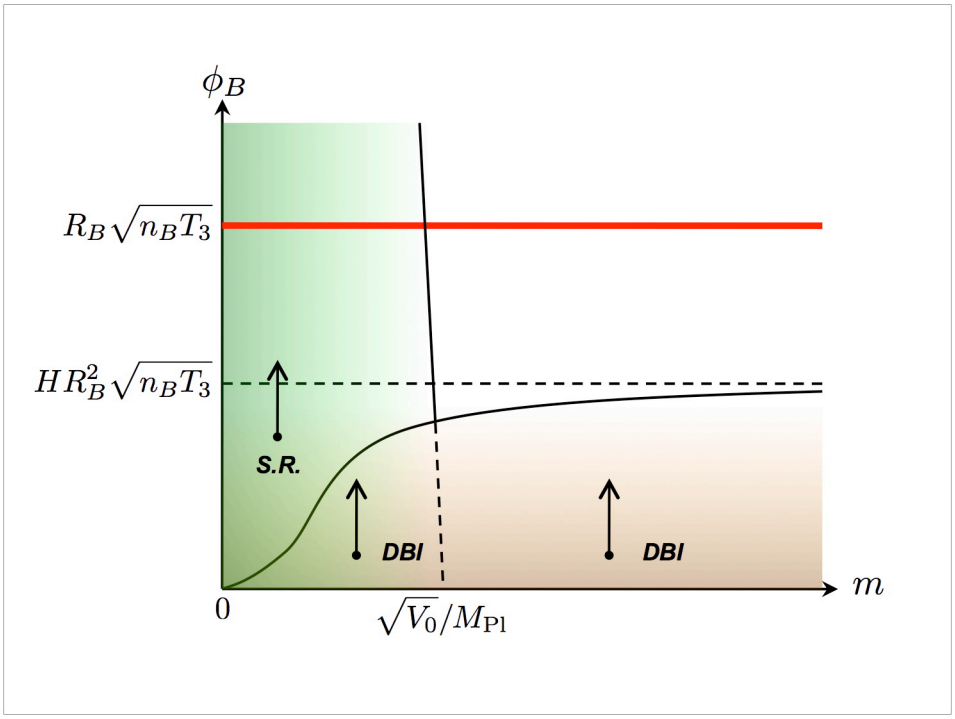

Figure 2.17: The inflation phase diagram for IR models. The notation used here is the same as in Fig. 2.3. The vertical line at $m = \sqrt{V_0}/M_{\rm Pl}$ corresponds to $|\eta_{\rm SR}| = \beta/3 = 1$. The unshaded region may support a certain amount of non-relativistic fast-roll inflation.

phase stays below the horizontal curve stretching from the origin to $\phi = HR_B^2\sqrt{n_B T_3}$ in Fig. 2.17. The DBI region always stays well below the maximum inflaton extension (the horizontal solid line at $\phi = R_B\sqrt{n_B T_3}$), since

$$\frac{HR_B^2\sqrt{n_B T_3}}{R_B\sqrt{n_B T_3}} = HR_B \lesssim \frac{\sqrt{n_A}h_A^2}{\sqrt{N_B}} \ll 1 \ , \tag{2.117}$$

where $V_0 = 2n_A h_A^4 T_3$ and (2.82) (2.83) are used, n_A being the number of antibranes that get annihilated. We see that IR DBI inflation is completed in a very small region at the tip of the B-throat. Unlike the UV DBI phase, the condition (2.105) is automatically satisfied. This also justifies the small field expansion in (2.113).

We have treated the Hubble parameter H as a constant. This can be verified using the

geometric constraints (2.82) and (2.83), because in the IR model the potential drop ΔV during inflation, estimated very conservatively, satisfies

$$\frac{\Delta V}{V_0} \lesssim \frac{m^2 R_B^2 n_B T_3}{2V_0} \sim \frac{\beta n_B}{N_B} \ . \tag{2.118}$$

As long as

$$\beta \ll N_B/n_B \ , \tag{2.119}$$

the inflationary energy is approximately a constant.

Therefore we see that in the IR models, inflation can occur for a large range of the mass parameter,

$$0 < m^2/H^2 \ll N_B \ , \tag{2.120}$$

around the generically expected magnitude $m \sim H$. The requirement is to start the inflatons from a small enough ϕ_B. In terms of the flux compactification this is easy to achieve, because the minimum warp factor is given by the flux numbers M and K in an exponential form [10]

$$h_{\rm min} \sim \exp(-2\pi K/3Mg_s) \ . \tag{2.121}$$

We emphasize that non-trivial constraints come from various back-reactions that cut off the IR regions of a throat. These include the back-reaction from the 4-d inflationary background [28, 51] and the back-reaction from the relativistic inflaton branes [13, 52]. The former is generally (for $\beta \sim 1$) more important than or comparable to the latter depending on the number of inflaton branes. It is estimated [28, 51] to cut off the throat at $\phi \sim HR_B^2\sqrt{n_B T_3}/\sqrt{N_B}$. This determines the maximum number of e-folds achievable by the DBI inflationary phase,[1] $N_{\rm tot}^{\rm DBI} \sim \sqrt{N_B}$. A more detailed understanding of this backreaction is important.

[1] This constraint is equally important for UV DBI models.

It is worth pointing out that, in terms of model building, the most important difference between the IR and UV DBI models is not whether branes are started from the IR or UV side of a warped space. It is the independence between the inflaton speed-limit and the inflationary energy, which allows a flexible shape of potential. We have seen that this naturally happens when branes are moving out of a throat, with inflationary energy provided by antibranes in other throats. Just in terms of field theory, even in the UV models, such an independence can be achieved by demanding the constant term V_0 in the potential (2.102) to be independent of the A-throat warp factor, for example by a hybrid of a different field around $\phi = 0$ to suddenly end inflation. The question is then how to realize it naturally in string models.

Having considered the phase diagram, we would like to first restrict the parameter space by comparing the predictions of the model with observational data, and then make predictions for future observations. This will be the main focus for the rest of the paper. We close this subsection with a few comments on the setup of the model.

First, as we demonstrated in Fig. 2.3, for UV models there is no inflation around $\eta_{\rm SR} \sim 1$ and a large parameter space beyond that. So for IR models, it is reasonable to consider the simplest case where, after branes come out of the B-throat, there is no significant amount of additional inflationary e-folds if they roll through the bulk or enter another A-throat to annihilate antibranes there. This simplest possibility represents a fairly generic class of models.

Second, more realistic throats such as the Klebanov-Strassler throat [15] have a scale-dependent charge. The characteristic scale R decreases slowly towards the tip of the throat. Especially the geometry around the tip region will be significantly different from the simple AdS form (2.61). For UV models such modifications can be important because the tip of the throat is the region around which the last 60 e-folds of inflation happens [36, 35]. For IR models, the situation is opposite. The last 60 e-folds of inflation

happens away from the bottom of a throat because generally the total e-folds is more than 60. Furthermore the relevant field range is very small. Therefore, under these conditions (which will be made more precise in Sec. 2.4.2), we can ignore both the deformation of the throat geometry and the running of the throat charge, and approximate the metric as (2.61) with the constant λ (or R) being the effective value at the relevant ϕ (or r).

Third, as we have mentioned, the realistic IR case almost always involves multiple inflaton branes. It is interesting to see whether the non-Abelian action plays an important role [53]. In our scenario, after the mobile branes are created in the IR end of the throat, they all have approximately the same radial coordinates and roll in the radial direction. In the angular directions, we either imagine that they are randomly distributed, in which case their average separation is $h_B R_B / n_B^{1/5}$ (the power of $1/5$ is due to the five-sphere) which is much larger than the local red-shifted string length along the extra dimensions, $h_B m_s^{-1}$; or we imagine that they stick together and roll with a fixed angular coordinate, which is different from them forming a higher dimensional brane and expanding around the center. In both cases, we expect the leading effects of a large number of branes on density perturbations to be well represented by the Abelian action. As in Ref. [28, 29], we will use this approximation in this paper.

Lastly, there is a trivial slow-roll region in IR models if we tune β to be near $\mathcal{O}(0.01)$. We skip this parameter space in this paper and start from $\beta \gtrsim \mathcal{O}(0.1)$.

2.4.2 Background Attractor Solutions

In regions where various back-reactions to the warped background are negligible and the Hubble energy stays below the red-shifted string scale, the low-energy dynamics of the inflaton branes is described by the DBI-CS action (1.5),

$$S = -\int d^4x\sqrt{-g}\left(\frac{\phi^4}{\lambda_B}\sqrt{1+\frac{\lambda_B}{\phi^4}g^{\mu\nu}\partial_\mu\phi\,\partial_\nu\phi}-\frac{\phi^4}{\lambda_B}+V(\phi)\right)\,, \tag{2.122}$$

where $V(\phi)$ is given by Eq.(2.113) . Subscripts A and B are used to denote quantities for the A and B throats.

The branes start from the tip of the throat and exit at the UV end of the throat, after which some of them quickly find antibranes and annihilate, diminishing the cosmological constant V_0. Among all the branes rolling out from the B-throat, only those which annihilate antibranes have significant contributions to the density perturbations. We will denote this number as n_B. The normalized inflaton field is

$$\phi = \sqrt{n_B T_3}\, r \ , \quad \lambda_B = n_B T_3 R_B^4 = \frac{n_B N_B}{2\pi^2 v_B} \ , \tag{2.123}$$

with N_B the background charge of the B throat, and v_B the B throat base volume / $\mathrm{Vol}(S^5)$. The UV end of the throat corresponds to $\phi_{\rm end} = R_B\sqrt{n_B T_3} = \sqrt{\lambda_B}/R_B$.

More generally, antibranes with number n_A that get annihilated can reside in different A-throats. Due to different warp factors, each annihilated brane pairs can have different contributions to reheating energy. These subtleties will only affect the microscopic interpretation of the parameters, such as $n_A h_A^4$. For our purpose, we define

$$V_0 \equiv 2 n_A h_A^4 T_3 \ , \tag{2.124}$$

The dynamics of the inflaton can be approximately described by two attractor solutions. The first is that of the IR DBI inflation. This is the phase where the effect of the speed-limit is important. The inflaton is traveling near the warped speed of light, and the attractor solution is

$$\phi = -\frac{\sqrt{\lambda_B}}{t} + \frac{9\sqrt{\lambda_B}}{2\beta^2 H^2 t^3} + \cdots \ , \tag{2.125}$$

where t is chosen to run from $-\infty$ for convenience. Recall that for $0 < \beta \ll N_B/(n_B)$, H is approximately a constant. This phase ends around $\phi \sim H\sqrt{\lambda_B}$ ($t \sim -H^{-1}$) for $\beta \gtrsim 1$ and $\phi \sim \beta H\sqrt{\lambda_B}$ ($t \sim -\beta^{-1}H^{-1}$) for $\beta < 1$. The inflationary e-folds as the function of ϕ can be estimated as

$$N_e^{\rm DBI} \approx \frac{H\sqrt{\lambda_B}}{\phi} - \beta^{-1} \ . \tag{2.126}$$

Here we have incorporated both the case $\beta < 1$ and $\beta \gtrsim 1$ by adding the term β^{-1}; this correction is negligible for $\beta \gtrsim 1$, and the validity of (2.125) requires $N_e^{\rm DBI} \gg \beta^{-1}$.

The second attractor solution describes the nonrelativistic rolling where the inflaton velocity stays far below the speed-limit. In this limit the equation of motion

$$\ddot{\phi} + 3H\dot{\phi} + \partial_\phi V(\phi) = 0 \tag{2.127}$$

has the following attractor solution

$$\phi = \phi_0 e^{\alpha\beta H(t-t_0)/3} , \quad \alpha = \frac{-9+\sqrt{81+36\beta}}{2\beta} . \tag{2.128}$$

The consistency condition that the inflaton velocity is non-relativistic $\dot{\phi} \ll \phi^2/\sqrt{\lambda_B}$ requires that $\phi \gg \alpha\beta H\sqrt{\lambda_B}/3$. This phase is smoothly connected to the previous DBI phase. The total number of inflationary e-folds provided by this period is given by

$$N_{\rm tot}^{\rm NR} \approx \frac{3}{\alpha\beta} \ln\phi \Big|_{\alpha\beta H\sqrt{\lambda_B}/3}^{\sqrt{\lambda_B}/R_B} \approx \frac{3}{\alpha\beta} |\ln HR_B| . \tag{2.129}$$

We emphasize that this nonrelativistic rolling region is slow-roll only if $\beta \ll 1$, while the above formulae are valid even if this condition is not satisfied. For example in Fig. 2.17 at around $\beta \sim 1$ ($m \sim \sqrt{V_0}/M_{\rm Pl}$), after the DBI phase it takes time for branes to go through the lightly-shaded region till it reaches the end of the throat. This is because the branes are originally very close to the top of the potential. It provides a certain amount of e-folds typically not corresponding to the scale of the CMB. These additional non-relativistic non-slow-roll inflationary e-folds is also interesting to us, because it affects the relevant e-folds in the DBI phase,

$$N_e = N_e^{\rm DBI} + N_{\rm tot}^{\rm NR} , \tag{2.130}$$

and hence predictions for observations.

In Fig. 2.18 we demonstrate numerical results and show that the two attractor solutions (2.125) and (2.128) give good analytical approximations for the inflaton dynamics. Any

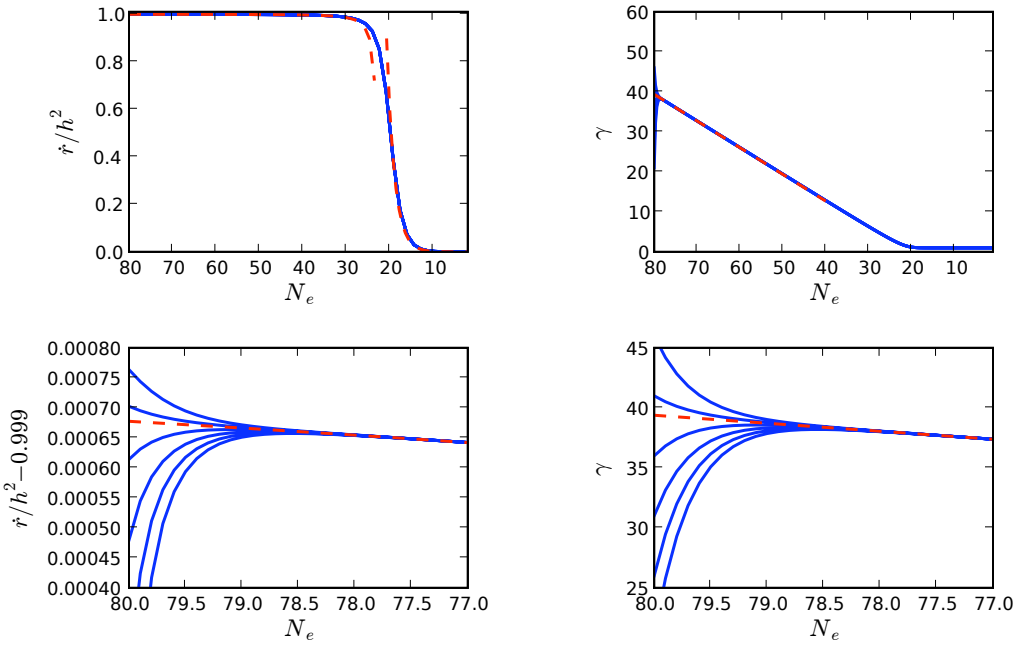

Figure 2.18: Attractor behavior of the background solution for IR-DBI model. The dashed lines are the analytical attractor solutions. The solid lines are numerical solutions with different initial velocities. The upper-left panel shows the evolution of the ratio of the inflaton-velocity $\dot{r}$ to the warped-speed-of-light h^2. The two dashed lines are DBI and non-relativistic rolling, respectively. The upper-right panel shows the evolution of the Lorentz factor γ. The lower panels are the blow-ups of the upper panels. The parameters are $\beta = 2$, $N_B = 10^9$, $n_B = 10^5$, $m_s g_s^{-1/4} = 10^{-6} M_{\rm Pl}$, $n_A h_A^4 = 1$. In the simulation, branes are started at $h_B = 2.9 \times 10^{-7}$.

initial angular motions will also be damped out due to the Hubble friction, because the inflaton potential considered here has only radial dependence.

In this chapter, we use the AdS_5 geometry with a length scale R to represent the warped space. The details of the geometry can be different for more realistic cases. We expect our example to capture the main properties of the model, and to be a good approximation for a certain generic parameter space. Let us consider, for example, the K-S throat,

$$h^{-4}(r) = \frac{27\pi g_s \alpha'^2}{4r^4}\left[N_{\rm tot} + \frac{3g_s M^2}{2\pi}\left(\ln\frac{r}{r_{max}} + \frac{1}{4}\right)\right] \equiv \frac{R_l^4}{r^4}\ , \qquad (2.131)$$

where we have defined a running R_l,

$$R_l^4 = \frac{27\pi}{4} g_s \alpha'^2 N_{\rm eff} \ , \tag{2.132}$$

with $N_{\rm eff} \equiv M K_{\rm eff} = M(K_{\rm tot} - l)$ for

$$r = r_{max} \exp(-2l\pi/3g_s M) \ . \tag{2.133}$$

So instead of the parameter N_B, here we have the parameter M. The effective $N_{\rm eff}$ and $K_{\rm eff}$ are now functions of r or l. From (2.133) we can estimate that, during IR DBI inflation, $\Delta l \approx g_s M$. Therefore as long as

$$K_{\rm eff} \gg g_s M \ , \tag{2.134}$$

we can neglect the running of $N_{\rm eff}$. The N_B in our analyses thus represents the $N_{\rm eff}$ in a small region of r relevant for IR DBI inflation. The condition (2.134) is most easily satisfied by having a small g_s. In addition, since the WMAP window is only a few e-folds, which corresponds to $\Delta l \approx 3 g_s M / N_e^{\rm DBI}$, we only need $K_{\rm eff} > g_s M$ to approximate $N_{\rm eff}$ as a constant in this window. In this case, the running of $N_{\rm eff}$ only slightly affects the total DBI e-folds, and hence the relation in (2.130). Another difference between the K-S throat and the geometry we use is that, in the latter, the UV edge of the warped space is cut off and glued to the bulk at R, while in the former it is given by an independent parameter r_{max}. This does not cause too much difference in the analyses, since the non-relativistic fast-roll inflation mostly happens near the top of the potential; hence $N_{\rm tot}^{\rm NR}$ is insensitive to the cutoff in generic cases.

2.4.3 The Power Spectrum and a Running Spectral Index

We first look at the density perturbations in the DBI phase. Its amplitude is given by the usual formula

$$P_\zeta = H^2 \delta t^2 \ , \tag{2.135}$$

where δt is the position-dependent time delay caused by the frozen quantum fluctuations of the inflaton, $\delta\phi = H/2\pi$. In this phase we approximate the inflaton zero-mode velocity as the speed of light, $\dot{\phi} = \phi^2/\sqrt{\lambda_B}$. So we have

$$P_\zeta = \frac{H^4}{4\pi^2\dot{\phi}^2} \approx \frac{(N_e^{\rm DBI})^4}{4\pi^2\lambda_B} \ . \tag{2.136}$$

If this is responsible for $P_\zeta \approx 23\times 10^{-10}$, we need $\lambda_B \sim 10^{13}$. Since the number of branes created after the flux-antibrane annihilation can be as large as $\mathcal{O}(\sqrt{N_B})$, this requires $N_B \gtrsim 10^9$. The formula (2.136) can be derived rigorously using the formalism of Garriga and Mukhanov [21] summarised in Chapter 2.2.1, where we can see that the main difference from the slow-roll case is the development of the sound speed c_s on the world-volume of the inflaton branes. This shrinks the Hubble horizon by a factor of c_s. The underlying physics can be most easily understood in the view of an instantaneous co-moving observer with the brane [14, 28]. For this observer the Hubble expansion rate is increased by the Lorentz factor

$$\gamma = 1/c_s = 1/\sqrt{1-\lambda_B\dot{\phi}^2/\phi^4} \approx \beta N_e^{\rm DBI}/3 \tag{2.137}$$

due to the relativistic time dilation. In the last step of (2.137), we have used the IR model solution (2.125) and (2.126). This Hubble parameter leads to a horizon of size c_sH^{-1}, which lies orthogonal to the brane velocity and hence appears the same to the lab observer (i.e. the observer that does not move with the branes).

In this model it is very important to realize the validity condition for the field theory analyses of density perturbations, and make estimates for the density perturbations when the field theory analyses break down [14, 28, 29]. There are the following several interesting regions as we extend the inflaton *back in time* towards the IR side of the warped space.

Firstly, open strings on the inflaton brane will be created when the Hubble energy density γ^4H^4 for the moving observer becomes larger than the red-shifted brane tension[2]

[2]If we replace the brane tension with the string scale m_s^4, we have an extra factor of $g_s^{1/8}$ in (2.138).

$h_B^4 T_3 = \phi^4/n_B\lambda_B$. Using (2.126) and (2.137), this happens at the critical e-fold

$$N_c \sim \frac{\lambda_B^{1/8}}{\beta^{1/2} n_B^{1/8}} \sim \frac{N_B^{1/8}}{\beta^{1/2}} \,. \tag{2.138}$$

Another observation that also indicates that we cannot naively extend the field-theoretic results too far down the IR side of the throat, is to look at the region $N_e > N_c$, where the brane fluctuations in the transverse directions become superluminal. This is impossible. The reason that such a superluminal speed even occurs under the DBI action can be understood as follows. When we calculate the primordial fluctuations, in the first step, the source of such fluctuations is the uncertainty principle, which *a priori* does not necessarily respect the speed-limit if we only consider the scalar field. In the next step, the later evolution of such fluctuations is governed by the DBI action and always follows the causality constraint. The superluminal fluctuation speeds to which we just referred come from the first step, if we naively extend the field theoretic calculation to the regions beyond (2.138).

Secondly, closed strings will be created when the Hubble energy H^4 for the lab observer becomes larger than the red-shifted brane tension. This happens at

$$N_e \sim \lambda_B^{1/4}/n_B^{1/4} \,. \tag{2.139}$$

Finally, when the closed string density created by the Hubble expansion overwhelms the source (fluxes or branes) for the warped geometry, the warped space gets cut off. As mentioned, this back-reaction determines the maximum number of inflationary e-folds in the DBI phase,

$$N_{\rm tot}^{\rm DBI} \sim \lambda_B^{1/2}/n_B^{1/2} \,. \tag{2.140}$$

It is important to note that the zero-mode dynamics of the inflaton are still valid as long as $N_e < N_{\rm tot}^{\rm DBI}$, since it only relies on the existence of the speed-limit and therefore on the condition (2.140) at which the warped space gets cut off.[3] In addition, the strings

[3] It will be interesting to understand better how branes move through a gas of strings and graviton KK modes, whose effects are ignored here.

and graviton KK-modes are only created in the tip of the throat and have energy density $\mathcal{O}(H^4)$. It does not backreact significantly on the Hubble expansion. However, the field-theoretic calculation of the density perturbation is no longer valid if $N_e \gtrsim N_c$, since not only scalar fields but also open strings will be created.

Estimate the Effect of Phase Transition on Spectral Index

While a rigorous treatment is currently unavailable, there are a couple of ways to estimate the density perturbations in this situation [28, 29].

We can estimate the part of energy that goes into scalar fluctuations to be saturated when the Hubble temperature reaches the brane tension $\phi^4/n_B\lambda_B$ at (2.138). Further relative increase of the Hubble energy excites strings and branes. The stringy excitations will be diluted by the exponential spatial expansion after the Hubble energy drops below the brane tension as branes move to the UV side, in the same way that the inflation dilutes relic densities. Only the scalar fluctuations are frozen and later translated into the position-dependent time-delay for the reheating. For the moving observer, the scalar field energy density is $(\delta\phi)^2_{\rm mov}\gamma^2H^2 \sim \phi^4/n_B\lambda_B$ and for the lab observer $\delta\phi = \delta\phi_{\rm mov}/\gamma$. This estimate leads to $\delta\phi = \sqrt{\lambda_B}H/\sqrt{n_B}(N_e^{\rm DBI})^2\gamma^2$. So for $N_e > N_c$, we estimate

$$P_\zeta = H^2\frac{\delta\phi^2}{\dot\phi^2} \sim \frac{324\pi^2}{n_B\beta^4(N_e^{\rm DBI})^4}\ . \tag{2.141}$$

This is also the result that we will get by looking at the transverse fluctuation speed of each brane. The field-theoretic analyses lead to the fluctuation speed (for the moving observer), $\dot r_{\rm mov} = \delta r/\delta t \approx \gamma H T_3^{-1/2}/(\gamma H)^{-1}$, which is the fluctuation amplitude divided by a Hubble time. This velocity reaches the warped speed of light precisely around (2.138). Above the phase transition, we assume the fluctuation speed saturates the warped speed of light h^2, so $\delta r_{\rm mov} \approx h^2(\gamma H)^{-1}$. The position-dependent time-delay is then

$$\delta t_{\rm lab} \approx \frac{\delta r_{\rm mov}/\dot r_0}{\gamma\sqrt{n_B}} \approx \gamma^{-2}H^{-1}/\sqrt{n_B}\ , \tag{2.142}$$

where $\dot{r}_0 = h_B^2$ is the zero-mode brane speed, and the factor $1/\sqrt{n_B}$ is due to the reduction of the root-mean-square of the fluctuations by the superposition of n_B independent branes. Eq. (2.142) reproduces (2.141).

To make the estimation more quantitative, consider a simple model where the density perturbations are caused by the scalar field fluctuations, which are the super-horizon ripples on branes in transverse directions. These ripples are generated during a Hubble time while they are still sub-horizon and then frozen. The amplitude of the ripples are given by the fluctuation speed of a Hubble-sized patch on the brane. This speed is determined by the energy pumped into the branes by the Hubble expansion. This model simplifies the underlying physics by focusing on only the overall fluctuation speed of a Hubble-sized patch while ignoring the detailed world-volume theory such as effects from specific stringy excitations.

According to the special relativity, an object with rest mass m_0 and energy $E = m_0 + \Delta E$ has velocity

$$v = c\sqrt{1 - \frac{m_0^2}{(m_0 + \Delta E)^2}} \ . \tag{2.143}$$

For the on-brane observer, a Hubble-sized patch has rest mass

$$m_0 = h_B^4 T_3 \Delta V = h_B^4 T_3 \left(\frac{\gamma H}{2\pi}\right)^{-3} \ , \tag{2.144}$$

where $h_B^4 T_3$ is the red-shifted brane tension. The Hubble energy is $\gamma H/2\pi$, half of which goes to the kinetic energy of the transverse oscillation of the brane $\Delta E = \gamma H/4\pi$, while the other half goes to the tension of oscillations in terms of spatial derivatives. We have restored the factor of 2π in the Hubble length and energy in order to quantitatively match the known results in the low energy limit. The local speed of light is $c = h_B^2$. The position-dependent time delay is

$$\delta t = \frac{v(\gamma H/2\pi)^{-1}/\gamma}{\dot{r}\sqrt{n_B}} \ , \tag{2.145}$$

where the numerator is the fluctuation amplitude within a Hubble time viewed from the lab observer (hence an extra factor of $1/\gamma$ due to Lorentz contraction), and the denominator is the overall brane velocity which is approximately the local speed of light $\dot{r} \approx c$. Here we also consider the case of n_B multiple branes where the superposition of independent fluctuations reduces the time-delay by a factor of $1/\sqrt{n_B}$. Using these estimates we obtain the power spectrum

$$P_\zeta = \frac{4\pi^2 v^2 T_3}{\gamma^4 \dot{\phi}^2} \ , \tag{2.146}$$

where

$$v^2 T_3 = h_B^4 T_3 \left[1 - \left(1 + \frac{\gamma^4 H^4}{32\pi^4 h_B^4 T_3} \right)^{-2} \right] \ . \tag{2.147}$$

This formula recovers the usual field theory result in the limit of non-relativistic fluctuation speed. This includes non-relativistic-(slow or fast)-roll inflation, and DBI inflation below the phase transition. This formula also gives an estimate on the effect of the Hubble-expansion induced stringy phase transition. The estimate is expected to provide the envelope behavior beyond the transition since it ignores detailed features such as specific resonant production of various stringy states.

It will be useful to extract the DBI inflation region in (2.146) and (2.147), and parametrize it in the following way,[4]

$$P_\zeta = H^2 \delta t^2 = \frac{324\pi^2}{n_B \beta^4 N_e^{\mathrm{DBI}\,4}} \left(1 - \frac{N_c^{16}}{(N_c^8 + N_e^{\mathrm{DBI}\,8})^2} \right) \ . \tag{2.148}$$

N_c is defined as

$$N_c \equiv 2^{5/8} \sqrt{3\pi} \frac{\lambda_B^{1/8}}{n_B^{1/8} \beta^{1/2}} = \sqrt{6} \pi^{1/4} \frac{N_B^{1/8}}{\beta^{1/2}} \ , \tag{2.149}$$

[4]More precisely, because of the sound horizon is time-dependent, we should replace N_e^{DBI} in (2.148) with $N_e^{\mathrm{DBI}} - \ln(c_s(k)H(k)^{-1})/(\hat{c}_s \hat{H}^{-1})$, where the variables with a hat are evaluated when the reference mode $\hat{k}$ (e.g. $\hat{k} = 0.002\,\mathrm{Mpc}^{-1}$ as in (2.163)) crosses the sound horizon. Because the relevant scales for (2.148) span only a few e-folds, the change of the sound horizon $c_s H^{-1}$ is very small and we neglect such corrections.

Taking the limits $N_e \ll N_c$ and $N_e \gg N_c$, we recover (2.136) and (2.141) respectively. The spectral index is

$$n_s - 1 = \frac{4}{N_e^{\rm DBI}} \frac{x^2+3x-2}{(x+1)(x+2)} , \quad x \equiv \left(\frac{N_e^{\rm DBI}}{N_c} \right)^8 . \tag{2.150}$$

This formula interpolates between two asymptotic values $4/N_e$ and $-4/N_e$. If we define the width of the transition region as the e-fold difference ΔN_e between $n_s - 1 = 2/N_e^{\rm DBI}$ and $-2/N_e^{\rm DBI}$, then we have

$$\Delta N_e \approx 0.2 N_c , \tag{2.151}$$

which can be quite large (for example, six if $N_c = 30$). But the running of n_s is still observably large in the transition region (for example, $\mathrm{d}n_s/\mathrm{d}\ln k \approx -0.02$ in the range of (2.151) for $N_c = 30$).

Regional Large Running of Spectral Index

From the last subsection, the spectral index is

$$n_s - 1 \approx -\frac{4}{N_e^{\rm DBI}} \qquad N_e^{\rm DBI} < N_c , \tag{2.152}$$

$$n_s - 1 \sim \frac{4}{N_e^{\rm DBI}} \qquad N_e^{\rm DBI} > N_c . \tag{2.153}$$

The most interesting information from (2.138) is its smallness due to the power $1/8$. For $\lambda_B \sim 10^{13}$, $\lambda_B^{1/8} \sim \mathscr{O}(100)$, which already makes N_c interestingly small. Considering the more realistic multi-brane case $n_B \lesssim \sqrt{N_B}$ leads to even smaller N_c of order $\mathscr{O}(10)$. So such an interesting phase transition may well have occurred within our CMB scale. Another interesting property is the fact that Eq. (2.138) is independent of the inflationary energy scale and the local warp factor of the inflaton branes, so it will be a rather generic prediction of the IR DBI models.

It is very important how sharp this transition is in terms of e-folds. In section 2.4.3, we give an estimate of the transition width based on the following approach. For the familiar case of field-theoretic density perturbations, the super-horizon perturbations can

be understood as being generated by the random walk of the transverse brane fluctuations within a Hubble time before the modes exit the horizon. Such a random walk velocity is given by the Hubble energy, and is non-relativistic. As we have discussed, during or above the stringy phase transition, the main difference is that the Hubble energy is comparable to or exceeds the rest mass of the brane in a Hubble-size patch. As a consequence the brane fluctuation speed becomes relativistic. We therefore use the same physical picture underlying the familiar theory, but generalize it relativistically to estimate the behavior of the density perturbations across the phase transition. The result is given in (2.146).

It is worth noting that this scenario has marked differences to several other cases commonly discussed in the literature. Firstly, this model has a scale-varying running of n_s, in contrast to the commonly investigated empirical ansatz, where the running of n_s is assumed to be constant. Here the large running of n_s is only regional, principally when $N_e^{\rm DBI} \lesssim N_c$. Secondly, this scenario can generate large running, in contrast to most slow-roll scenarios. A standard slow-roll potential predicts very small running of n_s. A transient, large $\mathrm{d}n_s/\mathrm{d}\ln k$ can be caused by some "mild features" in the potential. For example, for small field slow-roll inflation, to generate a large transition for n_s from blue to red, the mild feature should be a potential shape changing from concave to convex. Since the spectral index is still close to one, the slow-roll parameters for this case should still be at least of order 0.1. So such a case predicts unobservable non-Gaussianities. Lastly, non-standard choice of vacua may also cause observable running of spectral index. Such a running will be oscillatory in the WMAP window and phenomenologically distinguishable from the phase transition in IR DBI inflation. Interested reader are referred to the appendix of Ref.[54] for detailed discussions.

2.4.4 Large non-Gaussianity and Small Tensor Mode

The three-point function of the scalar perturbation is reviewed in Chapter 2.2.3. For DBI inflation, the result becomes

$$f_{\rm NL}^{\rm equil} \approx -0.32\, c_s^{-2} \ . \tag{2.154}$$

For IR DBI inflation, using the relation (2.137), we have [29]

$$f_{\rm NL}^{\rm equil} \approx -0.036\, \beta^2 (N_e^{\rm DBI})^2 \ . \tag{2.155}$$

The observational bound is $-256 < f_{\rm NL}^{\rm equil} < 332$ [55]. Comparing UV and IR DBI scenario, we see that the running of non-Gaussianities for these two cases are opposite, as dictated by the background geometry scanned through by the rolling inflatons.

However, we emphasize that the above results are derived in the regime where the primordial fluctuations are field-theoretic. Therefore the results can be different when the stringy phase transition happens. As we will see, data analysis suggests that the critical scale k_c for that transition lies somewhere near the largest scales. For those smaller scales, it seems reasonable to assume that the magnitude of Eq. (2.155) should be smoothly modified by the stringy corrections. So in this paper, we will use this field-theoretic approximation (2.155) and the bound $|f_{\rm NL}^{\rm equil}| < 256$.

For DBI inflation, the scalar and tensor perturbations can be written as follows,

$$P_\zeta = \frac{H^4}{4\pi^2 \dot\phi^2} = \frac{H^4}{4\pi^2 T(\phi)} \ , \tag{2.156}$$

$$P_h = \frac{2H^2}{\pi^2 M_{\rm Pl}^2} \ , \tag{2.157}$$

where $T(\phi) \approx \dot\phi^2$ is used since the brane if essentially moving at the speed limit. The tensor to scalar ratio is

$$r \equiv \frac{P_h}{P_\zeta} = \frac{24\phi^4}{\lambda_B V_0} \ . \tag{2.158}$$

Because $V_0 = 3H^2M_{\rm Pl}^2$ is almost a constant in this model, the fact that the scalar and tensor modes have different horizon sizes during inflation makes no difference to (2.158). From Section 2.4.2, we see that, at the scale of $N_e^{\rm DBI}$, $\phi \approx HR_B^2\sqrt{n_BT_3}/N_e^{\rm DBI}$. So we get

$$\begin{aligned} r &\approx \frac{8}{N_e^{\rm DBI}{}^4}(HR_B)^2\frac{n_BR_B^2T_3}{M_{\rm Pl}^2} \\ &\lesssim \frac{1}{N_e^{\rm DBI}{}^4}\frac{n_Ah_A^4}{N_B}\frac{n_B}{N_B}\ . \end{aligned} \tag{2.159}$$

This is of course consistent with the Lyth bound [45, 27, 56], since the r.h.s. of (2.159) is just the square of $\Delta\phi/\Delta N_e$ in Planck units divided by $(N_e^{\rm DBI})^2$, as we can see from (2.107), (2.117) and (2.126). To ignore the probe brane back-reactions we need $\gamma n_B \ll N_B$. So

$$r \ll \frac{1}{N_e^{\rm DBI}{}^4\gamma^2} < 10^{-6}\ , \tag{2.160}$$

which is unobservably small. Therefore in our data analyses, we always set $r = 0$.

2.4.5 Constraints on Microscopic Parameters

In this chapter we identify the set of microscopic parameters of the model, and list self-consistency constraints and the observables. As discussed in Chapter 2.4.3, we can estimate the power spectrum at all scales across the transition region by the following formula,

$$P_\zeta = \frac{4\pi^2v^2T_3}{\gamma^4\dot\phi^2}\ , \tag{2.161}$$

where

$$v^2T_3 = \frac{\phi^4}{n_B\lambda_B}\left[1-\left(1+\frac{n_B\lambda_B\gamma^4H^4}{32\pi^4\phi^4}\right)^{-2}\right]\ . \tag{2.162}$$

These equations relate the fundamental parameters to the observations. We will always choose initial position and velocity of branes so that all the observable scales are

within the attractor solution, namely the total e-folds is larger than the minimum requirement. So these initial conditions will not enter the observables. The parameters V_0 and β determine the scale and shape of the relevant part of the potential, λ_B/n_B characterizes the background geometry, and R_B tells us where to end the inflation (*i.e.* at $\phi_{\rm end} = \sqrt{32\pi^2/27}\sqrt{\lambda_B}/R_B$). So these four parameters determine the zero-mode evolution of the spacetime background and the inflaton dynamics in terms of the number of inflationary e-folds to the end of the inflation. In particular this determines the evolution of γ, $\phi/\sqrt{n_B}$ and H in (2.161) and (2.162). Note that we can write the factor $h_B^4 T_3$ in (2.162) in terms of $\phi/\sqrt{n_B}$ and $\lambda_B/n_B = 2\pi^2 N_B$, $h_B^4 T_3 = (\phi/\sqrt{n_B})^4/(\lambda_B/n_B)$, so this is also determined. Because the factor $\dot{\phi}^2$ appears in the denominator of (2.161), the parameter n_B affects the overall scale of P_ζ, but does not affect the spectral index once λ_B/n_B is fixed. In conclusion, we have five parameters $\{\lambda_B,\ n_B,\ R_B,\ V_0,\ \beta\}$. These parameters are equivalent to five even more fundamental microscopic parameters $\{N_B,\ n_B,\ m_s g_s^{-1/4},\ n_A h_A^4,\ \beta\}$.

We have the following observables:

1. The amplitude of the power spectrum $P_\zeta \approx 2.3 \times 10^{-9}$. Through (2.136) and (2.141) this roughly determines the order of magnitude of the parameters λ_B or $n_B\beta^4$ depending on whether the pivot point N_e is smaller or larger than N_c.

2. The scale-dependence of P_ζ. This determines the spectral index and its running. Since the spectral index of this model has a regional large running, the data will constrain at which scale (k_c) such a running happens and which DBI e-fold (N_c) it corresponds to. These are then transferred into some delicate relations with the microscopic parameters, e.g. (2.149) and (2.130).

3. Non-Gaussianity constraint $\gamma < 28$, will mainly constrain β (with some weak dependence on $N_e^{\rm DBI}$).

4. We have the following several consistency relations. First, a scale k is related to

the corresponding N_e by

$$N_e = 65 - \ln \frac{k}{0.002 \text{ Mpc}^{-1}} + \ln \frac{H/\hat{c}_s}{T_{\text{reheat}}} , \tag{2.163}$$

where the reheating is assumed to be efficient[5] so that $T_{\text{reheat}} = V_0^{1/4}$, and $\hat{c}_s$ is the sound speed when the mode $k = 0.002$ Mpc^{-1} crossed the sound horizon.

Second, according to the multi-throat brane inflationary scenario, the maximum number of the inflaton branes is bounded by the flux number M. Since $N_B = KM$ and we want to keep the minimum warp factor (2.121) small, we require

$$n_B \lesssim \sqrt{N_B/g_s} . \tag{2.164}$$

Third, the geometric constraints (2.82) and (2.83) give an upper bound on $m_s g_s^{-1/4}$,

$$\frac{m_s}{g_s^{1/4}} \lesssim 2^{3/2} \pi^{11/4} \frac{M_{\text{Pl}}}{N_B^{3/4}} , \tag{2.165}$$

where the approximate numerical factors come from the toroidal compactification, $M_{\text{Pl}}^2 = \frac{2}{(2\pi)^7} g_s^{-2} m_s^8 V_6$, which may change for more realistic setups.

Fourth, the warp factor $h_A \leq 1$ and $n_A = n_B$ [6], so

$$n_A h_A^4 \leq n_B . \tag{2.166}$$

Lastly, the inflationary scale and the string scale are both bounded below by TeV,

$$n_A h_A^4 T_3 \geq \text{TeV}^4 , \tag{2.167}$$

$$m_s g_s^{-1/4} \geq \text{TeV} . \tag{2.168}$$

[5] For single-throat reheating, the brane-antibrane pairs immediately (in terms of the Hubble time) annihilate and decay into relativistic particles and start the usual radiation-domination epoch. For tunneling reheating such as double-throat reheating, (2.163) may receive some small modifications due to a long intermediate matter-domination epoch [51].

[6] Among all the branes rolling out from the B-throat, only those which annihilate antibranes have significant contributions to the density perturbations. We will denote this number as n_B. More generally, antibranes that get annihilated can reside in different A-throats. Due to different warp factors, each annihilated brane pairs can have different contributions to reheating energy. These subtleties will only affect the microscopic interpretation of the parameters (such as $n_A h_A^4$).

(These two bounds turn out to be very weak. Much stronger ones will arise from the data analyses.)

We set $g_s = 0.1$ in our analysis. Reducing g_s may loosen some bounds and allow some microscopic parameters to take wider ranges. But this should not change the model predictions qualitatively.

2.4.6 Constraining IR-DBI Inflation Using CMB Data

First, as detailed in Chapter 2.4.3, we notice that the primordial power spectrum predicted by the IR DBI model can be approximated by the following analytical form:

$$P_\zeta = H^2 \delta t^2 = \frac{324\pi^2}{n_B \beta^4 {N_e^{\rm DBI}}^4} \left[1 - \frac{N_c^{16}}{(N_c^8 + {N_e^{\rm DBI}}^8)^2} \right] . \tag{2.169}$$

This is parameterized by three effective parameters: N_c, $\ln k_c$, and $n_B\beta^4$, where k_c is the critical scale near which the stringy phase transition happens,

$$N_e^{\rm DBI} = \ln(k_c/k) + N_c \ . \tag{2.170}$$

After verifying that these three parameters appear to have a simple likelihood surface in a trial MCMC analysis, we relate the five microscopic parameters to these three parameters through approximate analytical expressions.

The relation to N_c is simple and given by (2.149),

$$N_c = \sqrt{6}\pi^{1/4} \frac{N_B^{1/8}}{\beta^{1/2}} \ . \tag{2.171}$$

The k_c is defined as the value of k at $N_e^{\rm DBI} = N_c$. Using the relations (2.130) and (2.163), we get

$$N_c + N_{\rm tot}^{\rm NR} = 65 - \ln\left(\frac{k_c}{0.002\ {\rm Mpc}^{-1}} \right) + \ln\left(\frac{H}{\hat{c}_s T_{\rm reheat}} \right) \ . \tag{2.172}$$

Using the approximation (2.129), expressing H, R_B, V_0 in terms of N_B, $n_A h_A^4$ and g_s/m_s^4, we obtain

$$\begin{aligned}\ln\left(\frac{k_c}{0.002\ \mathrm{Mpc}^{-1}}\right) &\approx 65 - N_c + \ln\frac{1}{\sqrt{6}\pi^{3/4}\hat{c}_s} + \frac{3}{\alpha\beta}\ln\frac{1}{\sqrt{6}\pi^{5/4}} + \frac{3}{4\alpha\beta}\ln N_B \\ &+ \left(\frac{1}{4}+\frac{3}{2\alpha\beta}\right)\ln n_A h_A^4 - \left(\frac{1}{4}+\frac{3}{4\alpha\beta}\right)\ln\frac{g_s}{m_s^4}\ , \end{aligned} \tag{2.173}$$

where

$$\alpha\beta = (-9+\sqrt{81+36\beta})/2\ . \tag{2.174}$$

Here, $\hat{c}_s$ is the sound speed when the mode $k = 0.002\ \mathrm{Mpc}^{-1}$ crosses the sound horizon; we can also approximately express it in terms of the five microscopic parameters. But the detailed expression will complicate the relation. For our purpose, since $\hat{c}_s$ varies slowly from 0.01 to 0.1, treating it as a constant should not cause problems for the reparameterization.

These expressions suggest that the following set may prove to be a successful reparameterization of the microphysical parameters that can be effectively explored by MCMC:

$$\begin{aligned}\tilde{\alpha}_1 &= N_c = \sqrt{6}\pi^{1/4}\frac{N_B^{1/8}}{\beta^{1/2}}\ , \\ \tilde{\alpha}_2 &= \frac{3}{4\alpha\beta}\ln N_B\ , \\ \tilde{\alpha}_3 &= \left(\frac{1}{4}+\frac{3}{2\alpha\beta}\right)\ln n_A h_A^4\ , \\ \tilde{\alpha}_4 &= \left(\frac{1}{4}+\frac{3}{4\alpha\beta}\right)\ln\frac{g_s}{m_s^4} - \left(3\ln\frac{1}{\sqrt{6}\pi^{5/4}}\right)\frac{1}{\alpha\beta}\ , \\ \tilde{\alpha}_5 &= \ln n_B\beta^4\ . \end{aligned} \tag{2.175}$$

The relation between these new parameters, $\{\tilde{\alpha}\}$, and the effective parameters, $\{\theta\} = \{N_c, \ln k_c, n_B\beta^4\}$, is very clear. Two of them are identical, and the rest, $\tilde{\alpha}_2$, $\tilde{\alpha}_3$, and $\tilde{\alpha}_4$, all have approximately linear relationships to $\ln k_c$ through (2.173).

We adopt the reparametrized microscopic parameters $\{\tilde{\alpha}\}$ and the standard set of cosmological parameters $\{\omega_b \equiv \Omega_b h^2,\ \omega_m \equiv \Omega_m h^2,\ \theta_A, \tau\}$ as the model parameter set

sampled by the MCMC. Here, θ_A is the angular size of the acoustic horizon and functions as a proxy for the Hubble constant $H_0 \equiv 100h$ km/s/Mpc or Ω_m, and τ is the optical depth to reionization. The universe is assumed to be spatially flat. Constant priors are assumed over the previously specified parameter set $\{\tilde{\alpha}\}$, subject to the microphysical cuts described below.

For each set of $\{\tilde{\alpha}\}$ sampled by the MCMC, the relations (2.175) are numerically inverted to obtain the set of microscopic parameters $\{N_B,\ n_B,\ n_A h_A^4,\ g_s^{-1/4} m_s,\ \beta\}$. This inversion is bijective in the parameter ranges of interest. The microscopic parameters are then fed into a numerical code. After checking the input parameters for a set of conditions (2.164) (2.165) (2.166) (2.167) (2.168) which enforce model-building self-consistency, the code computes the primordial power spectrum of the curvature perturbation for the model specified by the input parameters. Input parameters which fail to satisfy the microphysical cuts are rejected through being assigned zero likelihood in the MCMC. The primordial power spectrum from this code is fed to the Boltzmann code CAMB [57], without significantly increasing the computational time, in order to calculate the cosmological observables.

We use a modified version of the CosmoMC code [44] to determine constraints placed on this parameter space by the WMAP three-year cosmic microwave background data [38, 41, 39, 40] and the SDSS Luminous Red Galaxy (LRG) galaxy power spectrum data [42]. We marginalize analytically over the linear bias factor b and the non-linearity parameter $Q_{\rm nl}$ of the SDSS LRG data as is done normally in the CosmoMC code. A properly derived and implemented MCMC draws from the joint posterior density once it has converged to the stationary distribution. We use eight Markov chains and a conservative Gelman-Rubin convergence criterion on the eigenvalues of the parameter covariance matrix to determine when the chains have converged to the stationary distribution. Then we re-weight the MCMC to switch to constant priors on the microscopic parame-

ters $\{\alpha\} = \{\log_{10} N_B,\ \log_{10} n_B,\ \beta,\ \log_{10} n_A h_A^4,\ \log_{10} m_s/g_s^{1/4}\}$.

Following this process, we would like to apply the observational non-Gaussianity bound $-256 < f_{\rm NL}^{\rm equil} < 332$ (95% C.L.) [55], as this should have a significant effect on restricting the allowed parameter range for β and other parameters which are correlated with it. This is because γ is roughly proportional to β, and $f_{\rm NL}^{\rm equil} = -0.32\gamma^2$. However, two approximations enter in applying this constraint. First, the observational constraint was obtained using an estimator that does not encode the specific scale-dependence of the IR DBI model, and it also does not restrict $f_{\rm NL}^{\rm equil} < 0$. Second, Ref. [55] only gives a 95% confidence level of the result, and hence a full Bayesian posterior is not available for this parameter. In order to make use of this constraint despite these limitations, firstly we assume that the constraint of Ref. [55] is the effective constraint at $k = 0.02$ Mpc^{-1}, which is approximately the best constrained scale with the current data compilation [58, 59]. Secondly, we choose a Gaussian prior on $f_{\rm NL}^{\rm eq}(0.02\ {\rm Mpc}^{-1})$ which has the 95% C.L. range found by Ref.[55], since the maximally uninformative prior in the case that only a single confidence range is available has a Gaussian form. We apply this prior to the chains, verifying that the convergence criteria still remain satisfied. Finally, we obtain parameter constraints on the microphysical parameters, cosmological parameters, cosmological observables, and derived model parameters, which we present in Tables 2.1–2.2 and Figs. 2.19–2.24.

2.4.7 Summaries and Discussions

We conclude this chapter by highlighting the main results and discussing their physical implications. The quoted ranges are at the 95% confidence level, and we have combined constraints from both the power spectrum and non-Gaussianity. The detailed 68% and 95% C.L. marginalized constraints and the maximum likelihood values are listed in Table 2.2.

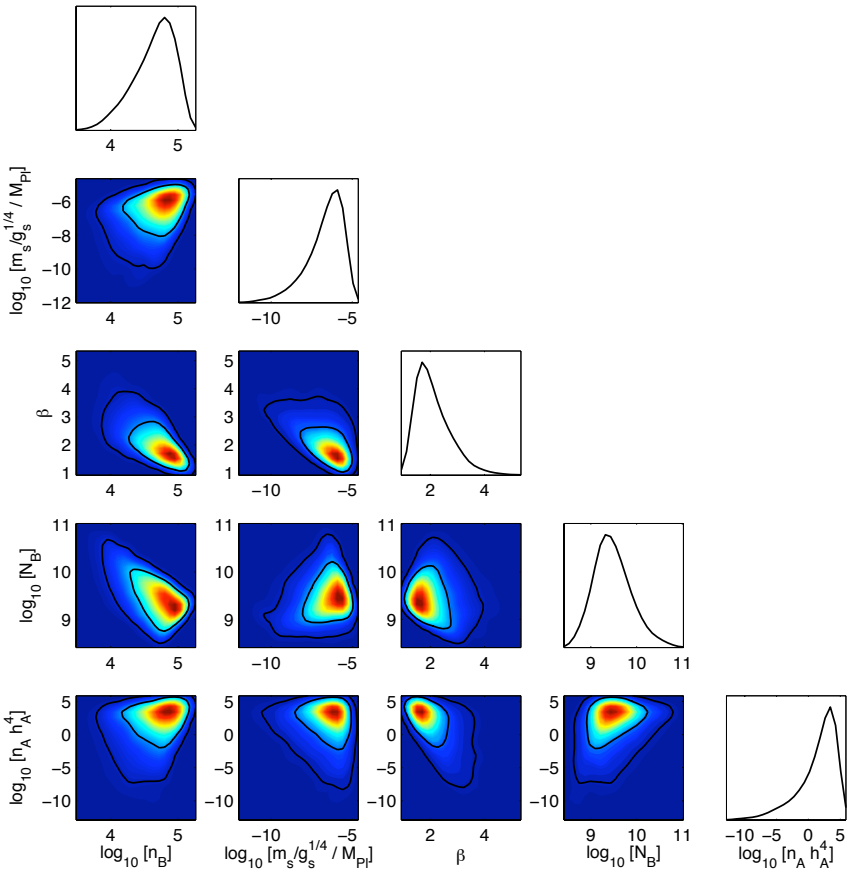

Figure 2.19: The marginalized 2D-joint 68% and 95% probability contours (solid lines in off-diagonal panels) and 1D marginalized probability distribution (diagonal panels) for the microphysical IR DBI parameters. The color coding shows the marginalized probability density in these 2D parameter spaces, ranging from red for the highest density to blue for the lowest.

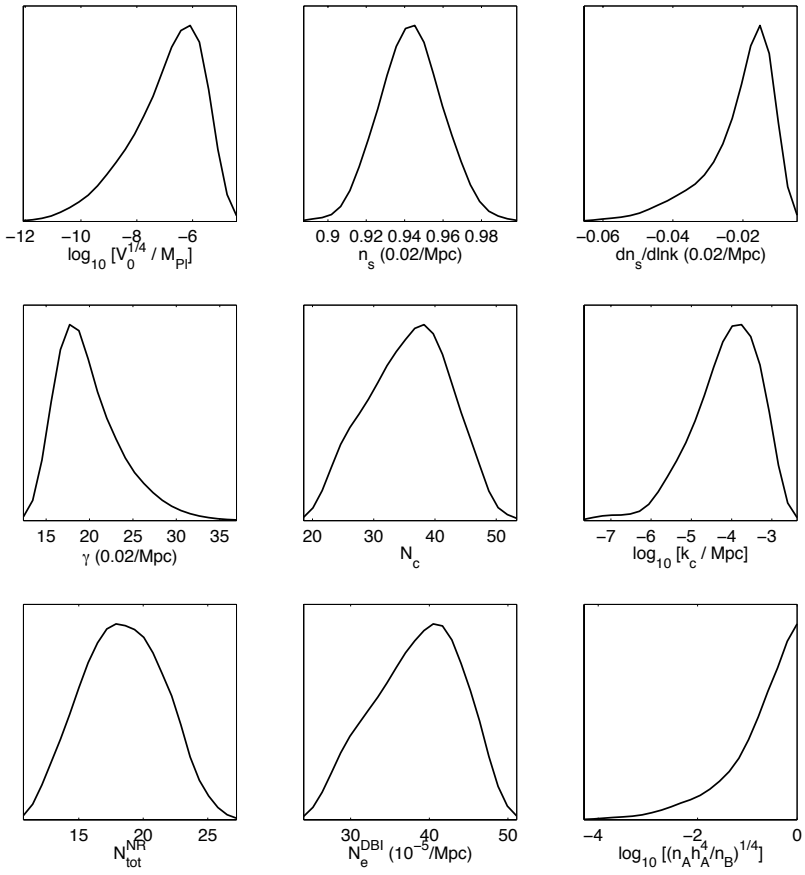

Figure 2.20: Marginalized posterior probability distribution functions obtained from the MCMC analysis for observables and derived quantities of interest. The functions are normalized such that the area under the curve is one.

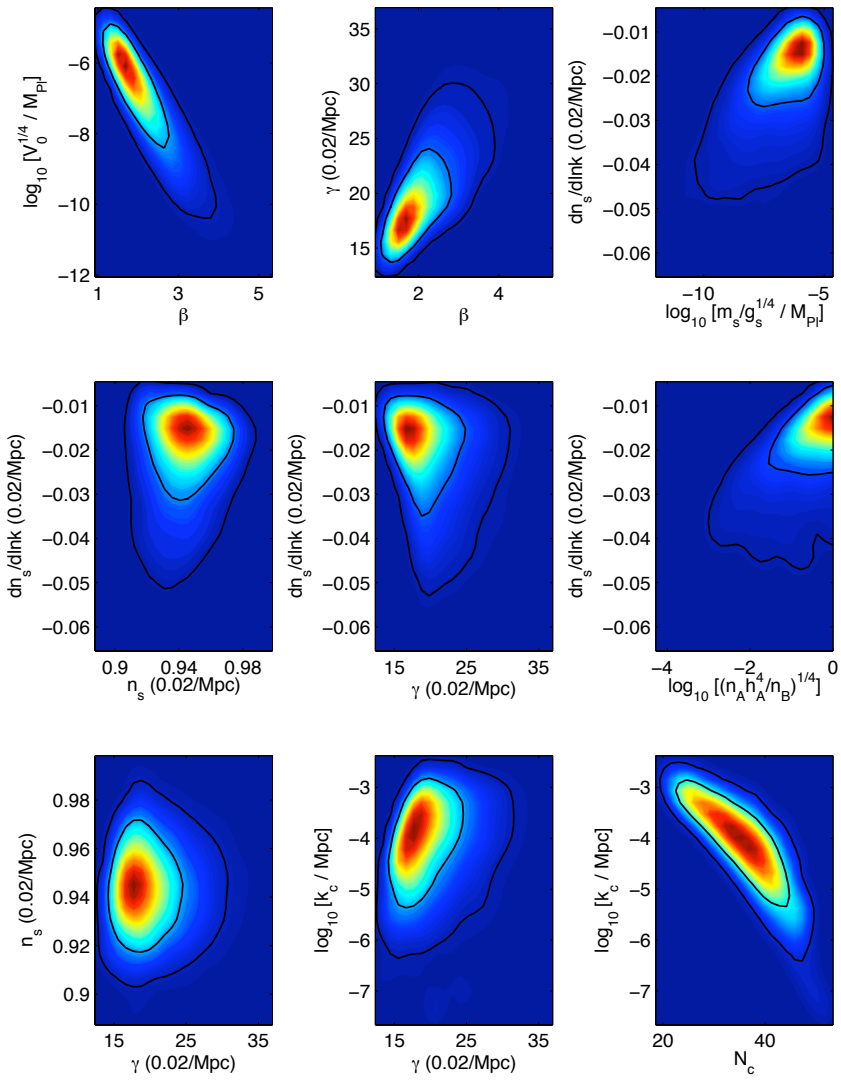

Figure 2.21: The marginalized 2D-joint 68% and 95% probability contours (solid lines) for observables and derived quantities of interest. The color coding shows the marginalized probability density in these 2D parameter spaces, ranging from red for the highest density to blue for the lowest.

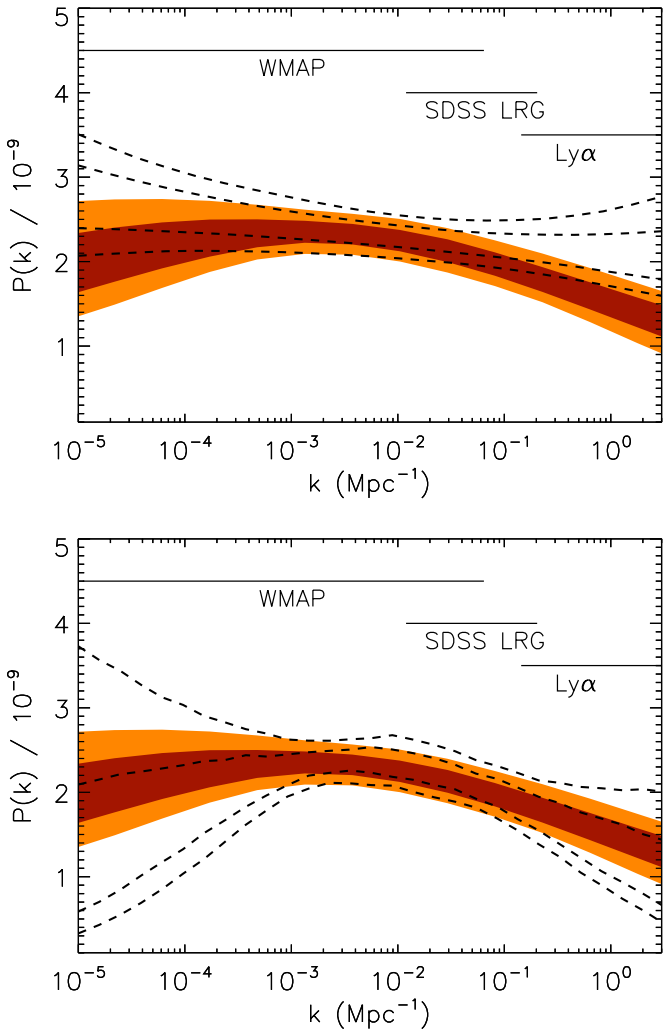

Figure 2.22: Reconstructed 68% (dark) and 95% (light) C.L. constraints on the primordial scalar power spectrum for the IR DBI model. The range of scales spanned by WMAP and SDSS LRG data (which were used in the fit) and the smaller scales covered by Lyman–α data (which were not) are shown for reference. For comparison, the dashed lines show the corresponding 68% and 95% constraints for (Upper) single-field slow-roll inflation, taken from Ref. [58] fitted to the WMAP and SDSS main galaxy sample data [60], and for (Lower) the empirical power law ansatz where the primordial power spectrum is described by its amplitude at a pivot scale, the spectral index n_s, and its running $\mathrm{d}n_s/\mathrm{d}\ln k$, fitted to WMAP, SDSS LRG and Supernova Legacy Survey [43] data.

Table 2.1: The best fit χ^2, defined as $\chi^2 = -2\ln\mathscr{L}_{\rm max}$ (where $\mathscr{L}_{\rm max}$ is the maximum likelihood with respect to the WMAP 3 year data and the SDSS LRG galaxy power spectrum data) for the standard ΛCDM model and the IR DBI scenario analyzed in this work. A Gaussian prior on $f_{\rm NL}^{\rm equil}$ has been applied based on the WMAP 3 year constraint on this parameter from Ref. [55]. For the ΛCDM model, the $f_{\rm NL}$ constraint has been applied assuming $f_{\rm NL}^{\rm equil} = 0$. The IR DBI model gives a slightly better (lower) χ^2 for this dataset than the ΛCDM model. The primordial power spectrum is described by five microphysical parameters in the former, and two empirical parameters (an amplitude and a power law index) in the latter. When we consider that the IR DBI observables are described phenomenologically by the three effective parameters N_c, $\ln k_c$, and $n_B\beta^4$, to which the microphysical parameters are related, we can see that the IR DBI model has roughly one extra degree of freedom over the ΛCDM model, which one expects to give a $\Delta\chi^2 \sim 1$ improvement in the fit. Since this is in fact what we see, there is no indication of a preference in the data for the IR DBI model.

Model	Best fit $-2\ln\mathscr{L}_{\rm max}$ (WMAP+SDSS LRG)
ΛCDM	5374.04
IR DBI	5373.11

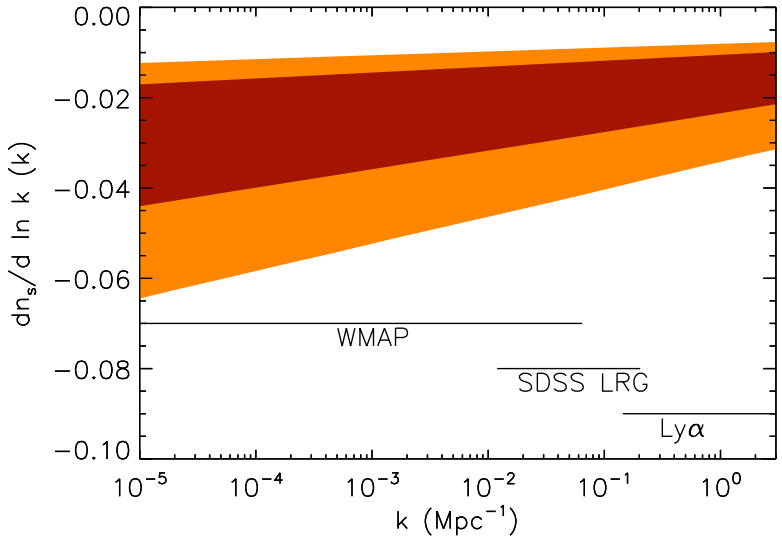

Figure 2.23: Reconstructed 68% (dark) and 95% (light) C.L. constraints on the scale dependence of the running of the spectral index, $dn_s/d\ln k$, showing a mild indication for a "running of the running".

Table 2.2: Constraints on the IR DBI model from the WMAP and SDSS LRG data-sets (mean, upper and lower 68% and 95% C.L., marginalizing over all other parameters), and the maximum likelihood values of the parameters found in the MCMC. A Gaussian prior on $f_{\rm NL}^{\rm equil}$ has been applied based on the WMAP 3 year constraint on this parameter from Ref. [55].

Parameter	Marginalized Constraint	Maximum Likelihood
$\Omega_b h^2$	$0.02145^{+0.00071+0.00138}_{-0.00071-0.00138}$	0.02162
$\Omega_c h^2$	$0.1070^{+0.0042+0.0086}_{-0.0044-0.0082}$	0.1058
τ	$0.089^{+0.030+0.060}_{-0.030-0.061}$	0.094
H_0	$71.2^{+1.8-3.9}_{-1.9-3.7}$	72.1
$\log_{10}[n_B]$	$4.64^{+0.30+0.45}_{-0.32-0.70}$	4.93
$\log_{10}[m_s/g_s^{1/4}/M_{\rm Pl}]$	$-6.71^{+1.04+1.43}_{-1.07-2.89}$	-5.91
β	$2.11^{+0.63+1.63}_{-0.60-0.85}$	1.77
$\log_{10}[N_B]$	$9.48^{+0.39+0.93}_{-0.39-0.70}$	9.15
$\log_{10}[n_A h_A^4]$	$1.41^{+2.64+3.34}_{-2.82-8.02}$	0.585
$\log_{10}[V_0^{1/4}/M_{\rm Pl}]$	$-6.95^{+1.25+1.83}_{-1.34-3.09}$	-6.36
N_c	$35.7^{+6.8+11.7}_{-7.3-12.6}$	34.1
$\log_{10}$ [k$_c$/Mpc]	$-4.15^{+0.81+1.21}_{-0.81-1.82}$	-3.86
$N_{\rm tot}^{\rm NR}$	$18.4^{+3.3+5.8}_{-3.2-5.7}$	20.5
$N_e^{\rm DBI}$ (10^{-5}/Mpc)	$38.4^{+5.6+9.1}_{-6.1-10.7}$	37.6
$\log_{10}[(n_A h_A^4/n_B)^{1/4}]$	> -2.36 (95% C.L.)	-1.09
$\log_{10}[(h_A m_s/g_s^{1/4})^2/(16\pi^2)/M_{\rm Pl}^2]$	$-17.2^{+2.4+3.5}_{-2.6-6.0}$	-16.2
n_s (0.02/Mpc)	$0.943^{+0.016+0.032}_{-0.016-0.031}$	0.946
$\mathrm{d}n_s/\mathrm{d}\ln k$ (0.02/Mpc)	$-0.021^{+0.008+0.011}_{-0.009-0.025}$	-0.021
γ (0.02/Mpc)	$19.9^{+3.6+9.3}_{-3.4-5.1}$	16.8
$f_{NL}^{\rm equil}$ (0.02/Mpc)	$-131^{+44+61}_{-45-141}$	-91

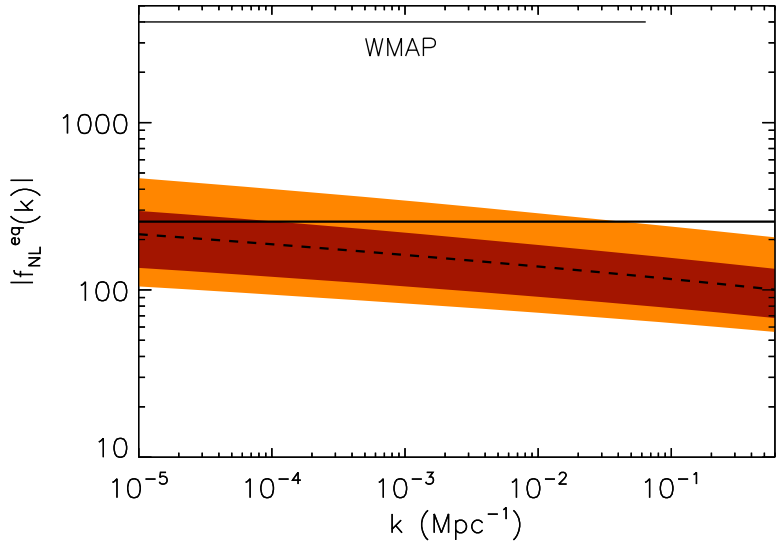

Figure 2.24: Reconstructed 68% (dark) and 95% (light) C.L. constraints and mean (dashed) for the non-linearity parameter $f_{\rm NL}^{\rm equil}$ for the IR DBI model, as a function of scale. Note that DBI inflation predicts $f_{\rm NL}^{\rm equil} < 0$, and the absolute value is plotted for convenience. The range of scales spanned by WMAP data are shown, as well as the WMAP 95% *lower limit* $f_{\rm NL}^{\rm equil} > -256$ (solid line), from an analysis which treated $f_{\rm NL}^{\rm equil}$ as scale-independent [55].

Microscopic Parameters

- *Shape of the inflaton brane moduli potential:* $1.3 < \beta < 3.7$. The lower bound is due to constraints from the power spectrum, while the upper bound is due to the non-Gaussianity constraint. It is encouraging that, while IR DBI inflation can happen for a range of β that varies over nearly 10 orders of magnitude, $0.1 \lesssim \beta < 10^9$ (see Eq. (2.120)), comparison with data picks out a very small range around $\mathcal{O}(1)$ which is generically expected theoretically. This makes an explicit construction of such potentials a more interesting question.

- *Fundamental string scale:* $-9.6 < \log_{10}(m_s/M_{\rm Pl})/g_s^{1/4} < -5.3$. The upper bound on the string scale is due to the large charge, and hence length scale, of the B-throat required to fit the amplitude of the density perturbations. The lower bound is due

to the fact that a smaller string scale tends to increase the total number of e-folds of non-relativistic fast-roll inflation, and make the running of the spectral index too large (Fig. 2.21). The model prefers an intermediate fundamental string scale, 10^8 GeV $< m_s/g_s^{1/4} < 10^{13}$ GeV, and therefore an intermediate large volume compactification, $8.9\times10^7 < V^{1/6}M_{\rm Pl} < 4.8\times10^{13}$, where V is the compactification volume.

- *B-throat charge:* $8.8 < \log_{10}N_B < 10.4$*; Number of inflaton branes:* $3.9 < \log_{10}n_B < 5.1$. In terms of the GKP-type warped compactification, this implies flux numbers $K \sim M \sim \sqrt{N_B} \sim \mathcal{O}(10^5)$. Explicit construction remains an open question. In the multi-throat brane inflation scenario, inflaton branes are generated from flux-antibrane annihilation. The number of branes generated in this process is roughly determined by the flux number M. Indeed, a small number of inflaton branes is ruled out by the data.

- *A-throat minimum warp factor:* $-2.4 < \log_{10}h_A \leq 0$. This is from combining the constraint on n_B and $n_A h_A^4$, $h_A = (n_A h_A^4/n_B)^{1/4}$. A smaller h_A leads to larger $N_{\rm tot}^{\rm NR}$ and larger running of the spectral index (Fig. 2.21). So the A-throat tends to be short. This makes tunneling reheating possible, where many interesting phenomena can occur, such as an intermediate matter-dominated epoch.

Secondary Derived Parameters

- *Inflationary phases.* In this model, not all e-folds comes from IR DBI inflation. The last $13 < N_{\rm tot}^{\rm NR} < 24$ e-folds come from non-relativistic fast-rolling inflation, which is possible because inflatons are close to the top of the potential.

- *The stringy phase transition.* The Hubble-expansion induced stringy phase transition happens at the largest scales in the sky, $-6.0 < \log_{10}k_c/{\rm Mpc} < -2.9$. However its impact on density perturbations extends over to shorter scales, such as

generating a transient large running of the spectral index.

- *Inflation scale:* $-10.0 < \log_{10} V_0^{1/4}/M_{\rm Pl} < -5.1$. This gives a very small tensor to scalar ratio $r_{TS} < 10^{-13}$.

- *Cosmic string tension:* $-23 < \log_{10} G\mu_D + \log_{10} g_s^{1/2} < -14$. Here the cosmic strings refer to the D-strings left over from the brane-antibrane annihilation in the A-throat, whose tension is $G\mu_D = (m_s h_A/g_s^{1/4} M_{\rm Pl})^2/(16\pi^2 g_s^{1/2})$. There is an unconstrained freedom coming from the additive factor $\log_{10} g_s^{1/2}$, but it is not expected to give any significant contributions. The F-string tension differs by a factor of g_s, $\mu_F = g_s \mu_D$.

Observational Predictions

- *Large, but regional, running of spectral index:* $-0.046 < {\rm d}n_s/{\rm d}\ln k(k = 0.02/{\rm Mpc}) < -0.010$. A reconstructed full-scale power spectrum and the running of the spectral index are shown in Fig. 2.22 & 2.23.

  This prediction is stringy in nature. A better understanding of the theoretical details and better measurements of both the power spectrum and non-Gaussianities on the relevant scales may reveal finer structures. In future experiments, Planck is expected to achieve $\sigma({\rm d}n_s/{\rm d}\ln k) = 0.005$ [61].

- *Large non-Gaussianities:* $-272 < f_{\rm NL}^{\rm equil}(k = 0.02/{\rm Mpc}) < -70$. A reconstructed full-scale prediction is in Fig. 2.24, which shows the running of the non-Gaussianities.

  This prediction is strictly speaking field-theoretic, but with strong string theory motivations, such as warped compactification and the DBI brane action. This field theoretic regime is $k > k_c$; the theoretical analysis for non-Gaussianities at $k \lesssim k_c$ is currently unavailable and remains an interesting open question. In future experiments, on CMB scales, Planck can achieve $\sigma(f_{\rm NL}^{\rm eq}) = 67$ [62, 63]; on

large scale structure scales, some high-z galaxy surveys can reach similar or better precision [33].

As seen from these results, constraints from cosmological data, and even relatively loose constraints such as the non-Gaussianity constraint, are already putting strong restrictions on the IR-DBI model. With more precise data coming in the near future, we expect even tighter constraints or detection of the above mentioned observable signatures.

2.5 Sharp Features in Brane Inflation

In this chapter, we show that brane inflation is very sensitive to tiny sharp features in extra dimensions, including those in the potential and in the warp factor [64]. This can show up as observational signatures in the power spectrum and/or non-Gaussianities of the cosmic microwave background radiation. One general example of such sharp features is a succession of small steps in a warped throat, caused by Seiberg duality cascade using gauge/gravity duality. We study the cosmological observational consequences of these steps in brane inflation. Since the steps come in a series, the prediction of other steps and their properties can be tested by future data and analysis. It is also possible that the steps are too close to be resolved in the power spectrum, in which case they may show up only in the non-Gaussianity of the CMB temperature fluctuations and/or EE polarization. We study two cases. In the slow-roll scenario where steps appear in the inflaton potential, the sensitivity of brane inflation to the height and width of the steps is increased by several orders of magnitude comparing to that in previously studied large field models. In the IR DBI scenario where steps appear in the warp factor, we find that the glitches in the power spectrum caused by these sharp features are generally small or even unobservable, but associated distinctive non-Gaussianity can be large. Together with its large negative running of the power spectrum index, this scenario clearly illustrates how rich and different a brane inflationary scenario can be when compared to generic slow-roll inflation. Such distinctive stringy features may provide a powerful probe of superstring theory.

2.5.1 Sharp Features from Duality Cascade

Let us consider the sharp features in the context of the IR-DBI scenario. The inflaton ϕ is related to the position of n_B 4-dimensional space-time filling $D3$-branes. They are

moving out of the B throat into the bulk and then falling into the A throat. For simplicity, we assume that the B throat is a K-S throat. The warped factor for the B throat around the p_l^{th} duality transition (starting from the bottom of the throat) is simplified to [47, 64]

$$h^4(r) \simeq \frac{r^4}{R_B^4}\frac{K}{p_l}(1+\Delta)\ , \quad \Delta = \sum_{p_i}^{K} \frac{3g_sM}{16\pi}\frac{1}{p^3}\left[1+\tanh\left(\frac{r-r_p}{d_p}\right)\right]\ , \tag{2.176}$$

where $h(r=R_B)\simeq 1$ at the edge of the throat. Here r_p is the positions of the steps, the initial $p_i \gg 1$ so that the warped factor formula is approximately good, and d_p controls the width of the step. The steps has a constant separation in $\ln r$, that is, $\ln r_{p+1} - \ln r_p \simeq 2\pi/3g_sM$. As one moves down the throat (r and p decreasing), note that the step in the warped factor $h^4(r)$ of the K-S throat is going down. See Figure 2.25. This stepping down happens at each Seiberg duality transition. Together, they form a cascade [65]. For large K, one encounters $K-1$ steps as one approaches the infrared. Note that we are ignoring smooth corrections to the shape of the warp factor even though they may be larger than the step size. This is a reasonable approximation since it is the sharp features that will show up as distinctive features in the CMBR. If the throat has relatively few steps, or if the steps are well separated, the impact of individual step on CMBR may be observable. Otherwise, the steps may be too close for them to show up in the power spectrum.

In the original K-S throat solution, they take the approximation where the dilaton is constant. Here the dilaton factor, $e^{-\Phi}$, runs in general and is ϕ dependent. However, for the IR DBI inflation model we discuss in this paper, most of the DBI e-folds are generated at the tip of the throat where $HR_B^2/N_e < r < HR_B^2$. At the same time, the brane moves across roughly g_sM steps [54]. The running of the dilaton can be ignored if $g_sM \ll p_l$, which is most easily satisfied with a small g_s. Furthermore, the WMAP data only covers a few e-folds, which corresponds to $3g_sM/N_e$ steps, so we only need $p_l \gtrsim g_sM$ to safely ignore the dilaton modification to the kinetic term. In this paper, when we discuss the IR DBI inflation, we always absorb e^{Φ} into g_s as a constant, so it

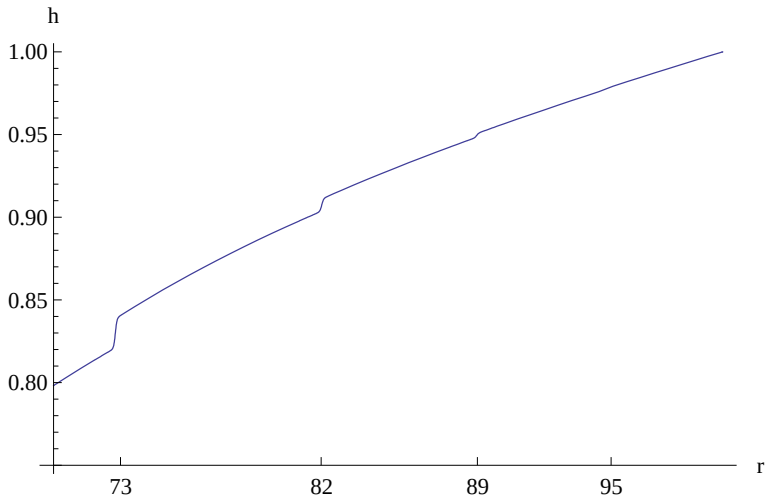

Figure 2.25: The warp factor $h(r)$ in the K-S throat, including the steps. Here r is measured in $\sqrt{\alpha'}$ with $R_B \simeq 100$, $g_s = 2$, M=20, $K = 10$ and $N = 200$. The width $d = 10^{-3}$. In this figure, there are actually 4 steps, located at $r \simeq 73$, $r \simeq 82$, $r \simeq 89$ and $r \simeq 95$, although the step at $r \simeq 95$ is too small to show up. Here, the parameters (in particular, a large $g_s M$) are chosen so that at least 3 steps are big enough to show up in the figure. This leads to relatively large corrections to the positions of the steps. Other parameters should be used in more realistic situations and in comparison with data.

will never appear explicitly in our analysis.

2.5.2 Steps in Slow-Roll Brane Inflation

In the slow-roll scenario, let us assume that inflation takes place as the brane moves down the throat. Since the dilaton runs, the slow-roll potential is given by

$$V_{SR}(\phi) = V(\phi) + T(\phi)(e^{-\Phi(\phi)} - 1) \ . \tag{2.177}$$

Here, the second term in the potential does not vanish, so the step in $T(\phi)$ shows up in the potential. Again, we may consider both step up and step down cases.

Before we proceed, we mention two other possibilities that will not be studied in more detail in this paper. Suppose the warp factor steps down as r increases. As the inflaton

moves down the throat, it encounters such steps. If the height of any particular step is too big, then the inflaton cannot overcome it so its classical motion towards the bottom of the throat is stopped. Let us say this happens at $r = r_p$. It can still move along the $S^3 \times S^2$ angular directions. In a realistic model, the $S^3 \times S^2$ symmetry is slightly broken so the inflaton would move along the steepest angular direction, until it reaches the lowest point at this radius r_p. If the step there is lessened so that the inflaton can roll over it, the inflaton can continue to roll down along r until it reaches the next step. This process can repeat some number of times. As a result, the inflaton path is substantially longer than just moving down along r. Effectively, this may substantially extend the field range and enough e-folds of inflation is much more likely.

Another possibility is that the brane can tunnel over the step barrier. Recent analysis of the tunneling of branes suggests that, under the right condition, the brane may tunnel very easily across a potential barrier that is not particularly small [66]. If this is the case, then the brane may roll along some angular direction until it reaches such a position and tunnel right over the potential barrier there. It can then roll down along r until it reaches the next step. Again, this process can repeat any number of times, as a result, the inflaton path is again substantially longer than just moving down along r, allowing the generation of many e-folds.

In the following, we consider the scenarios where the inflaton can roll over many steps in the potential.

The Position of the Steps

The duality cascade predicts more than one step, so it is interesting to ask where the steps are. Assume there is a step at the $l \simeq 20$ in the CMBR, which may be checked with a non-Gaussianity measurement. Let us further assume that there is another step at $l \simeq 2$, (the significance of the signal at $l = 2$ in power spectrum is much smaller than

that in $l \simeq 20$ due to the large cosmic variance, so we assume this mainly for the purpose of illustration). We now show that the location of all the steps in the duality cascade can be determined by given the locations of two such adjacent steps.

Using $l \sim 10^4 (k/\mathrm{Mpc}^{-1})$, we find

$$-\mathrm{d}N_e \simeq \mathrm{d}\ln k \simeq \mathrm{d}\ln l \simeq H\mathrm{d}t \simeq \frac{H}{\dot{\phi}}\mathrm{d}\phi \ , \tag{2.178}$$

Since both H and $\dot{\phi}$ are slowly varying during inflation, we have

$$\mathrm{d}\ln l \propto \mathrm{d}\phi \ . \tag{2.179}$$

Suppose ϕ is decreasing (going down a throat), also suppose that the step at $l = 2$ is at ϕ_{m_0} and that at $l = 20$ is at ϕ_{m_0+1}, we have

$$\frac{\phi_{m_0}}{\phi_{m_0+1}} \simeq \frac{\phi_{m_0+1}}{\phi_{m_0+2}} \simeq ... \simeq e^{2\pi/3g_sM}. \tag{2.180}$$

For large g_sM, this ratio is close to unity, $e^{2\pi/3g_sM} \simeq 1+\delta$, so $\phi_{m_0} - \phi_{m_0+1} \simeq \phi_{m_0+1} - \phi_{m_0+2} \simeq \phi_{m_0+1}\delta$. Due to (2.179), equal spacing in ϕ implies equal spacing in $\ln l$. So we find that the next two steps are at around $l \simeq 200$ and $l \simeq 2000$ respectively. In addition, the effect of the step at multiple moment l should span over Δl multiple moments with $\Delta l \propto l$.

The Power Spectrum

To see the full details of the effect of a step in potential, numerical calculation is necessary. However, the qualitative behavior can be estimated as follows. The step in the potential is typically characterized by two numbers: the depth which we describe as the ratio $\Delta V/V \approx 2c$, and the width $\Delta\phi = 2d$ in unit of Planck mass. We can divide the motion of inflaton into two parts: acceleration and relaxation. First, the inflaton, originally moving in its attractor solution, momentarily gets accelerated by the step. The potential energy ΔV gets converted to kinetic energy. Then after the inflaton moves across the

step, it starts to relax back to its attractor solution under $\ddot{\phi} + 3H\dot{\phi} \approx 0$, where the Hubble friction term dominates over the potential.

We first look at the power spectrum. The inflaton velocity in the original attractor solution is given by $|\dot{\phi}_{\rm attr}| \approx |V_\phi|/3H \approx \sqrt{\varepsilon V/3}$. After the acceleration of the step, $\dot{\phi} \approx \sqrt{V(3c+\varepsilon/3)}$. (It turns out that the best fit data give comparable $3c$ and $\varepsilon/3$, so for the purpose of order-of-magnitude estimate we later will also approximate $\dot{\phi}$ to be $\sqrt{3cV}$.) A useful formula to understand the dip of the glitch in the power spectrum caused by the step is $P_\zeta = H^2/(4\pi^2\dot{\phi}^2)$. The acceleration of inflaton does not change the H so it reduces the P_ζ. The ratio of P_ζ between the initial value and the value at the first dip is related to the corresponding ratio of $\dot{\phi}$, which is $\sqrt{1+9c/\varepsilon}$. For the large field quadratic inflation, Ref. [67, 68, 69] give the best-fit data, $c = 0.0018$, $\varepsilon = 0.009$. As we will see later, the values of c and ε will be rather model-dependent. However the discussion in this paragraph shows that their ratio should be fixed for a specific observed feature,

$$\frac{c}{\varepsilon} \approx 0.2 \, . \tag{2.181}$$

Although the above discussion indicates that the depth of the dip is relatively independent of d, the peak of the first bump is. When the inflaton moves across the step, energy conservation requires that $\frac{1}{2}\Delta\dot{\phi}^2 \leq \Delta V$, with the bound saturated when the Hubble friction is negligible. This will result in an upper bound in the change of ε

$$\Delta\varepsilon \approx \Delta V/H^2 \lesssim 5c \, . \tag{2.182}$$

We expect that the effect of decreasing d will first enhance the bump, since smaller d leads to more deviation from the attractor (larger $\Delta\varepsilon$), and will enhance the bumps in P_ζ during the relaxation period. However, as long as $\Delta\varepsilon$ saturates the upper bound (when d is small enough to ignore the Hubble friction), further decreasing d will not affect the bumps in P_ζ any more, since the relaxation period essentially starts with the same $\dot{\phi}$ no matter how small d is. So we expect the bump to depend sensitively on d if moving

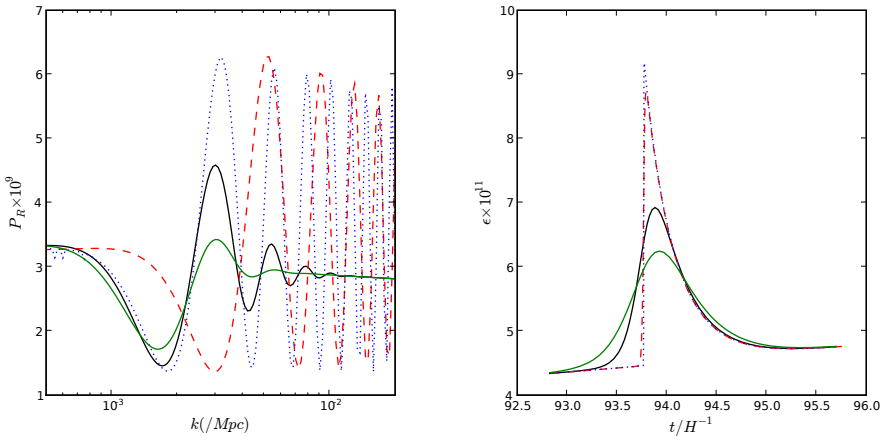

Figure 2.26: In the small field case, we show how the step in the inflaton potential changes the power spectrum. We show the power spectrum in the left panel and the behavior of ε around the step in the right panel. For illustration, we use the KKLMMT scenario with only the Coulomb potential. We choose the background flux $N = 2000$, so $\Delta\phi/M_{\rm Pl} \lesssim 0.01$. The inflation scale $V_0 \sim 10^{-17} M_{\rm Pl}^4$. ε is tiny, typically $\varepsilon \sim 10^{-11}$ as shown in the right panel. We introduce a step with $c = 8\times10^{-12}$ and calculate the power spectrum for four different values of d: (1) $d = 3\times10^{-6} M_{\rm Pl}$, green solid line. (2) $d = 1.7\times10^{-6} M_{\rm Pl}$, black solid line. (3) $d = 1.7\times10^{-7} M_{\rm Pl}$, red dashed line. (4) $d = 1.7\times10^{-8} M_{\rm Pl}$, blue dotted line. Note that the dip in the power spectrum depends weakly on d. In case (1) and (2), $\Delta\varepsilon$ has not saturated the bound Eq. 2.182, so decreasing d will enhance the bump in P_ζ significantly. In case (3) and (4), where $\Delta\varepsilon$ is maximized, the bump in P_ζ does not depend sensitively on d, but the range of the oscillations in k-space does. The black solid line is close to the best fit power spectrum given in Ref. [67, 68].

across the step takes $\mathcal{O}(1)$ e-folds, and it becomes relatively insensitive to d when the step is so sharp that moving across it takes only $\ll 1$ e-folds. In the latter situation, reducing d will only increase the extension of the oscillations in P_R,

$$\Delta k \sim \sqrt{\frac{z''}{z}} \sim k_0 \frac{\sqrt{c}}{d}\,, \tag{2.183}$$

where k_0 is the starting point of the feature. is used.

Ref. [67, 68] fit the $l \sim 20$ feature in the WMAP data introducing a step feature in

the large field slow-roll model and gives the best fit power spectrum. Here we have numerically reproduced a similar power spectrum for the small field case. We are not performing a complete data analysis to find the best fit model here, our major emphasis is to show how the width d comes into play. Fig. 2.26 shows the power spectrum and ε for four different values of d. The black solid line represents the power spectrum close to the best fit model given in Ref. [67, 68], with $c = 8 \times 10^{-12}$, we find that $d = 1.7 \times 10^{-6} M_{\rm Pl}$.

Non-Gaussianities

Now let us look at the bispectrum. For slow-roll inflation, the 3-point function of the scalar perturbation $\zeta(\tau_{end}, \mathbf{k})$ includes terms proportional to ε^2, ε^3, and $\varepsilon\eta'$ [31]. For the slow-roll potential without any features, the first terms dominate. Comparing to WMAP's ansatz, it gives the non-Gaussianities estimator $f_{\rm NL} = \mathscr{O}(\varepsilon)$.

In the presence of sharp features, from (2.182) we see that ε still remains small, $\lesssim \mathscr{O}(0.01)$. But η' can be much larger. Therefore, the leading three-point correlation function is given by the term proportional to $\varepsilon\eta'$ [49],

$$\begin{aligned} & \langle \zeta(\tau,\mathbf{k}_1)\zeta(\tau,\mathbf{k}_2)\zeta(\tau,\mathbf{k}_3)\rangle \\ = \;& i\left(\prod_i u_{k_i}(\tau)\right)\int_{-\infty}^{\tau} \mathrm{d}\tau' a^2 \varepsilon\eta' \left(u^*_{k_1}(\tau')u^*_{k_2}(\tau')\frac{d}{d\tau}u^*_{k_3}(\tau') + \text{perm}\right) \\ & \times (2\pi)^3 \delta\left(\sum_i \mathbf{k}_i\right) + \text{c.c.}\,, \end{aligned} \tag{2.184}$$

where the "perm" stands for two other terms that are symmetric under permutations of the indices 1, 2 and 3. The details of such an integration are quite complicated. Nonetheless we can estimate the order of magnitude of the non-Gaussianity estimator $f_{\rm NL}$ by comparing it to the slow-roll case. The most important difference is that here we replace a factor of ε by η', and also η' only gets large momentarily. Hence we estimate $f_{\rm NL}^{\rm feature} = \mathscr{O}(\eta'\Delta\tau) = \mathscr{O}(\Delta\eta)$, where $\Delta\tau$ is the conformal time that the inflaton spends

crossing the step.

To estimate the level of these non-Gaussianities, we now give a qualitative estimate for η' [49]. During the acceleration period, the ε is increased by

$$\Delta\varepsilon \approx \Delta V/H^2 \approx 5c \ . \tag{2.185}$$

The duration of this period is

$$\Delta t_{accel} \approx \Delta\phi/\dot{\phi} \approx d/\sqrt{cV} \ , \tag{2.186}$$

where we used $\dot{\phi}$ estimated in Chapter 2.5.2. These can be further used to estimate

$$\Delta\eta \approx \eta = \frac{\dot{\varepsilon}}{H\varepsilon} \approx \frac{7c^{3/2}}{d\varepsilon} \ , \tag{2.187}$$

The time scale for the relaxation period is of order H^{-1}, during which η is $\mathscr{O}(1)$ and $\dot{\tilde{\eta}}$ are of order $\mathscr{O}(H)$.

We sum over the contributions from both the acceleration and relaxation periods. The former gives $f_{\rm NL}^{\rm accel} \approx 7c^{3/2}/(d\varepsilon)$, the latter gives $f_{\rm NL}^{\rm relax} = \mathscr{O}(1)$. So for most interesting cases where non-Gaussianities are large enough to be observed, it can be estimated by the first contribution,

$$f_{\rm NL}^{\rm feature} \sim \frac{7c^{3/2}}{d\varepsilon} \ . \tag{2.188}$$

We note that this is only a crude order of magnitude estimation on the amplitude of this non-Gaussianity, since the integration (2.185) also involve mode functions u_k which will be modulated by the presence of the sharp feature, and the shape and running of such non-Gaussianities are very important. Details have to be done numerically, as in [49]. Qualitatively since we have argued in Chapter 2.5.2 that for a specific observed feature the c/ε is hold fixed model-independently, (2.188) implies that the value of d is very crucial to the level of the non-Gaussianities. There are two major constraints on d. First, in the power spectrum, as shown in Fig. 2.26 the bump in P_ζ may depend sensitively on d. Second, the range of oscillation in $P_\zeta(k)$ is also controlled by d. If d is too small, the

oscillation in $P_\zeta(k)$ might spread over to the well measured first acoustic peak in WMAP C_l curve. Numerically, we have found that $\sqrt{c}/d \sim \mathscr{O}(1)$, consistent with (2.183), so the magnitude of (2.188) should be close to that in Ref. [49].

It is instructive to split this expression to $f_{\rm NL}^{\rm feature} \sim 7c/\varepsilon \cdot \sqrt{c}/d$. The first factor is determined by the amplitude of the glitch from (2.181), while the second factor is the extension of the glitch from (2.183). Note both are in the k-space not the CMB multipole l-space. Therefore in principle a sharp feature can also appear only in the 3-point function. This is clear from our estimation (2.181) and (2.188), where one can reduce c/ε while increase $c^{3/2}/(d\varepsilon)$.

Our analyses so far do not depend on the whether the inflation is caused by large field or small field, but when it comes to the quantitative analyses the differences are interesting. For large field inflation $\varepsilon \sim \eta$ while for small field inflation $\varepsilon \ll \eta$. For example, previous numerical works focus on the large field quadratic potential, and give the best fit $\Delta V/V \sim c \sim 0.2\varepsilon \sim \mathscr{O}(10^{-3})$. Brane inflation is a small field inflation [37] and ε is much smaller, $\varepsilon \sim \mathscr{O}(10^{-6})$ or even $\mathscr{O}(10^{-12})$. Similarly the field range d (in units of $M_{\rm Pl}$) is also much smaller. So brane inflation is sensitive to very tiny steps present in the potential. This can be potentially used as a sensitive probe to the fundamental theory.

2.5.3 Steps in IR DBI Inflation

In the relativistic regime with $t \ll -H^{-1}$, the IR-DBI attractor solution is

$$\phi \simeq -\frac{\sqrt{\lambda_B}}{t}\left(1-\frac{9}{2\beta^2H^2t^2}\right), \quad \gamma \simeq \frac{\beta H}{3}|t| \,. \tag{2.189}$$

This zero mode evolution relies on the background warped geometry, so it is reliable in regions where the back-reaction deformation from Hubble expansion is small [28, 51]. This still leaves at least two interesting regions for primordial fluctuations: the field

theoretic region (corresponding to smaller N_e and shorter scales) and the stringy region (corresponding to bigger N_e and larger scales). The spectral index transitions from red to blue [28, 29]. Detailed estimates can be found in Ref. [54].

We now consider the effects of sharp features in the warped geometry on this IR DBI model. The duality cascade will leave sharp features on the warp factor $T(\phi)$ but not the inflaton potential $V(\phi)$. Since the WMAP window spans a few e-folds, corresponding to branes rolling across $\Delta l \approx 3g_s M/N_e^{\rm DBI}$ duality cascades in a Klebanov-Strassler throat. In this paper we will mainly treat the steps as individual sharp features, namely they are well separated in terms of e-folds and sufficiently sharp to generate observational signature individually. For this purpose, we would like to consider the situation where

$$g_s M \lesssim N_e^{\rm DBI} \ . \tag{2.190}$$

In the multi-throat brane inflation scenario, the number of inflaton branes generated in B-throat is roughly determined by the flux number M. Since the number of inflaton branes is constrained to be around $10^4 \sim 10^5$ [54], the condition (2.190) implies a small $g_s \lesssim 10^{-3}$.

It is also very natural that g_s takes value larger than 10^{-3}. In this case, the branes come across many steps within a single e-fold. We will discuss this case in Chapter 2.5.5.

The Properties of the Steps

Here we like to make a crude estimate on the positions, fractional heights and widths of the steps, along the line of Chapter 2.5.2 but with more detailed numbers. The input is the position, fractional height and width of the step at $l \sim 20$ as well as the position of the assumed step at $l \sim 2$. Let $r = r_0 \simeq R_B$ be the edge of the throat and $r = r_b$ at the bottom of the throat. They are related by the warp factor $h(\phi_b) = h_B$,

$$r_b \sim r_0 h_B \sim r_0 \exp\left(-\frac{2\pi K}{3g_s M}\right) \ . \tag{2.191}$$

We are interested at regions where $r_b \ll r \ll r_0$. Thus, given r_0 or r_b, we can determine all the other transition values r_p. Here p measures (starting at the bottom) the step in the duality cascade. In the large $K \gg p \gg 1$ limit, the correction is small, so we treat the steps as perturbations. The sharpness of the steps are controlled by the coefficient d_p. A step becomes infinitely sharp as $d_p \to 0$. We shall leave d_p as free parameters. Note we can introduce similar spreads to the running of the dilaton.

The position ϕ_p of the steps can be computed. The steps are at $\phi = \phi_p$, where

$$\ln \frac{\phi_p}{\phi_b} \simeq \frac{2\pi}{3g_s M}\left(p - \frac{1}{2p}\right) \sim \frac{2\pi p}{3g_s M} \,. \tag{2.192}$$

Same as Eq.(2.178) in the slow-roll case, we have

$$-\,\mathrm{d}N_e \simeq \mathrm{d}\ln k \simeq \mathrm{d}\ln l \simeq H\mathrm{d}t \,. \tag{2.193}$$

Suppose the pth step is at l_p (or ϕ_p), because $\phi \simeq -\sqrt{\lambda_B}/t$, we get

$$\frac{\phi_p}{\phi_{p-1}} \simeq \frac{t_{p-1}}{t_p} \simeq \frac{N_0 - \ln l_{p-1}}{N_0 - \ln l_p} \,, \tag{2.194}$$

where we have used the fact that H is approximately a constant, and N_0 is the number of e-folds (at the largest CMBR scale) to the end of DBI inflation, for example $N_0 \approx 38$ [54]. On the other hand, duality cascade relates the position of the adjacent steps

$$\frac{\phi_p}{\phi_{p-1}} = \exp\left(\frac{2\pi}{3g_s M}\right) \,. \tag{2.195}$$

Suppose the feature at $l_{p_i+1} \sim 20$ is due to such a step, and suppose the feature at $l_{p_i} \sim 2$ is also due to a step (not just cosmic variance). That is, p_i labels the initial or the first observable step. Then, taking $N_0 = 38$, we see that the next 2 steps should be at

$$l_{p_i+2} \sim 170 \qquad l_{p_i+3} \sim 1300 \,. \tag{2.196}$$

We also get a constraints on the microscopic parameters

$$g_s M \approx 33 \,. \tag{2.197}$$

Now we estimate the value of p_i by looking at the dip in the CMB power spectrum at $l \sim 20$. The power spectrum is

$$P_\zeta(k) = \frac{H^4}{4\pi^2\dot{\phi}^2}. \tag{2.198}$$

In IR DBI inflation, the Hubble scale is dominated by the constant $\sqrt{V_0}$, so it does not change across a step in the warp factor. However, since $\dot{\phi}$ closely tracks the speed limit $\dot{\phi}^2 \sim h^4(\phi)$, it is most sensitive to the step in the warp factor. $\dot{\phi}^2$ increasing by a factor of $(1+2b)$ across a step decreases P_ζ by a factor of $(1+2b)$. The CMB data shows that around $l \sim 20$, there is a dip in the power spectrum by about 20% in k-space, which gives $2b \sim 0.2$. Using (2.176), we have

$$\left(\frac{3g_sM}{8\pi}\right)\frac{1}{(p_i+1)^3} \sim 0.2\ . \tag{2.199}$$

Given that $g_sM \approx 33$ to fit the spacing of the steps, we immediately get

$$p_i = 2\ . \tag{2.200}$$

With input of 4 quantities : the position $l \sim 20$, the fractional height (size) $\Delta T/T \simeq 0.2$ and the width $\Delta l_p \sim 5$ of the 2nd step as well as the position (at $l \sim 2$) of the first step, we can use $\Delta l \propto l$ and $\Delta T/T \propto p^{-3}$ to get a complete set of predictions:

p	l	$\Delta T/T$	Δl_p
2	~ 2	~ 0.7	~ 1
3	~ 20	0.2	~ 5
4	~ 170	~ 0.08	~ 40
5	~ 1300	~ 0.04	~ 260

Note that $\Delta T/T \sim 0.7$ and $\Delta T/T = 0.2$ for the first two steps are probably too big to be treated as a perturbation. We shall take this to mean that the size of the first step can be very big.

We should point out that the warp factor Eq.(2.176) is a good approximation only when $p \gg 1$. This condition is also necessary to ignore the running of the dilaton. So $p = 3$ is already too small. Moreover, as we will see in Chapter 2.5.4, the glitch in the power spectrum around $l \sim 20$ may be too large to be explained by a step feature in the warp factor due to the duality cascades.

Qualitative Analyses around a Single Step

We consider a sharp step in the warped geometry $T(r)$. We parametrize the size of the step as $2b \equiv \Delta T/T$ and the width as $\Delta\phi \equiv 2d$. We use the tanh function interpolation between the two sides of the step, i.e.

$$T(r) \equiv T_3 \frac{r^4}{R^4}\left[1 + b\tanh\left(\frac{r - r_s}{d}\right)\right] . \tag{2.201}$$

The Evolution of the Sound Speed

We use the case of positive b to illustrate the evolution of the sound speed, the formulae are the same for negative b. The direction of the step is such that, for positive b, T steps up as r increases, i.e. the warp factor $h \propto T^{1/4}$ (or the speed-limit h^2) increases as r increases.

The first stage is when branes move across the step, where the speed-limit increases suddenly. Since the time that the branes spend to across the step is very short comparing to the Hubble time, during which we can ignore the Hubble expansion and the acceleration from the potential. So across the step, the behavior of the branes is approximated by the Lagrangian $\mathscr{L} = -T(r)\sqrt{1 - \dot{\phi}^2/T(r)}$. The corresponding energy $T\gamma = \text{const}$, where $\gamma = 1/c_s = (1 - \dot{\phi}^2/T)^{-1/2}$. Hence a sharp change in T results in a sharp change in c_s, and both changes are small,

$$\frac{\Delta c_s}{c_s} = \frac{\Delta T}{T} = 2b . \tag{2.202}$$

A small change in c_s also means that the velocity of the branes will closely track the change of the speed-limit in step.

The second stage is at the end of the step, where the previous change in c_s results in a deviation from the attractor solution. To see this, we note that in IR DBI inflation, the attractor solutions have $\gamma \approx \beta N_{e\rm DBI}/3$ and $N_{e\rm DBI} \approx HR/h$, so $c_s \approx 3h/\beta HR$. A fractional change in the warp factor $h = r/R$ means $\Delta R/R = -b/2$, which implies that the attractor solutions has a fractional change

$$\frac{\Delta c_s}{c_s} = b \ . \tag{2.203}$$

So the increase in c_s due to the first stage (2.202) over-shoots the new attractor solution, the branes will have to quickly relax to the new attractor solution. The Hubble expansion plays an important role here, so the energy $T\gamma$ is no longer conserved.

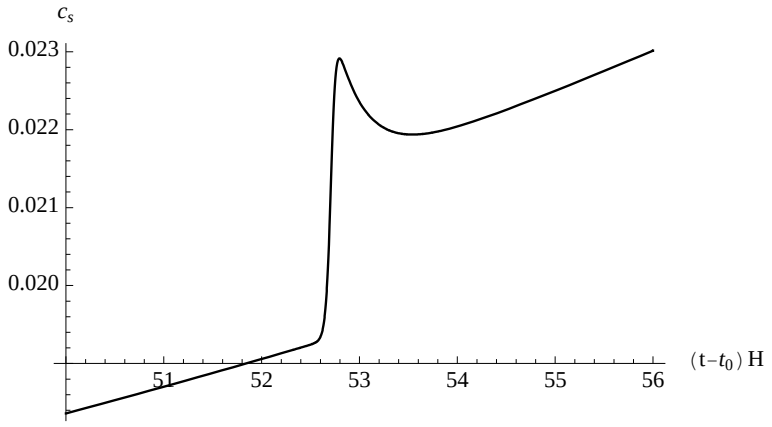

Figure 2.27: Evolution of c_s. Parameters are $b = 0.1$, step width $\Delta N_e = 0.05$, $\beta = 3$, $g_s m_s^{-4} = 10^{39}$, $N_B = 10^9$, $n_B = 10^4$, $n_A h_A^4 = 16$.

In summary, the behavior of c_s can be approximated by two step-functions side by side. In the first one, it jumps up from the original c_s to $c_s + 2bc_s$, during which the branes quickly fall down the step in warp geometry. The time scale is determined by d and is typically much smaller than $1/H$. The second one comes immediately afterwards, it jumps down from $c_s + 2bc_s$ to $c_s + bc_s$, during which the branes quickly approach the

new attractor solution. The time scale is of order $\mathcal{O}(1/H)$. The width of the second step function is much larger than the first for narrower step (i.e. smaller d). Note that in both stages, the velocity of branes increases. This evolution is illustrated in Fig. 2.27.

Because the width of step is very small, such a small change of c_s happens in a short period. This gives rise to large $s \equiv \dot{c}_s/(c_s H)$ and $\dot{s}/H$. This turns out to be the primary sources to various observable signatures in power spectrum and non-Gaussianities.

The Power Spectrum

The power spectrum is determined by the mode equation Eq.(2.23). We now estimate various parameters in Eq. (2.24) in terms of the size, b, and width, d, of the step feature in the warp factor. It is convenient to write d in terms of the e-fold that the brane spends moving across it,

$$\Delta N_e \equiv H\Delta t \approx H\frac{d}{\dot{\phi}} = \frac{d}{\sqrt{2c_s\varepsilon}} \ . \tag{2.204}$$

Note this is not the e-folds that the feature on CMB spans (denoted as Δl previously) which typically includes the oscillations and spreads much wider.

Using the continuity equation $\dot{\rho} = -3H(\rho + p)$, together with the energy density and pressure Eq.(2.7), we can solve for the evolution of s,

$$s = \frac{\dot{c}_s}{Hc_s} = 3(1-c_s^2) + \frac{c_s\dot{V}}{TH} + \frac{\dot{T}}{TH}(1-c_s) \ . \tag{2.205}$$

Here we can make more explicit the conditions under which the sharp features in warp factor dominate. On the right hand side of (2.205), to make the 3$^{\text{rd}}$ term larger than the first, i.e. to ignore the spatial expansion, we require $3 < \Delta T/(TH\Delta t) \approx 2b/\Delta N_e$; to ignore the 2$^{\text{nd}}$ term, i.e. the sharp features in potential, we require $c_s V_\phi < T_\phi$. Since the duality cascade leaves sharp steps on $T(\phi)$ but not $V(\phi)$, this condition is easily satisfied. Under these conditions, the last terms in the above equation dominates, so we

can approximate

$$s \approx \frac{\dot{T}}{TH} \sim \frac{b}{d}\sqrt{2\varepsilon c_s} \sim \mathscr{O}\left(\frac{b}{\Delta N_e}\right) . \tag{2.206}$$

This is consistent with (2.202).

Denote $X \equiv \dot{\phi}^2/2$, so $\varepsilon = X/(M_{\rm Pl}^2 H^2 c_s)$ for DBI inflation. We get

$$\eta = \frac{\dot{\varepsilon}}{H\varepsilon} = \frac{\dot{X}}{HX} + 2\varepsilon - s . \tag{2.207}$$

On the other hand, from the definition $c_s = \sqrt{1-2X/T(\phi)}$, we get

$$\frac{\dot{X}}{XH} = \frac{\dot{T}}{TH} - \frac{2c_s^2 s}{H(1-c_s^2)} . \tag{2.208}$$

Plug (2.208) into (2.207), and use (2.205) to get rid of $\dot{T}/TH$, we have

$$\begin{aligned} \eta &= \frac{c_s}{1+c_s}s - 3(1+c_s) - \frac{\dot{V}c_s}{HT(1-c_s)} + 2\varepsilon \\ &\approx c_s s - (3 + \frac{\dot{V}c_s}{HT}) . \end{aligned} \tag{2.209}$$

Except for the first term, the r.h.s. of this expression is affected little, $\mathscr{O}(b)$, by the feature. We use (2.209) to further estimate $\dot{\eta}/H$. Keeping the time derivatives on c_s, $\dot{\phi}$ and T, while ignoring those on V_ϕ and H, we get

$$\frac{\dot{\eta}}{H} \approx \frac{3}{2}s + c_s s^2 + c_s\frac{\dot{s}}{H} . \tag{2.210}$$

We have used the fact that the brane always tracks the speed-limit,

$$\dot{\phi} \approx \sqrt{T(\phi)} , \quad \ddot{\phi} \approx \frac{1}{2}\frac{T_\phi}{T}\dot{\phi}^2 , \tag{2.211}$$

since $c_s \ll 1$ even at the sharp feature as we know from Chapter 2.5.3. Eq. (2.206) is also used.

We further estimate $\dot{s}/H$,

$$\begin{aligned} \frac{\dot{s}}{H} &= \left(\frac{T_\phi}{T}\right)'\frac{\dot{\phi}^2}{H^2} + \frac{T_\phi}{T}\left(\frac{1}{H}\frac{d}{dt}\frac{\dot{\phi}}{H}\right) \\ &\approx \left(\frac{T_{\phi\phi}}{T} - \frac{T_\phi^2}{T^2}\right)\frac{\dot{\phi}^2}{H^2} + \frac{T_\phi}{T}\frac{\ddot{\phi}}{H^2} . \end{aligned} \tag{2.212}$$

Using Eq.(2.211) to eliminate the $\ddot{\phi}$ in Eq.(2.212), we get

$$\frac{\dot{s}}{H} \approx 2c_s\varepsilon\left(\frac{T_{\phi\phi}}{T}-\frac{1}{2}\frac{T_\phi^2}{T^2}\right)\approx 2c_s\varepsilon\left(\frac{T_{\phi\phi}}{T}\right)\sim b\,\frac{c_s\varepsilon}{d^2}\sim\mathscr{O}\left(\frac{b}{\Delta N_e{}^2}\right)\ , \quad (2.213)$$

where we have dropped the term T_ϕ^2/T^2, since $T_{\phi\phi}/T \gg T_\phi^2/T^2$ as long as $b \ll 1$.

We now can compare the amplitudes of various terms. Because both b and ΔN_e are small, from (2.206) and (2.213), we have

$$\frac{\dot{s}}{H} \gg s, s^2\ . \quad (2.214)$$

From (2.209) and (2.210),

$$s \gg \eta\ , \quad \frac{\dot{s}}{H} \gg \frac{\dot{\eta}}{H}\ . \quad (2.215)$$

So the only important contribution to z''/z is from $\dot{s}/H$, and we have

$$\frac{z''}{z} \approx 2a^2H^2\left(1-\frac{\dot{s}}{2H}\right)\approx 2a^2H^2\left(1-\frac{T_{\phi\phi}}{T}c_s\varepsilon\right)\ . \quad (2.216)$$

If we take T to be the form Eq.(2.201), we can evaluate

$$\begin{aligned}\frac{z''}{z} &\approx 2a^2H^2\left[1-b\frac{c_s\varepsilon}{d^2}\,\mathrm{sech}^2\left(\frac{\phi-\phi_s}{d}\right)\tanh\left(\frac{\phi-\phi_s}{d}\right)\right]\\ &\sim 2a^2H^2\left[1-\frac{b}{\Delta N_e^2}\,\mathrm{sech}^2\left(\frac{\phi-\phi_s}{d}\right)\tanh\left(\frac{\phi-\phi_s}{d}\right)\right]\ . \quad (2.217)\end{aligned}$$

The feature in z''/z is dictated by the $\mathrm{sech}^2\tanh$ term, and will affect the evolution of certain perturbation modes v_k. As moving across the step only generates $\sim N_e^{DBI}/M$ e-folds, typically $b/\Delta N_e^2 \gg 1$. The mode v_k will first see a dip in z''/z followed by a bump. Let us assume that the feature in z''/z shows up around conformal time τ_s, then modes with $c_s^2k^2 \gg (z''/z)|_{\tau_s}$ or $c_s^2k^2 \ll (z''/z)|_{\tau_s}$ will not be affected, because they are either oscillating well inside the sound horizon or have already crossed the sound horizon and got frozen. The major effect will be on the modes with $c_s^2k^2 \sim (z''/z)|_{\tau_s}$. The range of k affected by the sharp feature is determined by $b/\Delta N_e^2$. If P_ζ starts seeing the feature at k_0, the feature will disappear at

$$\Delta k \sim k_0\sqrt{b}/\Delta N_e\ . \quad (2.218)$$

Non-Gaussianities

Although Ref. [22, 31, 70] are only interested in non-Gaussianities without sharp features, the cubic expansion of the perturbations is exact and does not rely on the assumption that various inflationary parameters ε, η and s are small. For DBI inflation, among all the terms in Ref. [22], the leading term in the cubic action that is responsible for sharp features in non-Gaussianity is

$$\frac{a^3\varepsilon}{2c_s^2}\frac{d}{dt}\left(\frac{\eta}{c_s^2}\right)\zeta^2\dot{\zeta}\ . \tag{2.219}$$

In the absence of sharp features, a term such as $(a^3\varepsilon/c_s^4)\zeta\dot{\zeta}^2$ contributes to the non-Gaussianity estimator $f_{\rm NL}\sim 1/c_s^2$. Therefore as a rough estimate the term (2.219) contributes

$$f_{\rm NL}^{\rm feature}\sim\frac{d}{dt}\left(\frac{\eta}{c_s^2}\right)\Delta t\sim\Delta\left(\frac{\eta}{c_s^2}\right)\ . \tag{2.220}$$

The cases with large s are most interesting for non-Gaussianities. Using (2.209), $\eta\approx c_s s$, so

$$f_{\rm NL}^{\rm feature}\sim\frac{\Delta s}{c_s}\sim\frac{1}{c_s}\frac{b}{\Delta N_e}\ . \tag{2.221}$$

There is another term

$$-2\frac{a\varepsilon}{c_s^2}s\zeta(\partial\zeta)^2 \tag{2.222}$$

in the cubic action of Ref. [22] that contributes

$$f_{\rm NL}^{\rm feature}\supset\frac{s}{c_s^2}\Delta tH\sim\frac{\Delta c_s}{c_s^3}\sim\frac{b}{c_s^2}\ , \tag{2.223}$$

which is also possibly observable. The term (2.221) dominates for the most interesting cases.

The net observable effect will be a nearly-scale-invariant large non-Gaussianity of order $\mathcal{O}(1/c_s^2)$ plus the scale-dependent (oscillatory) modulation of order $\mathcal{O}(\Delta s/c_s)$.

Similar to the slow-roll case, we can write $f_{\rm NL}^{\rm feature} \sim (\sqrt{b}/c_s)(\sqrt{b}/\Delta N_e)$. As we have shown, the first factor determines the amplitude of the glitch in power spectrum through b, while the second factor determines the extension of its oscillations through (2.218). So there is a simple relation between the effects of sharp feature on the power spectrum and non-Gaussianity. For a same single visible glitch in power spectrum, the oscillatory amplitude of the bispectrum in DBI inflation is larger than that in slow-roll inflation mostly due to the factor of $1/c_s$ which can make $f_{\rm NL}^{\rm feature}$ larger than $\mathcal{O}(10)$; while for glitches that have long oscillatory extension (which can also be made invisible in power spectrum with tiny b), the associated bispectrum can be very large with tiny ΔN_e. The estimates of b and ΔN_e in Ref.[64] suggest that the well-separated steps in the duality cascade tend to fall into the latter category. We will later see independent evidence from fitting the power spectrum glitch to WMAP CMBR data.

2.5.4 Numerical Analyses and Data Fitting

We have analyzed qualitatively the behavior of the power spectrum around the step. However, due to the non-trivial behavior of z''/z, the mode equation is hard to solve analytically in general. To better understand the effect of the sharp feature, we numerically solve the equation of motion Eq.(2.8), evolve the mode equation Eq.(2.23) starting from when the mode is deep inside the sound horizon ($c_s^2 k^2 \gg z''/z$) until the mode is frozen when stretched out of the sound horizon ($c_s^2 k^2 \ll z''/z$), and evaluate the power spectrum numerically using Eq.(2.23). The numerical calculation also has the advantage that it is not necessary to assume certain simplification conditions in Chapter 2.5.3, such as $b/\Delta N_e \gg 1$. Our major results are shown in Fig. 2.28 and Fig. 2.29.

Fig. 2.28 shows the step feature in the power spectrum P_ζ for steps with different height b, but same width ΔN_e. We see clearly that in the power spectrum, a dip appears first with positive b and a bump appears first with negative b. However such a sequence

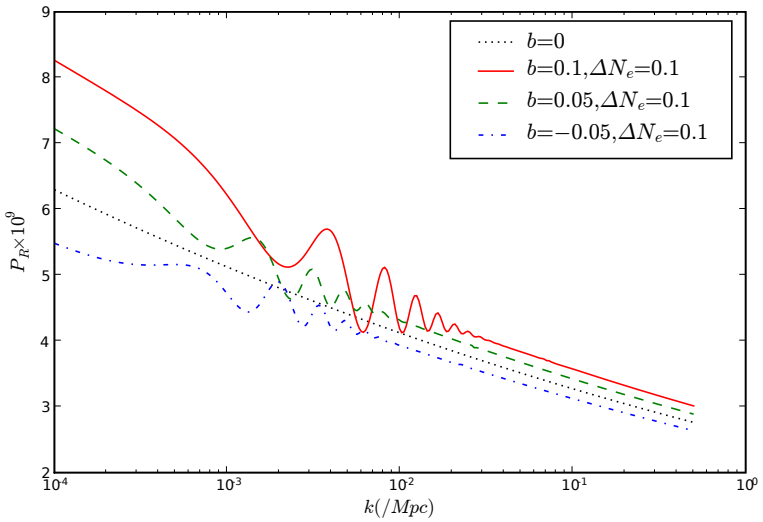

Figure 2.28: In the IR DBI scenario, we show the power spectrum, P_ζ, when there is a sharp step in the warp factor. For the same step width ΔN_e, we show three cases with different step size b. The amplitude of the first dip and bump increases as we increase the step height b. A bump appears first for $b < 0$ while a dip appears first for $b > 0$.

gets less clear after projecting from k-space to l-space.

In Fig. 2.29 we explore the step feature with different step width ΔN_e. We see that the oscillation amplitude in P_ζ is quite insensitive to the step width d. By the same argument in our slow-roll analysis, the steps are sharp so that $\Delta N_e \ll 1$. The c_s and $\dot{c}_s$ have reached their maximum values and so is the amplitude of the oscillation which is controlled by b.

In Fig. 2.30 we perform a χ^2 fit to the WMAP data. With one single step in the warp factor, we try to fit the $l \sim 20$ dip in WMAP temperature anisotropy. Here, instead of performing a full MCMC search for the best fit model, we only show an example to illustrate how the local step feature improves the quality of data fit. The example we show in Fig. 2.30 has the IR DBI model parameters $n_B = 6761, N_B = 4.315 \times 10^9, n_A h_A^4 = 0.01035, m_s/g_s^{1/4} = 2.567 \times 10^{-9} M_p, \beta = 4.021$, and the step parameters are $\Delta N_e =$

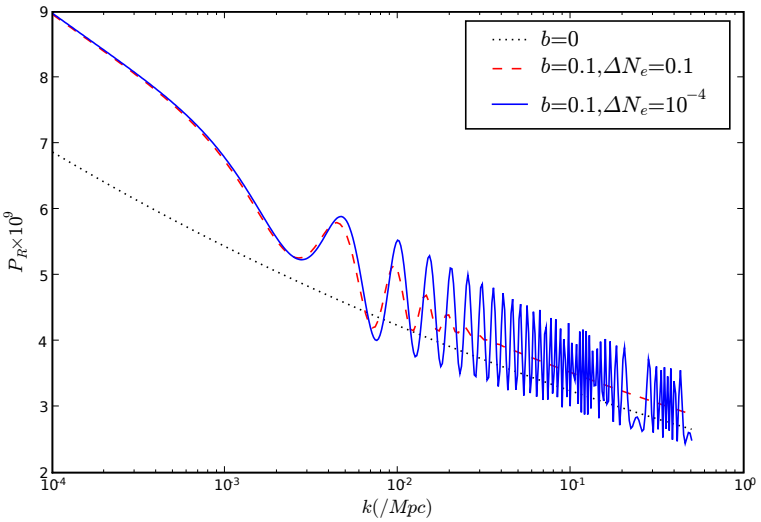

Figure 2.29: Same as Fig. 2.28, with the step size b fixed, we show two cases with different step width ΔN_e. Since in IR DBI model, the typical step width corresponds to $\Delta N_e \ll 1$, the dip and bump in the power spectrum is not sensitive to d. The width of the step affects only the range of oscillation in P_ζ.

0.105 and $b = -0.35$. The step model, with likelihood $\mathscr{L}$, $-2\ln\mathscr{L} = 5347.16$ when compared to WMAP 3-year temperature and polarization data [39, 38, 41, 40], has a better fit to the data, $\Delta\chi^2 = -2.76$, over the best-fit scenario with constant running of the spectral index, also shown. In light of the four extra degrees of freedom[7] determining the cascade power spectrum in comparison to the fiducial running model, however, this improvement in χ^2 is not statistically significant.

We also find that a positive b is not favored by data, so the first dip in the k-space does not necessarily transform into a clear dip in the l-space. Numerically we find that to fit the $l \sim 20$ dip, we need $|b| \sim 0.3$. However, if we take $b = +0.3$, it gives too much power on large scale, more than that is allowed by data.

The reason that the glitch appears to be less sharper than that in slow-roll case is

[7]Three of them specify the location, height and width of the step, another one is from IR DBI (versus LCDM).

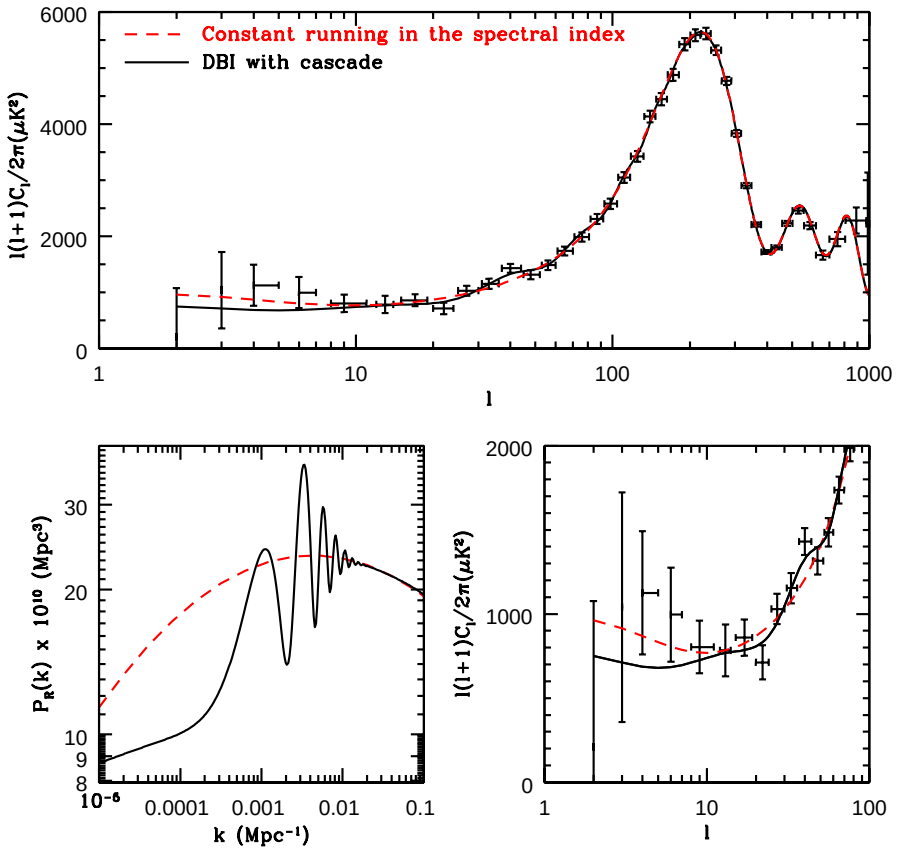

Figure 2.30: The CMB temperature power spectrum (top) and initial power spectrum (bottom left) in the presence of a step in the warp factor (full black line) and a best-fit scenario with constant running in the spectral index (red dashed line). The presence of large scale features in the cascade spectrum (bottom right) lead to an improved fit with the WMAP 3-year data of $\Delta\chi^2 = -2.76$ over the model with constant running in the spectral index.

the following. In DBI inflation, a step in warp factor not only causes oscillation in power spectrum, but also changes the asymptotic speed-limit of the inflaton. So in addition to glitches, it also introduces a step in the power spectrum. Both amplitudes are controlled by the relative height of the step b. It is more difficult to generate a sharp glitch while keeping the latter effect compatible with data. While in slow-roll case, asymptotic velocities of the inflaton is not affected by a local step in potential. In this sense, for DBI inflation the glitches in power spectrum can be made sharper if one introduces a bump (or anything that does not change the asymptotic behaviors of the warp factor) instead of a step in the warping.

We should also point out that $|b| \sim 0.3$ gives a step much larger than that given by Eq.(2.176) , which typically goes like $1/p^3$ with $p \gg 1$. This means that if we take the steps generated by the duality cascade, most probably we will not see any observable effects in the power spectrum. However, as we estimated in Eq. (2.221), the non-Gaussianities associated with the step can be very large depending on the height and width of the steps. This can leave distinctive features detectable by experiments.

2.5.5 Remarks on Closely Spaced Steps

We have been mainly concentrated on features that are sharp enough and well-separated (by at least one e-fold). We also see that there are parameter space where the feature is not sharp enough to show up in the CMB as observable signatures. In this case, the step is no longer important individually; but if there are parameter space such that, within one e-fold, the branes can go over many such small steps, a different kind of large non-Gaussianities can be generated through the "resonance mechanism" [71]. These closely spaced small steps induce small but high frequency oscillations of the background evolution in ε, η and s. This oscillation can resonant with the mode functions u_k when the mode is still within the horizon. As a result of this resonance, the non-Gaussianity

integration picks up a large contribution while the two-point function is only slightly affected. This non-Gaussianity has different signatures from the sharp feature case [71].

In slow-roll model, the condition to achieve this resonance mechanism relies on the shape of the potential. Naively, since we already have a series of steps, we can increase the tilt of the potential to make the branes roll faster so they come across many steps in one e-fold. Realistically, one needs to make sure that such a tilt will not significantly reduce the already-tuned total number of e-folds.

In IR DBI model, as we have discussed at the beginning of Chapter 2.5.3, there is actually a quite natural parameter space that such a condition can be satisfied, $1 > g_s > 10^{-3}$. We leave a more detailed study to a future publication.

CHAPTER 3

THE ISSUE OF ETERNAL INFLATION

In this chapter, we show that eternal inflation of the stochastic type is generically absent in the brane inflationary scenario [37]. Depending on how the brane inflationary universe originated, eternal inflation of the false vacuum type is still quite possible. Since the inflaton is the position of the $D3$-brane relative to the $\bar{D}3$-brane inside the compactified bulk with finite size, its value is bounded. In DBI inflation, the warped space also restricts the amplitude of the scalar fluctuation. These upper bounds impose strong constraints on the possibility of eternal inflation. We find that eternal inflation due to the random walk of the inflaton field is absent in both the slow roll scenario and the DBI scenario. In the multi-throat brane inflationary scenario, the branes may be generated by quantum tunneling and roll out the throat. Eternal inflation of the false vacuum type inevitably happens in this scenario due to the tunneling process.

3.1 Two Types of Eternal Inflation

The idea of eternal inflation was introduced more than 20 years ago, and has been considered as a generic phenomenon common to a wide class of inflationary models [72, 73, 74, 75]. If eternal inflation is present in the inflationary universe, the inflating part of the universe is exponentially larger than the non-inflating part (which includes our observable universe) today. This suggests that it is exponentially more likely for a random occurrence to take place in the part of the universe that is still inflating. This will force us to invoke something like the anthropic principle in order to explain our very existence. Although a weak form of such an anthropic principle may be acceptable, philosophically at least, the absence/presence of eternal inflation is an interesting question.

There are two types of mechanisms that drive eternal inflation. The first type involves a meta-stable false vacuum in the inflaton potential [74]. The false vacuum decays through bubble nucleation. If the decay rate Γ is slower than the expansion rate H, the false vacuum never totally disappears and the total volume of it, once inflation starts, continues to grow exponentially with time. So there are always bubbles of false vacuum in the entire universe where inflation continues. We call this eternal inflation of the false vacuum type.

The second type of eternal inflation was the stochastic eternal inflation. Let us think about the chaotic inflation scenario. Within one Hubble time, the inflaton field classically rolls down the potential by an amount

$$\Delta\phi = \dot{\phi} H^{-1} \ , \tag{3.1}$$

while at the same time, the intrinsic de-Sitter quantum fluctuation is

$$\delta\phi = \frac{H}{2\pi} \ . \tag{3.2}$$

If there is a regime where

$$\delta\phi > \Delta\phi \ , \tag{3.3}$$

The inflaton field could fluctuate up the potential quantum mechanically, and inflation will never end.

It is interesting to note that the ratio between $\delta\phi$ and $\Delta\phi$ is

$$\frac{\delta\phi}{\Delta\phi} = \frac{H^2}{2\pi|\dot{\phi}|} \sim \sqrt{P_\zeta} \ . \tag{3.4}$$

We know from observations that the primordial perturbation has an amplitude $\sqrt{P_\zeta} \sim 10^{-5} \ll 1$, at 55 e-folds from the end of inflation. Therefore, eternal inflation cannot happen if inflation only lasts for 55 e-folds, and the spectral index is red ($n_S < 1$). However, in most inflationary models, the range of inflaton field is unbounded, and one can

always start inflation high up on the potential, where quantum fluctuation is large. This is the main reason why eternal inflation in unavoidable in field theory models. However, as we will see in the next section, string compactification provides a bound on the inflaton field range, which exclude the possibility of stochastic eternal inflation for slow-roll brane inflation in the warped throat.

3.2 Absence of Eternal Inflation in the Slow Roll Scenario

In this chapter, we show that stochastic eternal inflation is absent in the simplest slow-roll scenario. The inflaton potential for the slow-roll scenario is,

$$V(\phi) = V_0 \left(1 - \frac{V_0}{4\pi^2 v}\frac{1}{\phi^4} + \frac{\beta}{6}\frac{\phi^2}{M_{\rm Pl}^2}\right) , \quad V_0 = 2T_3 h_A^4 \tag{3.5}$$

The slow roll parameters are

$$\begin{aligned} \eta_{\rm SR} &= M_{\rm Pl}^2 \left|\frac{V''}{V}\right| = \frac{\beta}{3} - \frac{20 M_{\rm Pl}^2 \phi_A^4}{N\phi^6} , \\ \varepsilon_{\rm SR} &= \frac{M_{\rm Pl}^2}{2}\left(\frac{V'}{V}\right)^2 = \frac{1}{2}\left[\frac{4M_{\rm Pl}\phi_A^4}{N\phi^5} + \frac{\beta\phi}{3M_{\rm Pl}}\right]^2 . \end{aligned}$$

The end of inflation is given by $\eta_{\rm SR} = -1$

$$\phi_E^6 = \frac{1}{1+\beta/3}\left(\frac{20\phi_A^4}{NM_{\rm Pl}^4}\right) M_{\rm Pl}^6 . \tag{3.6}$$

The inflaton field ϕ_N is at N_e e-fold before the end of inflation, and the scalar density perturbation δ_H are given by [23]

$$\phi_N^6 = \frac{\phi_A^4}{NM_{\rm Pl}^4}(24N_e + 20)\Omega(\beta) M_{\rm Pl}^6 , \tag{3.7}$$

$$\delta_H = \frac{2}{45}(24N_e+20)^{5/6}\left(\frac{\phi_A^4}{M_{\rm Pl}^4 N}\right)^{1/3} f(\beta) , \tag{3.8}$$

$$\begin{aligned} \Omega(\beta) &\equiv \frac{(1+2\beta)e^{2\beta N_e} - (1+\beta/3)}{2\beta(N_e+5/6)(1+\beta/3)} , \\ f(\beta) &\equiv \frac{1+\beta/3}{1+2\beta}\Omega(\beta)^{5/6} e^{-2\beta N_e} . \end{aligned}$$

We can use (3.8) to express ϕ_A^4/N as a function of β,

$$\frac{\phi_A^4}{M_{\rm Pl}^4 N} = \left(\frac{45\delta_H}{2}\right)^3 (24N_e+20)^{-5/2} f(\beta)^{-3} \ . \tag{3.9}$$

Given the value of β, we can impose the COBE normalization $\delta_H = 1.9\times 10^{-5}$ at $N_e = 55$ [3], and fix ϕ_A^4/N. For the slow roll regime $0 \le \beta \le 1/7$, we get

$$1.2\times 10^{-18} \le \frac{\phi_A^4}{M_{\rm Pl}^4 N} \le 3.5\times 10^{-12} \ , \tag{3.10}$$

Using (3.2) and (3.1), the quantum fluctuation and classical motion of ϕ are given respectively as

$$\delta\phi = \frac{4}{9}\sqrt{\frac{\phi_A^4}{NM_{\rm Pl}^4}} M_{\rm Pl} \ , \tag{3.11}$$

$$\Delta\phi = \frac{4\phi_A^4}{NM_{\rm Pl}^4}\left(\frac{\phi}{M_{\rm Pl}}\right)^{-5} M_{\rm Pl} + \frac{1}{3}\beta\phi \ . \tag{3.12}$$

To compare the magnitude of quantum fluctuation and classical motion, it is important to notice that $\Delta\phi$ has a minima,

$$(\Delta\phi)_{\rm min} = \frac{24}{60^{5/6}}\left[\frac{\phi_A^4}{NM_{\rm Pl}^4}\beta^5\right]^{1/6} M_{\rm Pl} \ . \tag{3.13}$$

If for certain values of β, $\Delta\phi_{\rm min} > \delta\phi$, the classical motion always dominates over the quantum fluctuation, and eternal inflation will never happen. Using (3.11)(3.13), the range of β is determined by

$$\frac{4}{9}\sqrt{\frac{\phi_A^4}{NM_{\rm Pl}^4}} < \frac{24}{60^{5/6}}\left[\frac{\phi_A^4}{NM_{\rm Pl}^4}\beta^5\right]^{1/6} \ ,$$

where ϕ_A^4/N is also a function of β as seen in (3.9). Solving the inequality numerically, we get

$$3.4\times 10^{-8} < \beta \le 1/7 \ . \tag{3.14}$$

Apparently for the slow roll regime $0 \le \beta \le 1/7$, eternal inflation is possible only when

$$\beta < 10^{-8} \ . \tag{3.15}$$

A significant amount of fine tuning is needed to achieve this value, since the moduli stabilization generically gives $\beta \sim 1$ [12].

For the range $0 \leq \beta \leq 10^{-8}$, $f(\beta) \approx 1$, $\Omega(\beta) \approx 1$, the β dependence becomes so small that it is safe to simply set $\beta = 0$. Now, using Eq.(3.11), $\Delta\phi < \delta\phi$ indicates that eternal inflation happens when

$$\phi > \phi_c = \left(\frac{81\phi_A^4}{NM_{\rm Pl}^4}\right)^{1/10} M_{\rm Pl} = 0.025 M_{\rm Pl} \ . \tag{3.16}$$

There appears a critical value of the inflaton field $\phi_c = 0.025 M_{\rm Pl}$. Inflation will be eternal if it starts with $\phi_i > \phi_c$.

For brane inflation in the warped throat, we require that at least 55 e-folds are achieved in side the throat, i.e.

$$\phi_A < \phi_E < \phi_{55} \leq \phi_{\rm edge} \ . \tag{3.17}$$

Here, inflation ends when ϕ reaches ϕ_E, where tachyons appear and the $D3-\bar{D}3$ brane annihilation begins. ϕ_{55} corresponds to the position of the $D3$-brane at 55 e-fold before inflation ends, ϕ_i is the initial position where inflation starts, and $\phi_{\rm edge} \equiv \sqrt{T_3}R$ is the edge of the throat.

Using (3.7), we get $\phi_{55} = 3.4 \times 10^{-3} M_{\rm Pl} \ll \phi_c$, so we will surely get enough number of e-fold if inflation starts with ϕ_c. However, the constraint $\phi_c < \phi_{\rm edge}$ is non-trivial, since $\phi_{\rm edge}$ depends on T_3 and N,

$$\phi_{\rm edge} = \sqrt{T_3}R = \left(\frac{27NT_3}{32\pi^2}\right)^{1/4} \ ,$$

where $\phi_c/\phi_{\rm edge} < 1$ requires

$$N > \frac{256\pi^5}{27} g_s \left(\frac{\phi_c}{M_{\rm Pl}}\right)^4 (\alpha' M_{\rm Pl}^2)^2 \approx 10^{-3} g_s (\alpha' M_{\rm Pl}^2)^2 \ . \tag{3.18}$$

There is another constraint we have to take into account. Assuming the Planck mass is dominantly contributed by the bulk volume, as it typically happens to a warped compactification, we have

$$M_{\rm Pl}^2 = \frac{m_s^8 L^6}{\pi g_s^2} \ , \tag{3.19}$$

where g_s is the string coupling and $m_s = 1/\sqrt{\alpha'}$. Here $2\pi L$ is roughly the dimension of the bulk. Since the throat is part of the bulk, we naturally require

$$L > R \ . \tag{3.20}$$

The requirement (3.20) implies an upper bound for the AdS throat charge,

$$N < \frac{4}{27}\left(\frac{g_s}{\pi}\right)^{1/3}(\alpha' M_{\rm Pl}^2)^{2/3} \ . \tag{3.21}$$

It is obvious that the lower bound of N (3.18) cannot exceed the upper bound (3.21), so we require

$$\frac{256\pi^5}{27} g_s \left(\frac{\phi_c}{M_{\rm Pl}}\right)^4 (\alpha' M_{\rm Pl}^2)^2 < \frac{4}{27}\left(\frac{g_s}{\pi}\right)^{1/3}(\alpha' M_{\rm Pl}^2)^{2/3} \ ,$$

which leads to a constraint on α'

$$\alpha' M_{\rm Pl}^2 < \frac{1}{(2\pi)^4\sqrt{2g_s}}\left(\frac{\phi_c}{M_{\rm Pl}}\right)^{-3} \ . \tag{3.22}$$

The upper bound of N (3.21) is maximized if we push α' to the upper bound given in (3.22). Thus to make eternal inflation possible, the largest value of N is

$$N < \frac{1}{(2\pi)^3}\frac{4}{27}\left(\frac{\phi_c}{M_{\rm Pl}}\right)^{-2} = 0.95 \ . \tag{3.23}$$

In the KKLMMT scenario, typically $N \gg 1$. This means that if we assume the inflaton potential in the bulk is not very flat and inflation only happens in the throat, the critical initial value ϕ_c is impossible to be consistently realized in the KKLMMT scenario. That is, the stochastic eternal inflation is absent.

There are at least 3 possible ways for stochastic eternal inflation to be present in this scenario:

1. The potential has additional contributions [20]. That may change the above analysis if the potential is changed substantially.

2. The brane can start in the bulk instead of only from the UV side of the throat; this may allow us to evade the constraint (3.23). The antibrane in the end of the throat provides a red-shifted Coulomb attraction source and the potential is similar to the first two terms in the (3.5). Assume one can tune away the potential from the moduli stabilization (in the same sense as requiring an extremely small β), the relaxed constraint on ϕ_c is $\phi_c < L\sqrt{T_3}$, which implies

$$L > (2\pi)^3 g_s \alpha'^2 \phi_c^2 \ . \tag{3.24}$$

The condition (3.20) still applies here so we still have the same upper bound of N as in (3.21). It is obvious that (3.24) and (3.21) are not contradictory and by choosing appropriate values of L and α', we can have $N \gg 1$. So in the case when we get a good fraction of e-folds from the bulk, eternal inflation is possible when $\beta < 10^{-8}$ and inflation starts with $\phi_i > \phi_c$.

3. If the throat is a long narrow throat (that is, its width is much smaller than its length), then the bound (3.20) is relaxed. Orbi-folding a deformed conifold can be a way to achieve this. Even if this bound is relaxed, we note that the bound (3.15) is still very tight.

3.3 Absence of Eternal Inflation in the DBI Scenario

For UV-DBI inflation in the ultra-relativistic regime, we have seen in Chapter 2.3.2 that the background solution can be solved using Eq.(2.79). $H = c\,\phi$, which gives $c_s^{-1} = \gamma \sim M_{\rm Pl}^2/\phi^2$, and $\varepsilon \sim$ const. Therefore, the primordial power spectrum is

$$P_\zeta = \frac{H^2}{8\pi^2 M_{\rm Pl}^2 \varepsilon\, c_s} \sim \text{const} \ . \tag{3.25}$$

This means if we impose the normalization $P_\zeta \sim 10^{-9}$ at $N_e = 55$, we'll have the same normalization at any number of e-folds. The fact that P_ζ has no ϕ dependence is largely

due to the ultra-relativistic motion of the brane. Recall the argument (3.4), we see that for ultra-relativistic fast roll inflation, $\delta\phi \ll \Delta\phi$ all the way through the throat no matter where inflation starts. For UV model with $\gamma \gg 1$ and quadratic potential, eternal inflation will not happen.

In the IR model of the DBI inflation, the brane is moving out from the IR side of the warped space. During most of the inflationary epoch, the Hubble parameter is approximately a constant and a de Sitter phase of inflation is triggered. The field theory calculations [14, 28] show that the spectral index is red and the inflaton can be extended back in time to the deep IR region of the AdS throat. So naively the eternal inflation of random walk type is possible. But interestingly as we will see, by considering the validity of the field theory analyses, a rather different mechanism [28, 29] kicks in before the condition (3.4) can be satisfied.

When calculating the quantum fluctuations in the expanding background, for the field theory to work, we require that the Hubble energy be smaller than the (red-shifted) string scale,

$$\gamma H \lesssim T(\phi)^{1/4} , \tag{3.26}$$

where H is the Hubble constant, $T(\phi) = \phi^4/\lambda$ is the warped brane tension. It is easiest to get Eq. (3.26) on the moving frame on the brane, where the Hubble expansion is faster by a factor of γ because of the relativistic time dilation. A closely related consequence is the reduction of the horizon size by a factor of γ^{-1}.

The evolution of the brane position (inflaton) is given by

$$\phi \approx -\frac{\sqrt{\lambda}}{t} , \tag{3.27}$$

where t runs from $-\infty$. The inflation ends when $t \sim -1/H$. The number of inflationary e-folds to the end of the inflation is

$$N_e \approx -Ht . \tag{3.28}$$

During inflation the inflaton travels ultra-relativistically,

$$\gamma \approx \frac{\beta N_e}{3} \ , \tag{3.29}$$

where β again parameterizes the steepness of the potential $V = V_0 - \frac{1}{2}\beta H^2\phi^2$. Using these field theory results of the IR DBI inflation, we translate (3.26) into

$$N_e \lesssim \frac{\lambda^{1/8}}{\beta^{1/2}} \ , \tag{3.30}$$

where λ is the $D3$-charge of the background, e.g. given by three-form fluxes. Namely the field theory results only applies to the short scales satisfying (3.30). Above that, the quantum fluctuations become stringy. (The zero-mode inflation still proceeds as long as back-reactions on the background throat, including those from the relativistic probe brane [13, 28, 52] and those from the de Sitter expansion [28], can be neglected.)

Although a full understanding of this stringy phase requires a full string theory treatment, we can see a bound on the scalar fluctuation amplitude in the following way. In expanding background, the quantum fluctuations are generated during a Hubble time $\gamma^{-1}H^{-1}$, and then get stretched out of the horizon and lose causal contact. Within this period, the brane fluctuates in the transverse directions, but the fluctuation speed is limited by the local speed of light h^2. So the maximal amplitude for a moving frame observer is

$$\Delta r_{max} \approx \gamma^{-1}H^{-1}h^2 \ . \tag{3.31}$$

To see that it is consistent with our previous arguments, we note that from field theory, the density perturbation in IR DBI is

$$\delta_H \approx H\delta t \approx N_e^2/\lambda^{1/2} \ , \tag{3.32}$$

and the brane fluctuation is

$$\Delta r = \gamma\delta r \approx \gamma\dot{r}\delta t \approx \gamma h^2\delta t \ , \tag{3.33}$$

where δt is the time delay measured by a lab observer, $\dot{r}$ is the brane speed (zero-mode scalar speed) which is approximately the speed of light h^2 because the brane travels ultra-relativistically in DBI inflation. Requiring

$$\Delta r \leq \Delta r_{max} \tag{3.34}$$

gives the same condition as (3.30).

But the condition (3.34) is more transparent in terms of the scalar fluctuation amplitude. We get

$$\delta_H \approx H\delta t \lesssim H\frac{\Delta r_{max}/\gamma}{h^2} \approx 1/\gamma^2 \ . \tag{3.35}$$

(Note that in this formula the time decay δt is measured in the non-moving lab frame. That's why the Lorentz contraction factor $1/\gamma$ arises in $\Delta r_{max}/\gamma$.) This means that, although naively from field theory results (3.32) that δ_H can grow to one as we look at large enough N_e , it actually has a upper bound far below one, since $\gamma \gg 1$. The type of eternal inflation caused by the random walk of the scalar field is forbidden. We note that this type of constraint applies to general DBI inflation models.

3.4 Possible Presence of Eternal Inflation in Brane Inflation

On Top of the Potential in the Bulk

Because of the compactness of the extra dimensions, it is inevitable that some parts of the inflaton potential profile may have vanishing first derivative. Especially for those potentials that grow toward the bulk, such as those we have considered in the KKLMMT slow-roll or UV DBI inflation, at somewhere in the bulk $V_{\phi_i} = 0$ and $V_{\phi_i\phi_j} < 0$ will appear. Classically the inflaton velocity can be infinitely small if it stays on the top of such a potential. So it is interesting to look in more details the conditions for the random walk type eternal inflation to happen.

Let us simplify the form of such a potential to be $V = V_0 - \frac{1}{2}m^2\phi^2$, where ϕ is measured with respect to the top of the potential. Using the standard slow-roll results, we know that the density perturbation δ_H becomes one at the place

$$\hat{\phi} = \frac{V_0^{3/2}}{5\sqrt{3}\pi M_p^3 m^2} \ . \tag{3.36}$$

Because of the quantum fluctuations of the inflaton, the precision of putting a brane on the top of potential is given by $\delta\phi = H/2\pi$. Therefore we require $\hat{\phi} > H/2\pi$. This is always satisfied given that $m^2 \ll H^2$, i.e. the condition that the inflation happens on the top of such a potential. Therefore eternal inflation of the random walk type happens in the bulk if such an inflationary potential can be obtained by fine-tuning, for example in the models of Ref. [9, 76].

It is worthwhile to point out another key difference between brane inflation and a more traditional inflationary scenario such as chaotic inflation. In chaotic inflation, if we are willing to accept a random value for the initial inflaton field in the presence of many causally disconnected patches, it is reasonable that the inflaton field takes an initial value larger than the critical value in at least one patch, thus leading to eternal inflation. Even if the inflationary universe was created spontaneously with only one patch, one may argue it is more likely that $\phi_{\rm ini} > \phi_c$, since $\phi_{\rm ini}$ can apriori take an arbitrarily large value in the absence of any selection principle (such as the wavefunction of the universe). In brane inflation, the inflationary universe typically starts with one or more pairs of $D3 - \bar{D}3$ branes, where all values of ϕ s are bounded by the size of the bulk. First consider the case with only one pair inside one causal patch. There is no reason that the $\bar{D}3$ brane starts out sitting precisely at the bottom of a throat. In general, it will start somewhere in the bulk and then, due to the attractive force, move relatively quickly towards the bottom of the throat. While this is happening, its tension will start dropping and the potential for the $D3$ brane will approach the eventual one that is adopted above. That is, the $D3$ brane is seeing a rapidly changing potential as it is moving in the bulk. While

this is happening, both the position and the height of the inflaton potential at the top of the hill discussed above have not even emerged yet. We expect the $D3$ brane to be dragged towards the throat during this time. So, it seems some fine-tuning is needed for the $D3$ brane to end up at the top of the hill after the $\bar{D}3$ brane has settled at the bottom of the throat. Clearly a more careful analysis is warranted. Obviously, this pictures gets much more complicated if we start with multi-pairs of $D3-\bar{D}3$ branes or some other arrangements. However, in this case it seems that the random walk type eternal inflation is possible but absent under generic initial conditions. Of course, if inflation comes only from the motion of the D3 brane (that is, no $\bar{D}3$ brane), then the random walk type eternal inflation becomes more likely.

We may apply the same argument if the inflaton potential has a local shallow minimum in the bulk. The attractive force of the $\bar{D}3$ brane plus its motion tend to drag the $D3$ brane towards the throat. Of course, if the minimum is deep enough, then the $D3$ brane may be stuck there. This leads to eternal inflation of the tunneling type.

At the Tip of the IR Throat

The top-of-a-hill like potential is also possible when we extend the potential to the tip of a throat, analogous to the potential in the IR DBI model. The difference is that we are now interested in a fine-tuned slow-roll shape, $|\beta| \ll 1$. The same discussion of the last subsection applies except for the following complication. If the throat is very long, i.e. extends to $\phi \to 0$, the slow-roll inflationary phase will smoothly transit to the DBI inflationary phase at $\phi_{\rm DBI} = \beta\sqrt{N}H$ for $N > \beta^{-2}$ [28]. This is because towards the IR end of the throat, the speed-limit constraint becomes more important and have to be taken into account. So if the IR end of the throat is terminated at $\phi > \phi_{\rm DBI}$, the warping does not change beyond the cutoff, and we get stochastic eternal inflation near $\hat{\phi}$. Otherwise, if the throat is terminated at $\phi < \phi_{\rm DBI}$, the inflation will become the DBI

type before the slow-roll inflation can reach the critical point of eternal inflation. In DBI region, the stochastic eternal inflation is forbidden as we saw in Chapter 3.3. However, the warping of a throat cannot extend to infinity in the IR end, either because of a cutoff or the back-reaction of the dS space which will smooth out the warping in the IR end of the warped space starting at $\phi \approx H$ [28, 51]. Hence the speed limit constraint will not further increase beyond this point, and the inflation smoothly changes back to be the slow-roll type on the top of the hill. In this case it is this period of slow-roll inflation that may be responsible for random walk eternal inflation, if the branes start from there.

Multi-throat Brane Inflation

So far we have concentrated on the eternal inflation of the Brownian type. We saw that in brane inflation such a mechanism is either tightly constrained or forbidden for various different reasons. As mentioned in the introduction, however, eternal inflation is also possible through a first order phase transition of false vacuum bubble nucleation. In this and next subsection, we discuss this mechanism in brane inflation.

Warped compactification in type IIB string theory is a natural place to realize the brane inflation. In such a case, there is a very natural mechanism to generate candidate inflaton branes in the multi-throat brane inflationary scenario [14, 28]. The AdS throats are sourced by RR and NSNS three-form fluxes localized at conifold singularities on a Calabi-Yau manifold. The $\bar{D}3$-branes will naturally settle down in throats, since they carry opposite $D3$ charge to the throats and will be attracted to the IR end. These antibranes have different lifetimes in different throats depending on the numbers of fluxes and antibranes, and they will eventually annihilate against the fluxes which source the throats [50, 77]. If the number p of antibranes is much smaller than the number M of the RR fluxes, such an annihilation process proceeds through a quantum tunneling. At the end of this annihilation, $M - p$ number of $D3$ branes will be created to conserve the

total $D3$ charge. These $D3$ branes will either stay or come out of the throats, depending on the sign of the mass-squared of the moduli potential. In the latter case, they become a direct source of inflaton for IR DBI inflation; or when they move into the bulk and re-settle down elsewhere, become an indirect source of inflaton for other types of brane inflation such as KKLMMT type slow-roll inflation or UV DBI inflation. Therefore, in this multi-throat scenario, the quantum tunneling in the flux-antibrane annihilation is responsible for creating successful inflation bubbles. As we know such a bubble creation process is naturally eternal.

CHAPTER 4

COSMIC INFLATION IN THE STRING LANDSCAPE

4.1 The Meandering Inflaton Scenario

The study of the inflationary universe is mainly on the slow-roll model with a single inflaton field. An important reason to focus on the single field case is simplicity. A typical multi-field inflationary scenario is clearly very complicated and not predictive. If the inflaton fields couple to each other during inflation and reheating, the problem seems rather intractable. Motivated by the realization of inflation in superstring theory, we expect a multi-field inflationary scenario. The scenario could apply to brane inflation in the compactified bulk. A generic bulk compactification must be very complicated, with different type of warped throats in different regions. An inflaton brane could move inside the bulk, before it falls into one of the throat; or it could come out of a throat, wanders in the bulk, and fall into another throat. This scenario could also happen if inflation takes place in the stringy cosmic landscape[11], where the number of moduli is probably as large as hundreds. Even if not all of them participate in inflation, it is likely that a large subset of moduli contribute directly or indirectly to the inflationary scenario. Their interaction can be rather complicated (maybe strongly interacting as well), generating a cosmic landscape that is random (aperiodic) in some directions and quasi-periodic (within certain field range) in others.

In a generic string compactification, one expects the string scale to be in between the Hubble and the Planck scale, $H \ll m_s \ll M_{\rm Pl}$, so that a single Planck scale field range in the landscape naturally contains many string scale features. For our purpose here, the cosmic landscape may be approximated by a d-dimensional random potential, and the inflaton (the scalar mode for inflation) path appears smooth in the coarse-grained limit, but is actually rugged with fine-grained string scale features [78, 79]. The generic

properties of such an inflationary scenario are:

1. At least 60 e-folds of inflation is necessary in an inflationary scenario to solve the well-konwn cosmological problems such as the flatness and the horizon problems. To achieve this in the slow-roll inflationary scenario usually requires an almost flat smooth potential. Without any fundamental theory, one can always invent such a potential. However, in the context of string theory, such an almost flat potential requires some fine-tuning. While a generic potential may not be flat enough, it is not necessarily smooth either. A rugged d-dimensional potential is more realistic in the context of the cosmic landscape (Fig.4.1), where $d \gg 1$. For large enough d, percolation probability approahes unity so the wave function of the universe is mobile in the landscape [80, 81, 82]. For a Planck scale field range, one expects many string scale features and consequently the inflaton takes a meandering path. Since the de-Sitter quantum fluctuation (H) is smaller than the size of the features (m_s), the turns of the inflaton path may be treated as classical scatterings. We will prove that an arbitrary detour of the inflaton path always increases the travel time, leading to more e-folds than given by the corresponding coarse-grained smooth potential. With appropriately many features in the potential, enough e-folds of inflation becomes generic. Although the scenario is motivated by the cosmic landscape, if a specific string compactification is complicated enough, a brane motion inside the bulk can exhibit similar meandering behavior.

2. The above scenario naturally leads to fluctuations in the the cosmic microwave background radiation (CMB) temperature (TT) and polarization (TE/EE) power spectra. These fluctuations are due to the turns and detours of the inflaton path in the d-dimensinal potential. Due to the randomness of the features in the potential, such fluctuations appear with irregular spacings, magnitudes and shapes [78]. While some of these features are probably too fine and/or small to be detected,

a few big fluctuations may already have been observed in the data [83, 84, 85]. With more data coming in the future, one expects this prediction to be well tested. The existence of such fluctuations will have a profound impact on the inflationary scenario, on the origin of our universe and on the existence and properties of the cosmic landscape.

3. Non-Gaussianity is generically suppressed by the growth of adiabatic perturbations on super-horizon scales, and is negligible in the weakly random scenario. However, non-Gaussianity can possibly be enhanced by resonant effects in the strongly random scenario or arise from the entropic perturbations during the onset of (p)reheating if the background inflaton trajectory exhibits particular properties.

4.1.1 Detours Always Lead To More *e*-folds

Let $\vec{\phi} \equiv (\phi_1, \phi_2, \ldots, \phi_d)$ be the canonical inflaton field in the d-dimensional field space (indices are raised by δ^{IJ}), and let $V(\vec{\phi})$ be the actual d dimensional scalar potential. We assume that over relatively large field distances, the potential appears coarse-grained smooth, denoted by $V_c(\vec{\phi})$, which may or may not be flat enough to support 60 e-folds of inflation, and may suffer from the η problem. For a small enough field range, we are safe to keep only the linear term in the Taylor-expansion of $V_c(\vec{\phi})$. Without loss of generality, for a specific small field range, we can rotate to the basis $\vec{\phi} = \{\phi_{I'}, \sigma\}$ (I' denotes all directions transverse to σ.), so that $V_c(\vec{\phi})$ for this segment has gradient only along the σ field,

$$V_c(\vec{\phi}) = V_0 - b\,\sigma\ , \quad 0 \leq \sigma \leq \sigma_f\ . \tag{4.1}$$

where the constant $b > 0$ and σ_f denotes the validity range of the linear expansion. This yields a straight inflaton path from $\vec{\phi} = \mathbf{0}$ to $(0, \ldots, \sigma_f)$. When the inflaton moves beyond σ_f, one needs to re-expand the potential with a new slope b' and a new σ direction. In

this way, one can approximate an arbitrary coarse-grained smooth potential using a set of piecewise linear segments.

In this chapter, we take the Hubble parameter $H \approx$ const and we use the slow-roll approximation ($3H\dot{\phi}_I = -\nabla_I V$) for the field range $[0, \sigma_f]$. The qualitative properties are robust even when these approximations are relaxed.

Now the actual potential is rugged instead of smooth. Let us introduce fine grained features to $V_c(\vec{\phi})$ (4.1) to reproduce or to better approximate the actual potential. Starting with $\vec{\phi} = \mathbf{0}$ at $t = t_1 = 0$, the slope $\vec{s} \equiv (s_1, s_2, \ldots, s_d)$ changes at t_k from $\vec{s}(k-1)$ to $\vec{s}(k)$ ($t_{k+1} > t_k$,$k = 1, \ldots, K-1$),

$$s_I(k) = b\,\delta_{dI} + \sum_{j=1}^{k} \delta_I(j) \tag{4.2}$$

where $\vec{\delta}(j)$ is a constant vector parameter for the j-th step. The potential for $t_k \le t < t_{k+1}$ now becomes (denote $\vec{\phi}(j) \equiv \vec{\phi}(t_j)$)

$$V(\vec{\phi}) = V_0 - \sum_{j=1}^{k-1} \vec{s}(j) \cdot \left[\vec{\phi}(j+1) - \vec{\phi}(j)\right] - \vec{s}(k) \cdot \left[\vec{\phi} - \vec{\phi}(k)\right] \ . \tag{4.3}$$

Since we are treating $V_c(\vec{\phi})$ as the background potential, we require that, after K steps, $\vec{\phi}$ will reach $\vec{\phi}(K) \equiv (0, \ldots, \sigma_f)$, i.e.

$$\phi_{I'}(K) = \sum_{j=1}^{K-1} \frac{s_{I'}(j)}{3H}\,(t_{j+1} - t_j) = 0 \ , \tag{4.4}$$

$$\sigma(K) = \frac{b\,t_K}{3H} + \sum_{j=1}^{K-1} \frac{s_\sigma(j)}{3H}\,(t_{j+1} - t_j) = \sigma_f \ . \tag{4.5}$$

We also require that both the coarse-grained smooth potential $V_c(\phi)$ (4.1) and the actual potential $V(\phi)$ (4.3) begin at $\vec{\phi} = \mathbf{0}$ with value V_0 and end at $\vec{\phi} = (0, \ldots, 0, \sigma_f)$ with value $V_c(\sigma_f)$ (as illustrated in Fig.4.1), namely

$$\sum_{j=1}^{K-1} \sum_{I',\sigma} s_I(j) \left[\phi^I(j+1) - \phi^I(j)\right] = b\,\sigma_f \ . \tag{4.6}$$

Let us count the number of free parameters. For K steps, we introduce $K-1$ time parameters t_k ($2 \le k \le K$). For each $\phi_{I'}$ and σ, we introduce $K-1$ fluctuation parameters

$\delta_I(i)$, altogether $(K-1)d$ parameters. Taking into account the $d+1$ constraints from Eq.(4.4), Eq.(4.5) and Eq.(4.6), the number of parameters is $(K-1)+(K-1)d-(d+1)=(K-2)(d+1)$. The actual potential can be approached in the $K\to\infty$ limit.

To proceed, we need to properly choose σ_f, so that not only the linear expansion is valid, but also the σ field is monotonic and can be used as our "clock". (Otherwise, we have to choose a finer-grained piece-wise linear approximation.) As we shall see, this also limits the sizes of the kinks. We now show that *an arbitrary detour from $V_c(\vec{\phi})$ (4.1) will take longer to reach $V_c(\sigma_f)$*. Such an increase in the number of e-folds of inflation is unbounded from above.

Using σ as the variable, we can rewrite the d-dimensional potential $V(\vec{\phi})$ as an effective 1-dimensional potential $V_{\rm eff}(\sigma)$. For $d=1$, $V_{\rm eff}(\sigma)$ reduces to $V(\phi)$.

$$V_{\rm eff}(\sigma) \;=\; V_0 - b\,\sigma - \hat{S}(k)\,[\sigma-\sigma(k)] - \sum_{j=1}^{k-1}\hat{S}(j)\,[\sigma(j+1)-\sigma(j)]\;, \qquad (4.7)$$

$$\hat{S}(j) \;=\; \hat{s}_\sigma(j) + \sum_{I'}\frac{\hat{s}^2_{I'}(j)}{b+\hat{s}_\sigma(j)}\;, \quad \sum_{j=1}^{K-1}\hat{S}(j)[\sigma(j+1)-\sigma(j)] \;=\; 0\;. \qquad (4.8)$$

where the last equation is simply the constraint (4.6). In this sense, Fig.4.1 may also represent the $V_{\rm eff}(\sigma)$ for $d>1$.

We now show how arbitrary features of the potential increases the number of e-folds when compared to the smooth linear potential. Let us also generalize the piecewise constants $\hat{s}_I$ and $\hat{S}$ to continuous functions of σ (one may view this as a $K\to\infty$ limit) so the number of e-folds can be expressed as $N_e=\int {\rm d}\sigma\, 3H^2/(b+\hat{s}_\sigma(\sigma))$. Here $\hat{s}(\sigma)\equiv\vec{s}(\sigma)-\vec{b}$, i.e., $\hat{s}_\sigma = s_\sigma - b$, $\hat{s}_{I'}=s_{I'}$.

Now N_e can be regarded as functional of $\hat{s}_I(\sigma)$,

$$N_e[\hat{s}] = \int\frac{{\rm d}\sigma\, 3H^2}{b+\hat{s}_\sigma(\sigma)} + \lambda_d\int {\rm d}\sigma\,\hat{S}(\sigma) + \sum_{I'}\int\frac{{\rm d}\sigma\,\lambda_{I'}\hat{s}_{I'}(\sigma)}{b+\hat{s}_\sigma(\sigma)} \qquad (4.9)$$

where, following the constraint (4.5), all the integrals are over the range $[0,\sigma_f]$. We have employed the Lagrangian multipliers $\{\lambda_{I'},\lambda_d\}$ to impose the constraints (4.4) and (4.8).

Using the variational method to find the stationary solution, we first require $\delta N_e/\delta\lambda_{I'} = \delta N_e/\delta\hat{s}_{I'} = 0$, so that

$$\int \mathrm{d}\sigma \, \frac{\hat{s}_{I'}}{b+\hat{s}_\sigma} = 0, \quad \lambda_{I'} = 2\lambda_d \hat{s}_{I'} \, . \tag{4.10}$$

We get the solutions $\hat{s}_{I'}(\sigma) = 0$, $\lambda_{I'} = 0$ for $\lambda_d \neq 0$. This means turning off transverse motions decreases the e-folds of inflation, i.e., for an arbitrary path along the σ direction, any detour in the transverse directions always increases the travel time. In fact, the increase is unbounded from above.

If we further set $\delta N_e/\delta\lambda_d = \delta N_e/\delta\hat{s}_\sigma = 0$, we have

$$\frac{3H^2}{(b+\hat{s}_\sigma)^2} = \lambda_d \, , \quad \int \mathrm{d}\sigma \, \hat{s}_\sigma = 0 \, , \tag{4.11}$$

which gives the solution $\hat{s}_\sigma(\sigma) = 0$ and $\lambda_d = 3H^2/b^2$. This stationary solution is the minimum of the functional $N_e[\hat{s}]$, that is, $N_e[0] = 3H^2\sigma_f/b$, which corresponds to turning off all the kinks in the potential. We therefore conclude that whenever $\hat{s}(\sigma) \neq 0$, the number of e-folds always increases, that is, any detour from $V_c(\vec{\phi})$ (4.1) increases the e-folds of inflation. Again, the increase is unbounded from above.

To understand the mechanism better, let us give an alternative proof. We introduce

$$\bar{s}_\sigma \equiv -\frac{1}{\sigma_f}\int \hat{s}_\sigma \, \mathrm{d}\sigma = \frac{1}{\sigma_f}\sum_{I'}\int \mathrm{d}\sigma \, \frac{\hat{s}_{I'}^2}{b+\hat{s}_\sigma} \geq 0 \, . \tag{4.12}$$

which simply follows from the constraint (4.8). Here $\bar{s}_\sigma = 0$ if and only if $d = 1$ or $\hat{s}_{I'} = 0$. With transverse motion, $\bar{s}_\sigma > 0$. Since σ is locally monotonic by construction, $b+\hat{s}_\sigma(\sigma) > 0$ in the range $0 \leq \sigma \leq \sigma_f$, and we have $0 < b - \bar{s}_\sigma \leq b$. Now we consider the increase in e-folds due to the kinks (with $N_e[0] = 3H^2\sigma_f/b$),

$$\frac{N_e[\hat{s}] - N_e[0]}{N_e[0]} = \frac{b}{\sigma_f}\int \frac{\mathrm{d}\sigma}{b+\hat{s}_\sigma(\sigma)} - 1 = \frac{\bar{s}_\sigma}{b-\bar{s}_\sigma} + \left(\frac{b}{\sigma_f}\int \frac{\mathrm{d}\sigma}{b+\hat{s}_\sigma(\sigma)} - \frac{b}{b-\bar{s}_\sigma}\right) \geq 0$$

where we have introduced an intermediate term containing $\bar{s}_\sigma \geq 0$. Actually, both terms are semi-positive. The first term in Eq.(4.13) is always positive with transverse motion. In the presence of non-zero $\hat{s}_I(\sigma)$, positivity of the second term follows from the

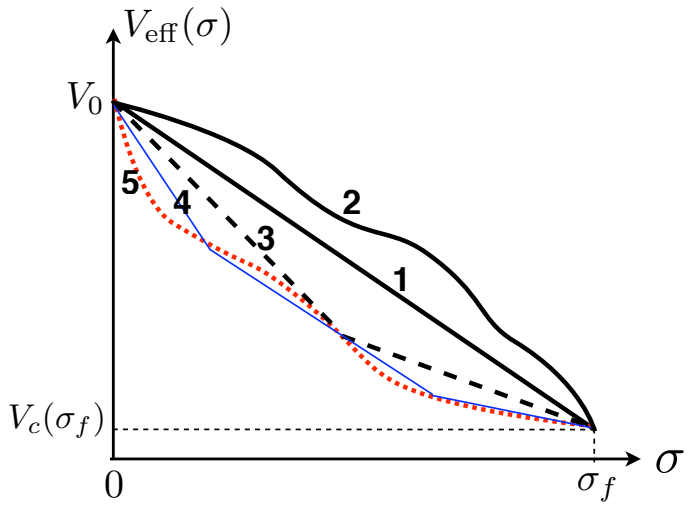

Figure 4.1: Consider a potential segment that begins at $\sigma = 0$ at V_0 and ends at σ_f at $V_c(\sigma_f)$, each curve above can be regarded as either the *actual* potential $V(\phi)$ for $d = 1$ or the *effective* potential $V_{\rm eff}(\sigma)$ for $d > 1$. For $d = 1$, in the slow-roll approximation, the linear segment $^{\#}1$ yields the smallest number of e-folds. Suppose $^{\#}5$ (red dotted curve) is the actual potential, then $^{\#}1$, $^{\#}3$ ($K = 3$) and $^{\#}4$ (blue solid thin line, with $K = 4$) are successively finer approximations of potential $^{\#}5$, yielding increasing number of e-folds, $N_e(^{\#}5) > N_e(^{\#}4) > N_e(^{\#}3) > N_e(^{\#}1)$. For $d > 1$, small transverse motions always increase N_e. That is, $V_{\rm eff}(\sigma)$ always yields more e-folds than the corresponding potential shown in the figure.

inequality between the harmonic mean and the arithmetic mean, i.e., for $x_i > 0$ and $\sum \omega_i = 1$, $\sum \omega_i/x_i \geq (\sum \omega_i x_i)^{-1}$ (with the equality reached if and only if all the x_i's are equal), where $\omega_i \to d\sigma/\sigma_f$ and $x_i \to b + \hat{s}_\sigma$. We therefore see explicitly from Eq.(4.13) that $N_e[\hat{s}] \geq N_e[0]$. For $d = 1$, or no transverse motion, the increase is from the second term in Eq.(4.13) alone. For $d > 1$, if there is transverse motion, the first term always increases the e-folds of inflation.

To get an intuitive sense of the picture, consider Fig.4.1 for the $d = 1$ case when $V_{\rm eff}(\sigma) = V(\phi)$. Potential $^{\#}1$ is the piecewise linear part of $V_c(\phi)$ from $\phi = 0$ to $\phi = \sigma_f$. Potentials $^{\#}3$ ($K = 3$) and $^{\#}4$ ($K = 4$) can be considered as successively finer-grained

approximations of the actual potential $^{\#}5$, i.e., we can treat $^{\#}3$ to be a coarse-grained potential with 2 linear segments and $^{\#}4$ has a kink (with $K = 3$) for each of the 2 segments of $^{\#}3$. For an arbitrary curve, we can break it into $K = 3$ pieces, and the more we break it, the better it approximates the actual potential. More fine-grained features will always increase e-folds; here we have $N_e(^{\#}5) > N_e(^{\#}4) > N_e(^{\#}3) > N_e(^{\#}1)$. For $d > 1$ with transverse motions, the curves in Fig.4.1 now represent $V_{\rm eff}(\sigma)$ (4.7). The *actual* d-dimensional potential represented by $V_{\rm eff}(\sigma)$ always yields more e-folds than the corresponding $d = 1$ potential shown, due to the detours of the inflaton field.

Most e-folds come from the regions with the smallest slope, where the constant H and the slow-roll approximations are most valid. Still one can also relax the $H \approx$ const and the slow-roll approximations. In this case, the linear segments of $V_c(\vec{\phi})$ should be replaced by the corresponding solutions to the respective brachistochrone problem, which are expected to be close to linear anyway. It is clear that an arbitrary detour from such paths will again lead to an increase in e-folds. So the qualitative properties of the scenario reman intact.

We expect the string scale and/or the Hubble scale to provide the cut-off on how fine-grained the actual potential can be. With appropriate characteristics of the actual potential, the enhancement can be large enough to give 60 or more e-folds.

We have assumed that the slope is always monotonic, $s_\sigma(\sigma) > 0$. It is argued in Ref.[80, 82] that the percolation probability $p \to 1$ in a random potential for large d. This is intuitively reasonable, since the inflaton has more choices of directions to move classically down a random potential as d is large. For the cosmic landscape, we expect $d \gg 1$, so the assumption $s_\sigma(\sigma) > 0$ is quite natural. For small d, percolation is not assured. For $d = 1$, the system typically does not percolate, so the monotonic condition on the slope is imposed by hand.

For our later purpose to analyze the primordial power spectrum, we now derive the

relation between the parameters $\vec{\delta}^{(i)}$ and the properties of the scalar potential. If we model the effect of inflaton scattering by turning on $V_{IJ} \equiv \partial^2 V/\partial\phi^I\partial\phi^J$ instantaneously, i.e., we assume

$$V_{IJ} = 3H\Delta_{IJ}\delta(t-t_k) \tag{4.13}$$

The factor $3H$ is for latter convenience. Such a defect changes the slope of the potential according to

$$s_I^{(k)} = s_I^{(k-1)} + 3H\Delta_{IJ}^{(k)}\dot{\phi}^J(t_k) \tag{4.14}$$

If we further assume that the acceleration $\ddot{\phi}_I$ is important only at the moment of scattering, and between scatterings, the inflaton motion is close to slow-roll, Eq.(4.14) becomes

$$s_I^{(k)} = s_I^{(k-1)} + \Delta_{IJ}^{(k)} s^{(k-1)J} \tag{4.15}$$

Starting with $s_I^{(0)} = b_I$, we can easily work out

$$\begin{aligned}
s_I^{(1)} &= b_I + \Delta_{IJ}^{(1)} b^J \ , \\
s_I^{(2)} &= b_I + \Delta_{IJ}^{(1)} b^J + \Delta_{IJ}^{(2)} b^J + \Delta_{IK}^{(2)} \Delta^{(1)}{}_J^K b^J \ , \\
&\cdots \\
s_I^{(k)} &= b_I + \sum_{i=1}^{k} \Delta_{IJ}^{(i)} b^J + \mathscr{O}(\Delta^2, \Delta^3, \ldots, \Delta^k) \ .
\end{aligned}$$

Comparing with Eq.(4.14), we can identify

$$\delta_I^{(i)} = \Delta_{IJ}^{(i)} b^J \ . \tag{4.16}$$

The terms non-linear in Δ_{IJ} can be neglected in the perturbative regime $\Delta_{IJ} \ll 1$, but could play an important role if the scattering is strong, i.e. $\Delta_{IJ} \sim 1$. On the other hand, if the potential is sufficiently random, adjacent scatterings are weakly correlated, $\Delta^{(i)}{}_I^K \Delta_{KJ}^{(i+1)}$ tends to become negligible.

4.1.2 A Langevin Fokker-Planck Analysis

We describe the inflaton's motion in the landscape using the Langevin Equation,

$$\ddot{\phi}_I + 3H\dot{\phi}_I + \partial_I V_c(\vec{\phi}) = \xi_I(t) \tag{4.17}$$

The coarse-grain potential $V_c(\vec{\phi}) = 3H^2 M_{\rm Pl}^2$ is smooth while its fine-grain random features are represented by the fluctuating force $\vec{\xi}(t)$, which leads to the random scatterings of the inflaton,

$$\langle \xi_I(t)\xi_J(t')\rangle = 2D_{IJ}\,\delta(t-t')\ , \tag{4.18}$$

where D_{IJ} is the constant diffusion tensor. The bracket $\langle\ldots\rangle$ denotes average over different realizations of the random walk. Note that, in the absence of quantum fluctuation, every causal patch of the universe undergoes the same random-looking classical trajectory under the same random force $\vec{\xi}(t)$ during inflation, and therefore no density perturbation is generated. Density perturbation is generated by quantum effects only. The ending of inflation can be brought about through a variety of ways that do not concern us here.

Considering a relatively small range of ϕ, we may Taylor expand the potential around $\vec{\phi} = \mathbf{0}$ and keep only the linear term,

$$V_c(\vec{\phi}) = V_0 - b^I\phi_I\ . \tag{4.19}$$

To solve the Langevin Equation, we define

$$\vec{y} \equiv \vec{\phi} - \frac{\vec{b}}{3H}t\ , \quad Y \equiv (\vec{y},\dot{\vec{y}})\ , \tag{4.20}$$

and rewrite the Langevin equation into the matrix form,

$$\frac{{\rm d}Y}{{\rm d}t} = AY + B\vec{\xi}(t)\ , \tag{4.21}$$

where

$$A = \begin{pmatrix} 0 & 1 \\ 0 & -3H \end{pmatrix} \quad B = \begin{pmatrix} 0 \\ 1 \end{pmatrix}\ .$$

The solution can be formally written as

$$Y(t) = e^{At}\, Y(0) + \int_0^t \mathrm{d}s\, e^{A(t-s)}\, \xi(s) B \ , \tag{4.22}$$

with the matrix exponent e^{At} given by

$$e^{At} = \begin{pmatrix} 1 & \frac{1}{3H}(1-e^{-3Ht}) \\ 0 & e^{-3Ht} \end{pmatrix} \tag{4.23}$$

So in terms of $\phi(t)$ and $\dot{\phi}(t)$, we get (setting $\vec{\phi}(0) = 0$ and $\dot{\vec{\phi}}(0) = \dot{\vec{\phi}}_0$),

$$\dot{\vec{\phi}}(t) = \frac{\vec{b}}{3H}\left(1 - e^{-3Ht}\right) + \int_0^t \mathrm{d}s\, \vec{\xi}(s)\, e^{3H(s-t)} \tag{4.24}$$

$$\vec{\phi}(t) = \frac{\vec{b}}{3H} t + \frac{1}{3H}\left(1 - e^{-3Ht}\right)\left(\dot{\vec{\phi}}_0 - \frac{\vec{b}}{3H}\right) + \int_0^t \mathrm{d}s\, \frac{\vec{\xi}(s)}{3H}\left[1 - e^{3H(s-t)}\right] \tag{4.25}$$

It readily follows that the sample mean speed (when $3Ht \gg 1$) is

$$u_I \equiv \langle \dot{\phi}_I(t) \rangle \approx \frac{b_I}{3H} \ , \tag{4.26}$$

with the sample variance

$$\langle (\dot{\phi}_I(t) - u_I)(\dot{\phi}_J(t) - u_J) \rangle = \int\int \mathrm{d}s_1 \mathrm{d}s_2\, e^{3H(s_1+s_2-2t)} \langle \xi_I(s_1) \xi_J(s_2) \rangle = \frac{D_{IJ}}{3H} \ . \tag{4.27}$$

An alternative way to describe the random walk is to use the probability density function $P(\vec{\phi}, \dot{\vec{\phi}}, t)$ for the inflaton. The probability density function obeys the Klein-Kramers equation,

$$\frac{\partial P}{\partial t} = -\dot{\phi}_I \frac{\partial P}{\partial \phi_I} + \partial_I V \frac{\partial P}{\partial \dot{\phi}_I} + 3H \frac{\partial}{\partial \dot{\phi}_I}\left(\dot{\phi}^I P\right) + D_{IJ} \frac{\partial^2 P}{\partial \dot{\phi}_I \partial \dot{\phi}_J} \tag{4.28}$$

A trick to solve the above equation is to first integrate $P(\vec{\phi}, \dot{\vec{\phi}}, t)$ over $\vec{\phi}$. We first define

$$\tilde{P}(\dot{\vec{\phi}}, t) \equiv \int \mathrm{d}^d \dot{\vec{\phi}}\, P(\vec{\phi}, \dot{\vec{\phi}}, t) \ . \tag{4.29}$$

Integrating Eq.(4.28) over $\vec{\phi}$, we find that $\tilde{P}$ satisfies the velocity space Fokker-Planck equation

$$\frac{\partial \tilde{P}}{\partial t} = b_I \frac{\partial \tilde{P}}{\partial \dot{\phi}_I} + 3H \frac{\partial}{\partial \dot{\phi}_I}\left(\dot{\phi}^I \tilde{P}\right) + D_{IJ} \frac{\partial^2 \tilde{P}}{\partial \dot{\phi}_I \partial \dot{\phi}_J} \tag{4.30}$$

Again, for $3Ht \gg 1$, we get the solution

$$P(\vec{\dot{\phi}},t) = \left(\frac{3H}{2\pi}\right)^{d/2} (\det D)^{-1/2} \exp\left[-\frac{3H}{2}(\dot{\phi}_I - u_I)D^{-1}_{IJ}(\dot{\phi}_J - u_J)\right] , \qquad (4.31)$$

where D^{-1}_{IJ} is the IJ component of the inverse D^{-1}.

In both approaches, we see that the sample mean velocity $\langle\dot{\phi}_I\rangle$ approaches the slow-roll velocity $b_I/3H$ quickly. The actual inflaton velocity distribution centers around $\langle\dot{\phi}_I\rangle$ with a spread dictated by the diffusion matrix D_{IJ}.

The fact that $\langle\dot{\phi}_I\rangle$ equals the slow roll speed naively leads one to think that the random walk path generically gives the same amount of e-folds as the corresponding coarse-grained smooth potential. However, the number of e-folds over a time period T is given by

$$N_e = \int_0^T H dt = \int \frac{H}{\dot{\phi}^2}\,\dot{\phi}_I \mathrm{d}\phi_I , \quad \dot{\phi} \equiv \left|\vec{\dot{\phi}}\right| , \qquad (4.32)$$

It appears that $\langle 1/\dot{\phi}\rangle$ rather than $\langle\dot{\phi}\rangle$ may be more indicative of the underlying physics, where

$$\left\langle 1/\dot{\phi}\right\rangle = \int d^d\dot{\phi}_I \frac{1}{\dot{\phi}} P(\dot{\phi}_I,t) \to \infty \qquad (4.33)$$

That is, $\langle 1/\dot{\phi}\rangle \neq 1/\langle\dot{\phi}\rangle$. The reason is simple: while large speeds dominate $\langle\dot{\phi}\rangle$, it is the smallest speeds that dominate $\langle 1/\dot{\phi}\rangle$. This clearly suggests that even if the average (over samples) speed of the inflaton is the same with or without the random forces, the presence of the random forces will typically increase the number of e-folds for any specific path.

4.2 The Non-Slow-Roll Generalization

4.2.1 The Inflationary Trajectory with Minimal E-folds

The analysis in Chapter 4.1.1 relies on the slow-roll approximation and a constant Hubble parameter. Here we would like to generalize the analysis to non-slow-roll case. We

will see that the exponential potential corresponds to the minimal number of e-folds and any deviation from that increases the number of e-folds. In the limit where ε is small, the exponential potential become the linear potential in Chapter 4.1.1.

To begin, let us describe the dynamics of the single canonical inflaton field in the Hamilton-Jacobi formalism [86], where we write every quantity as a function of the scalar field ϕ, i.e., we choose ϕ as the "clock".

$$3M_{\rm Pl}^2 H^2 = \frac{1}{2}\dot{\phi}^2 + V(\phi)\,, \tag{4.34}$$

$$\dot{\phi} = -2M_{\rm Pl}^2 H'(\phi)\,. \tag{4.35}$$

The ε and η parameters in this formalism is given by

$$\varepsilon \equiv -\frac{\dot{H}}{H^2} = 2M_{\rm Pl}^2\left(\frac{H'}{H}\right)^2\,, \tag{4.36}$$

$$\eta \equiv \frac{\dot{\varepsilon}}{H\varepsilon} = 4M_{\rm Pl}^2\left[\left(\frac{H'}{H}\right)^2 - \frac{H''}{H}\right]\,. \tag{4.37}$$

The number of e-folds is given by

$$N_e = \int {\rm d}\phi \frac{H}{\dot{\phi}} = \frac{1}{2M_{\rm Pl}^2}\int_{\phi_f}^{\phi_i} {\rm d}\phi \frac{H(\phi)}{H'(\phi)} \tag{4.38}$$

Consider the case with fixed initial and final Hubble scale $H_i \equiv H(\phi_i)$ and $H_f \equiv H(\phi_f)$, and we can ask what kind of function $H(\phi)$ gives the minimum number of e-folds between the two fixed boundary points. One can write down the Euler-Lagrangian equation,

$$\frac{\partial}{\partial H}\left(\frac{H}{H'}\right) = \frac{\partial}{\partial \phi}\frac{\partial}{\partial H'}\left(\frac{H}{H'}\right) \tag{4.39}$$

which gives

$$\frac{H''}{H} - \left(\frac{H'}{H}\right)^2 = 0 \tag{4.40}$$

Comparing with the definition of η in Eq.(4.37), the Euler-Lagrangian equation is equivalent to saying that $\eta = 0$ for the trajectory with minimum e-folds.

The solution to Eq.(4.40) is given by

$$H(\phi) = H_i \exp\left(-C\frac{\phi}{M_{\rm Pl}}\right) \tag{4.41}$$

where the integration constant C is determined through requiring that $H(\phi_f) = H_f$. Without losing generality, we set $\phi_i = 0$, and introduce two parameters α and β such that

$$\alpha \equiv \frac{H_f}{H_i} < 1 \ , \quad \beta \equiv \frac{\phi_f}{M_{\rm Pl}} \ . \tag{4.42}$$

We therefore can write

$$H(\phi) = H_i \exp\left(\frac{\ln\alpha}{\beta}\frac{\phi}{M_{\rm Pl}}\right) \tag{4.43}$$

We now look at the ε and η parameters to make sure that Eq.(4.43) is an inflationary solution. It is already evident that $\eta = 0$. Furthermore using Eq.(4.36), we get

$$\varepsilon = \frac{2\ln^2\alpha}{\beta^2} \ . \tag{4.44}$$

Inflation requires that $\varepsilon < 1$, so we need

$$\beta > -\sqrt{2}\ln\alpha \tag{4.45}$$

From $H(\phi)$ above, we can reconstruct the potential through Eq.(4.34) and Eq.(4.35),

$$V(\phi) = (3-\varepsilon)H_i^2 M_{\rm Pl}^2 \exp\left(-\sqrt{2\varepsilon}\,\frac{\phi}{M_{\rm Pl}}\right) \ . \tag{4.46}$$

In the limit $\varepsilon \ll 1$, the potential becomes linear

$$V_S(\phi) \approx 3M_{\rm Pl}^2 H_i^2 \left(1 - \sqrt{2\varepsilon}\,\frac{\phi}{M_{\rm Pl}}\right) \ , \tag{4.47}$$

which agrees with previous analysis in the slow-roll scenario with large damping [79]. Note that, to get the correct power spectrum index, we have to keep the ϕ^2 term in $V_S(\phi)$. Using

$$\frac{{\rm d}\phi}{{\rm d}\ln k} = \frac{-2H'/H}{1-\varepsilon} \tag{4.48}$$

one obtains, for

$$P_\zeta(k) = \frac{H^2}{8\pi^2\varepsilon} \tag{4.49}$$

the power spectrum index

$$n_s - 1 = \frac{\mathrm{d}\ln P}{\mathrm{d}\ln k} = -(2\varepsilon+\eta)/(1-\varepsilon) \simeq -2\varepsilon - \eta \simeq -6\varepsilon + 2\eta_{SR} \tag{4.50}$$

where the last equality is taken in the slow-roll approximation. We see that $\eta = 0$ for $H_1(\phi)$.

One can now calculate the value of the minimum number of e-folds based on Eq.(4.43)

$$N_e^{\min} = \frac{1}{2M_{\rm Pl}^2}\int_{\phi_f}^{\phi_i} \mathrm{d}\phi \frac{H(\phi)}{H'(\phi)} = \frac{-\beta^2}{2\ln\alpha} \tag{4.51}$$

We conclude here that, given the field distance $\Delta\phi = \beta M_{\rm Pl}$, and the change in Hubble scale $\Delta H = (1-\alpha)H_i$, the exponential form $H(\phi)$ in Eq.(4.43) corresponds to the minimum number of e-folds $N_e^{\min} = -\beta^2/(2\ln\alpha)$.

A few comments on the above conclusion:

- Let us denote the functional space of all the functions interpolating between $H(\phi_i) = H_i$ and $H(\phi_f) = H_f$ by $\mathscr{H}$. The solution Eq.(4.43) minimizes the functional $N_e[H(\phi), H'(\phi)]$ among all the functions in $\mathscr{H}$. But we are only interested in the inflationary subspace $\mathscr{I} \subset \mathscr{H}$, which only contains functions $H(\phi)$ that: 1) supports inflation everywhere in between ϕ_i and ϕ_f. 2) gives a monotonic behavior of $\phi(t)$, i.e. $\dot\phi > 0$, $H'(\phi) < 0$. The first condition is satisfied by Eq.(4.43) if $\varepsilon < 1$, i.e., $\beta > -\sqrt{2}\ln\alpha$, while the second condition is apparent from Eq.(4.43). Once we make sure the solution Eq.(4.43) is contained in the inflationary functional space $\mathscr{I}$, we can conclude that it is the trajectory that gives the minimum number of e-folds.
- If $\beta < -\sqrt{2}\ln\alpha$, the solution Eq.(4.43) itself does not give inflation, i.e., it is not within the inflationary functional space $\mathscr{I}$. We have no conclusion on the minimal e-fold trajectory between H_i and H_f.

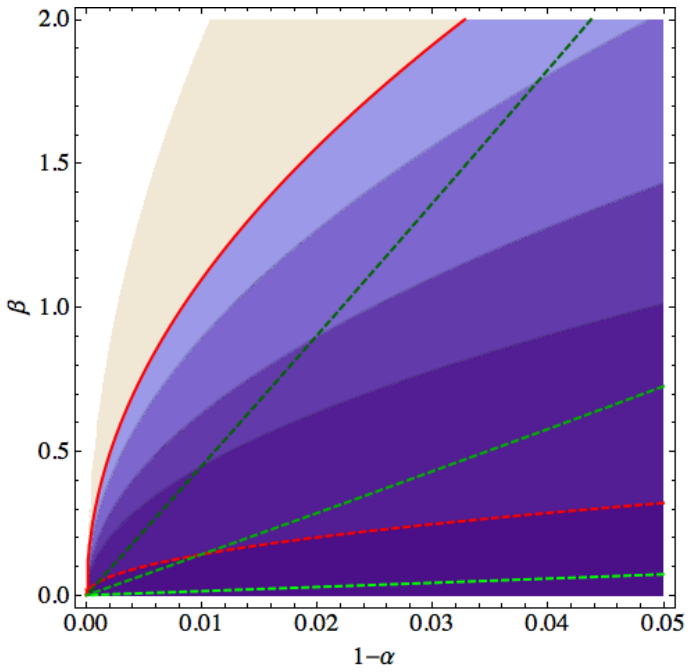

Figure 4.2: Contour plot (blue regions) for the value of minimum e-folds, with lighter blue denoting larger $N_e^{\min}$. The red dashed line is $N_e^{\min} = 1$ and the red solid line is $N_e^{\min} = 60$. The green dashed lines are constant ε curves, with $\varepsilon = 1, 10^{-2}, 10^{-3}$ from the lighter to the darker green lines.

4.2.2 Deviation from the Minimal E-fold Path

Since the minimal e-fold path corresponds to $\eta = 0$, we can turn on the η parameter to characterize the deviation away from the minimal e-fold path. Let us consider $H_2(\phi)$ first. We now need to solve the equation

$$\left(\frac{H'}{H}\right)^2 - \frac{H''}{H} = \frac{\eta(\phi)}{4M_{\rm Pl}^2} \,. \tag{4.52}$$

The solution can be formally written as

$$H(\phi) = H_i \exp\left[C'x - \frac{1}{4}\int_0^x \mathrm{d}x_1 \int_0^{x_1} \mathrm{d}x_2 \eta(x_2)\right] \,, \quad x \equiv \frac{\phi}{M_{\rm Pl}} \tag{4.53}$$

We can fix the integration constant C' by matching $H(\phi_f) = H_f = \alpha H_i$ with $\phi_f = \beta M_{\rm Pl}$. Therefore

$$C' = \frac{\ln\alpha}{\beta} + \frac{1}{4\beta}\int_0^\beta \mathrm{d}x_1 \int_0^{x_1} \mathrm{d}x_2 \eta(x_2) \tag{4.54}$$

Now the number of e-folds is

$$N_e = \frac{1}{2M_{\rm Pl}^2}\int_{\phi_f}^{\phi_i}\frac{H(\phi)}{H'(\phi)}{\rm d}\phi = \frac{1}{2}\int_0^{\beta}{\rm d}x\frac{1}{C' - \frac{1}{4}\int_0^x \eta(x'){\rm d}x'} \tag{4.55}$$

In principle, one can consider arbitrary function of $\eta(\phi)$, as long as $|\eta(\phi)| < 1$. Here we will illustrate with the case $\eta = const$, where the solution Eq.(4.53) can be simplified,

$$H(\phi) = H_i \exp\left(C'\frac{\phi}{M_{\rm Pl}} - \frac{\eta}{8}\frac{\phi^2}{M_{\rm Pl}^2}\right) \tag{4.56}$$

$$C' = \frac{\ln\alpha}{\beta} + \frac{\eta\beta}{8} \tag{4.57}$$

$$N_e = \frac{2}{\eta}\ln\left(\frac{\ln\alpha - \frac{1}{8}\eta\beta^2}{\ln\alpha + \frac{1}{8}\eta\beta^2}\right) \tag{4.58}$$

In the small η expansion, we can write

$$N_e = -\frac{\beta^2}{2\ln\alpha} - \frac{\beta^6\eta^2}{384(\ln\alpha)^3} + \mathscr{O}(\eta^4) + \dots\ , \tag{4.59}$$

which further verifies that $\eta \to 0$, N_e approaches minimum.

4.3 Primordial Power Spectrum

The standard approach to perturbations in multifield inflation is to decompose the perturbations into modes tangent to the background path (the adiabatic mode) and modes orthogonal to the background path (the entropic modes). Such an approach is not quite useful in our scenario, as the background path is convoluted making the adiabatic and entropic decomposition artificial. Here we will treat perturbation in all directions on equal footing and follow their evolution using the perturbed Klein-Gordon equation. There are two subtleties here. First, the perturbations evolves even after horizon exit, because the convoluted background path creates non-adiabatic pressure. As a result, we will need to trace the evolution of the perturbations towards the end of inflation. Second, even if we trace the perturbation for every ϕ_I, it is the projection along the adiabatic direction that translates into the observable relevant for CMB temperature anisotropies.

We now write down the standard evolution equation for the scalar perturbation $v_I(k,\tau)$,

$$v_I'' + \left(k^2 - \frac{a''}{a}\right) v_I + \left[a^2 V_{IJ} - \frac{1}{a^2}\left(\frac{a}{H}\phi_I'\phi_J'\right)'\right] v^J = 0 \,. \tag{4.60}$$

Here τ is the conformal time, and $v_I \equiv Q_I/a$ with Q_I the perturbation of ϕ_I in the spatially flat gauge.

The last term above is negligible as it is suppressed by ε. According to the setup in Eq.(4.13), V_{IJ} is important only when the inflaton scatters, $a^2 V_{IJ} = 3aH\sum_i^K \Delta_{IJ}^{(i)}\delta(\tau-\tau_i)$ to leading order in $\Delta^{(j)}$, so

$$\vec{v}'' + \left(k^2 - \frac{a''}{a}\right)\vec{v} - 3aH\sum_{i=1}^{K}\Delta^{(i)}\,\delta(\tau-\tau_i)\vec{v} = 0 \,. \tag{4.61}$$

with $\vec{v} \equiv (v_1, v_2, \cdots v_d)^T$. Between the i-th and the $(i+1)$-th scattering, i.e. $\tau_i \le \tau \le \tau_{i+1}$, we can write

$$\vec{v}(k,\tau) = \vec{\alpha}^i v^-(k,\tau) + \vec{\beta}^i v^+(k,\tau) \,, \tag{4.62}$$

$$v^{\pm}(k,\tau) = \frac{1}{\sqrt{2k}} e^{\pm ik\tau}\left(1 \pm \frac{i}{k\tau}\right) \tag{4.63}$$

Generalizing the approach in Ref.[87], we derive the coefficients $(\vec{\alpha}^i, \vec{\beta}^i)$ recursively, by matching the boundary conditions at each τ_i,

$$\vec{v}(k,\tau_i^+) - \vec{v}(k,\tau_i^-) = 0 \,, \quad \vec{v}'(k,\tau_i^+) - \vec{v}'(k,\tau_i^-) = 3aH\Delta^{(i)}\,\vec{v}(k,\tau_i^+) \,. \tag{4.64}$$

The result can be written in the form,

$$\begin{pmatrix} \vec{\alpha}_j \\ \vec{\beta}_j \end{pmatrix} = T_{j,j-1}\begin{pmatrix} \vec{\alpha}_{j-1} \\ \vec{\beta}_{j-1} \end{pmatrix} \tag{4.65}$$

with

$$T_{j,j-1} \equiv \begin{pmatrix} 1 + \frac{3i}{2}\Delta^{(j)}(x_j^{-1} + x_j^{-3}) & \frac{3i}{2}\Delta^{(j)} e^{-2ix_j}(-i + x_j)^2 \\ -\frac{3i}{2}\Delta^{(j)} e^{2ix_j}(i + x_j)^2 & 1 - \frac{3i}{2}\Delta^{(j)}(x_j^{-1} + x_j^{-3}) \end{pmatrix} \,, \quad x_j \equiv \frac{k}{aH}\Big|_{\tau_j} \tag{4.66}$$

Starting with the Bunch-Davies vacuum $(\alpha_I^0, \beta_I^0) = (1,0)$ at $\tau = -\infty$, we get (to leading order in $\Delta^{(j)}$),

$$\alpha_I^n = \alpha_I^0 + \sum_{j=1}^{n} \frac{3i}{2} \Delta^{(j)}{}_I^J \alpha_J^0 \, (x_j^{-1} + x_j^{-3}) \, , \tag{4.67}$$

$$\beta_I^n = -\sum_{j=1}^{n} \frac{3i}{2} \Delta^{(j)}{}_I^J \alpha_J^0 \, e^{2ix_j} (i + x_j)^2 \, . \tag{4.68}$$

As discussed at the beginning of the section, the observable is the gauge invariant adiabatic scalar perturbation ζ defined by

$$\zeta \equiv \frac{H}{\dot{\phi}^2} \frac{v_I}{a} \dot{\phi}^I \, , \quad \dot{\phi}^2 \equiv \dot{\phi}^I \dot{\phi}_I \tag{4.69}$$

Assuming $\langle v^I v^J \rangle \propto \delta^{IJ}$, the power spectrum P_ζ is

$$P_\zeta(k) = \frac{H^4}{4\pi^2 \dot{\phi}^2} \sum_{I=1}^{d} \frac{|\beta_I - \alpha_I|^2}{d} \Big|_{\tau \to 0} \, . \tag{4.70}$$

Using Eq.(4.67) and Eq.(4.68), we get

$$P_\zeta(k) = \frac{H^4}{4\pi^2 \dot{\phi}^2} \times \left(1 + \sum_{i=1}^{K} B^i p_1(x_i) + C^i p_2(x_i) \right) \, , \tag{4.71}$$

$$B^i \equiv \frac{1}{d} \sum_{I,J} \Delta_{IJ}^{(i)} \, , \quad C^i \equiv \frac{1}{d} \sum_{I,J,K} \Delta_{KI}^{(i)} \Delta_{IJ}^{(i)} \, , \tag{4.72}$$

where B^i is the leading order effect due to inflaton scattering. The detailed shape of the fluctuation is given by

$$p_1(x_i) = 3(x_i^{-3} - x_i^{-1}) \sin 2x_i - 6x_i^{-2} \cos 2x_i \, ,$$

$$p_2(x_i) = 9(x_i^{-6} + x_i^{-4})(\sin x_i - x_i \cos x_i) \, .$$

Note that the power spectrum derived above contains terms quadratic in Δ. Naively, one may think that we need to calculate the (α_I, β_I) to the same order to be consistent. However, a careful examination shows that (α_I, β_I) only contains quadratic terms like $\Delta^{(i)}\Delta^{(i+1)}$, and by our assumption that adjacent scatterings are uncorrelated, they are negligible. So we only need (α_I, β_I) to linear order in Δ to get the power spectrum to

quadratic order in Δ. Furthermore, terms like $\Delta^{(i)}\Delta^{(i+1)}$ are dropped when expanding $|\alpha_I - \beta_I|^2$ for the same reason. We see that the assumption of randomness on the scalar potential simplifies the power spectrum to a great extent.

In the above analysis, we have assumed H to be a constant. Incorporating the time dependence of H, as dictated by the potential in Eq.(4.3), we can parametrize

$$\frac{H^4}{4\pi^2\dot{\phi}^2} \equiv A_s \left(\frac{k}{k_0}\right)^{n_s-1} \tag{4.73}$$

with $A_s = 2.41 \times 10^{-9}$ and $k_0 = 0.002\,\mathrm{Mpc}^{-1}$ [4]. The fluctuation part of the power spectrum is essentially unchanged except that now $x_i \to x_i/(1-\varepsilon)$.

We see that the primordial power spectrum Eq.(4.71) nicely factors. The smooth part represents the gross feature of the power spectrum like the amplitude A_s and the tilt n_s, and the fluctuation part leads to features of magnitude B_i. Fig.4.3 shows an example of the power spectrum with $n_s = 0.95$ and seven random fluctuations.

4.4 Fluctuations on the CMB Power Spectrum

We consider an experiment which maps a fraction f_{sky} of the sky using a Gaussian beam with full width at half maximum $\Delta\theta$ and a pixel noise ΔT_{pix}. Treating the noise as Gaussian and ignoring any correlations between pixels, the uncertainties in C_l can be approximated by the following expression [88],

$$\delta C_l = \sqrt{\frac{2}{(2l+1)f_{\mathrm{sky}}}} \left(C_l + \omega^{-1} e^{l^2\sigma_b^2}\right) , \tag{4.74}$$

where $\sigma_b = 7.42 \times 10^{-3}(\Delta\theta/1^\circ)$, $\omega^{-1} = (\Delta T_{\mathrm{pix}})^2 \Delta\theta^2$. Assuming $f_{\mathrm{sky}} = 0.8$, $C_l \sim 10^4\, l^{-2}(\mu K)^2$, and using the experimental specifications [89] for WMAP and PLANCK (Table I), the calculated uncertainties $\delta C_l/C_l$ (Fig.4.4) show that PLANCK can provide cosmic variance limited measurements up to $l \sim 2000$, while WMAP does so only up to

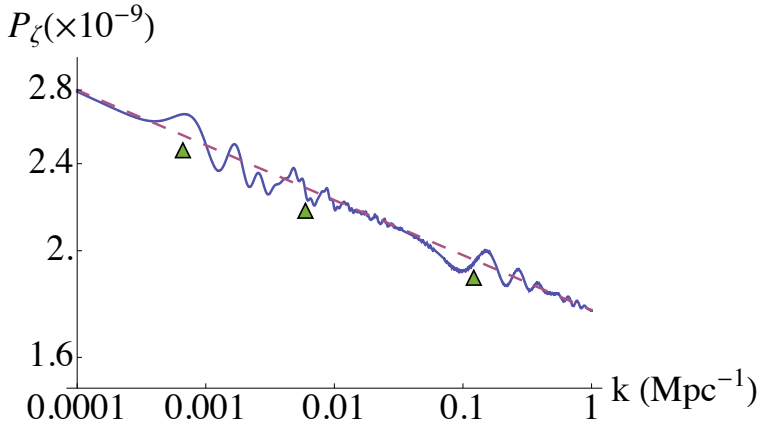

Figure 4.3: We show the smooth power spectrum with $n_s = 0.95$ (dashed line), and an illustration of the power spectrum with three features labeled by the triangles. We choose the magnitudes of the features $B^i \sim 0.01$. For single field $d = 1$, the features correspond to $\sim 1\%$ sudden change in the potential gradient. However, for multifield $d \gg 1$, the features arise due to the turning of inflaton trajectory. The turning angle can be quite large $\Delta_{IJ} \sim 1$, and still be compatible with data since $B^i \sim \Delta_{IJ}/d$ for the multifield case. Although features arise due to different reasons in the single field and multifield scenario, one can not tell the difference from their appearance in the power spectrum.

$l \lesssim 800$. [1]

Looking at the un-binned TT CMB power spectrum released by WMAP [83], one clearly sees that it fluctuates for about 10% (in the range $100 \lesssim l \lesssim 800$). However, due to the large error bars of the same magnitude (10%), it is hard to claim any features based on current data. The usual approach to reduce the error bars by binning a few tens of multiple moments together gives a relatively smooth TT power spectrum over all angular scales. On the other hand, given that each e-fold of inflation corresponds to roughly 300 multiple moments, the data binning approach will have smoothed out fluctuations in the power spectrum if the inflaton scatters too frequently , say more than

[1] We assume an ideal case of complete foreground removal, marginalizing over foregrounds will generically degrade $\delta C_l/C_l$ further.

Table 4.1: Experiment specifications for WMAP and PLANCK

	WMAP		PLANCK		
ν (GHz)	61	94	70	100	143
$\Delta\theta$ (arcmin)	19.8	12.6	14	9.5	7.1
$\Delta T_{\rm pix}$ (μK)	21.1	31.9	12.8	6.8	6.0

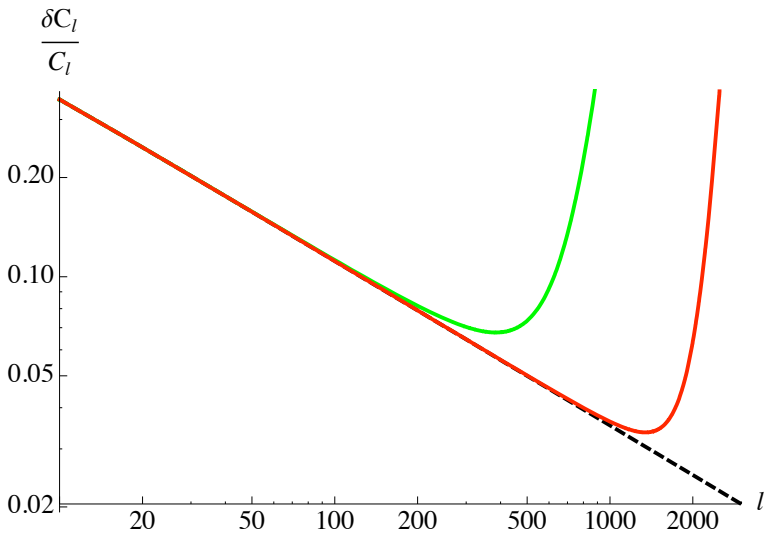

Figure 4.4: $\delta C_l/C_l$ for WMAP 4-year data (green) and PLANCK 14-month data (red). The black dashed line is the uncertainty due to cosmic variance.

20 times per e-fold.

We see that $\delta C_l^{TT}/C_l^{TT} \lesssim 5\%$ for PLANCK in the range $500 \lesssim l \lesssim 2000$. So each 10% fluctuation in C_l^{TT} will be a 2σ effect for PLANCK. Once such features are revealed in the TT power spectrum, they must appear in the TE/EE power spectrum at the same angular scales. Although the noise ($\Delta T_{\rm pix}$) in the TE/EE correlation will be $\sqrt{2}$ times larger than that of the TT correlation, PLANCK still has the sensitivity to detect 10% fluctuations as 2σ effects for $500 \lesssim l \lesssim 1500$ in the TE/EE power spectrum. The appearance of fluctuations in the different power spectra (TT/TE/EE) will be an important

consistency check on our prediction.

If we assume that a few of such features already have been detected in the data [83, 84, 85], two possible scenarios seem to emerge : (1) the spacings between fluctuations (i.e., scatterings) can be many units of l, say $\Delta l \sim 100$; (2) although the spacings between fluctuations are too small to be resolved, an occasional fluctuation is big enough to be observed. Such observable fluctuations are relatively well spaced.

We end this chapter with some remarks. If the inflaton is trapped at a local minimum in the potential, the CMB power spectrum will be scale-invariant ($n_s = 1$), which is certainly not the case. The red tilt of the power spectrum ($n_s < 1$) implies that the inflaton is mobile at least during the epoch that generates the CMB temperature perturbations. If the inflaton reaches a local minimum, it will stay there for a time roughly given by the lifetime of this false vacuum t_F. Mobility of the inflaton implies that $Ht_F \ll 1$. The typical time delay due to this quantum tunneling effect is t_F, so that we can easily estimate the amplitude of density perturbation [90, 91], $\Delta = \delta N \simeq H\delta t \sim Ht_F \sim 10^{-5}$. Some of the features in the power spectrum can be due to such a fast tunneling event in the cosmic landscape.

The presence of fluctuations in the power spectrum implies that the inflaton is mobile in the random potential, i.e., the cosmic landscape. This suggests that there is no eternal infaltion, which will arise only if the inflaton is trapped at a local site for more than an e-fold. Since our universe has gone through the cosmic landscape only once in this scenario, the fluctuations will reveal this particular path of our past history.

CHAPTER 5

COMMENTS AND OUTLOOKS

Brane inflation in the warped throat has very rich observable features on the CMB power spectrum, provinding explicit comparisons between fundamental theory and cosmological observations. Generally speaking, when the inflaton mass is much smaller than the Hubble scale, we have the slow roll scenario, which can easily fit current observations by adjusting the mass parameter. Unfornately, such slow-roll scenario does not generate large tensor perturbations or primordial non-Gaussianities, making it almost impossible to be distinguished from field theory models (except that it can produce cosmic strings at the end of inflation). The slow-roll scenario also suffers from the η problem; Kähler moduli stabilization induced a inflaton mass of order the Hubble scale, so 1% tuning is needed for the slow-roll model to work.

When the inflaton mass is around or above the Hubble scale, we may have DBI inflation, where the full non-linear DBI action come into play and the inflaton speed is bounded by the warped brane tension. In this work, we studied the UV and IR DBI scenarios in detail. In the UV scenario, we found that before imposing the bulk volume bound (2.108), the ultra-relativistic scenario is compatible with the present data, predicting a large non-Gaussianity. We also found in the intermediate regime that the tensor mode can be large and the $n_t - r$ relation deviates from the usual slow-roll consistency relation. However, imposing the bulk volume bound excludes both regions in the simplest scenario. UV DBI inflation still remains a valid effective field theory model, however, its embedding in the GKP type compactification [10] is excluded by current observations (especially the bound on $f_{\rm NL}$). Searching for UV completion of such a scenario is an interesting question remaining to be explored.

The IR DBI model, in which the brane rolls out of the throat under a negative mass term, agrees with current observations very well. It produces negligible tensor perturba-

tions due to its low inflation scale, while primordial non-Gaussianity is distinctive. The running of $f_{\rm NL}$ in the IR model is opposite to that in the UV model. During the early stage of inflation, when the brane tension is warped below the Hubble scale, there is a phase transition which suppresses the amplitude of primordial perturbations. If such a transition happens not too far from the observable scales of CMB experiments, we will be able to observe a negative running of the spectral index. Understanding the nature of such a phase transition will be crucial if future data from PLANCK see significant running of the power spectrum index ($\mathrm{d}n_S/\mathrm{d}\ln k$) and primordial non-Gaussianity ($f_{\rm NL}$) at the same time. The negative mass term in the IR model still has not been explicitly constructed from string theory to date, it will be interesting to search for such a construction using the recent advancement in string theory [92].

In addition to the global properties of the primordial perturbations, such as $f_{\rm NL}$ and $\mathrm{d}n_S/\mathrm{d}\ln k$, we also studied localized features in warped brane inflation scenarios. In particular, Sieberg duality cascade provides a natural motivations for step features in the K-S warp factor. Such features show up in the inflaton potential in the slow-roll scenario, and the speed limit in the DBI scenario. The magnitude and location of such steps are all correlated, such that if more than two adjacent features are revealed by CMB data, we can predict where to look for other features. The features shows up not only in the CMB power spectrum, but also leads to large oscillatory non-Gaussianity, providing a consistency check on their existence. Current estimator for non-Gaussianity is most sensitive to the local form $f_{\rm NL}^{\rm local}$. To study the oscillatory non-Gaussianity from features, a new estimator needs to be developed.

Aside from brane inflation in the warp throat, inflation could also happen in the string landscape. There the resulting inflationary picture is quite different. Due to the randomness in the inflaton potential, the inflaton path exhibits Brownian like motion. We have proved that detours of the inflaton in the landscape always increase the number of *e*-

folds. Furthermore, when the inflaton makes a turn in the landscape, the resulting power spectrum has a feature at the corresponding scale. The Brownian like motion of the inflaton will show up on the CMB power spectrum as random features, with their location, shape, and magnitude all uncorrelated. Such features are extremely hard to be picked out in data analysis. However, if the fluctuation is about 10%, PLANCK may have a chance to see it at $500 \lesssim l \lesssim 2000$. Furthermore, a combined $TT/TE/EE$ analysis will help to distinguish features from noises.

While this work studied the observational signatures of brane inflation in great detail, many open questions still remain in both model building and data analysis. I will leave these questions for future research.

BIBLIOGRAPHY

[1] A. H. Guth, *The Inflationary Universe: A Possible Solution to the Horizon and Flatness Problems*, *Phys. Rev.* **D23** (1981) 347–356.

[2] G. F. Smoot *et. al.*, *Structure in the COBE DMR first year maps*, *Astrophys. J.* **396** (1992) L1–L5.

[3] C. L. Bennett *et. al.*, *4-Year COBE DMR Cosmic Microwave Background Observations: Maps and Basic Results*, *Astrophys. J.* **464** (1996) L1–L4, [astro-ph/9601067].

[4] **WMAP** Collaboration, E. Komatsu *et. al.*, *Five-Year Wilkinson Microwave Anisotropy Probe (WMAP) Observations:Cosmological Interpretation*, *Astrophys. J. Suppl.* **180** (2009) 330–376, [arXiv:0803.0547].

[5] A. D. Linde, *A New Inflationary Universe Scenario: A Possible Solution of The Horizon, Flatness, Homogeneity, Isotropy and Primordial Monopole Problems*, *Phys. Lett.* **B108** (1982) 389–393.

[6] A. Albrecht and P. J. Steinhardt, *Cosmology for Grand Unified Theories With Radiatively Induced Symmetry Breaking*, *Phys. Rev. Lett.* **48** (1982) 1220–1223.

[7] S. H. H. Tye, *Brane Inflation: String Theory Viewed from the Cosmos*, hep-th/0610221.

[8] G. R. Dvali and S. H. H. Tye, *Brane Inflation*, *Phys. Lett.* **B450** (1999) 72–82, [hep-ph/9812483].

[9] C. P. Burgess, M. Majumdar, D. Nolte, F. Quevedo, G. Rajesh, and R. Zhang, *The Inflationary Brane-antibrane Universe*, *JHEP* **07** (2001) 047, [hep-th/0105204].

[10] S. B. Giddings, S. Kachru, and J. Polchinski, *Hierarchies from Fluxes in String Compactifications*, *Phys. Rev.* **D66** (2002) 106006, [hep-th/0105097].

[11] S. Kachru, R. Kallosh, A. Linde, and S. P. Trivedi, *De Sitter Vacua in String Theory*, *Phys. Rev.* **D68** (2003) 046005, [hep-th/0301240].

[12] S. Kachru, R. Kallosh, A. Linde, J. Maldacena, L. McAllister, and S. P. Trivedi, *Towards Inflation in String Theory*, *JCAP* **0310** (2003) 013, [hep-th/0308055].

[13] E. Silverstein and D. Tong, *Scalar Speed Limits and Cosmology: Acceleration from D- cceleration*, hep-th/0310221.

[14] X. Chen, *Multi-throat Brane Inflation*, hep-th/0408084.

[15] I. R. Klebanov and M. J. Strassler, *Supergravity and a Confining Gauge Theory: Duality Cascades and χSB-resolution of Naked Singularities*, *JHEP* **08** (2000) 052, [hep-th/0007191].

[16] E. S. Fradkin and A. A. Tseytlin, *Nonlinear Electrodynamics from Quantized Strings*, *Phys. Lett.* **B163** (1985) 123.

[17] A. Abouelsaood, J. Callan, Curtis G., C. R. Nappi, and S. A. Yost, *Open Strings in Background Gauge Fields*, *Nucl. Phys.* **B280** (1987) 599.

[18] R. G. Leigh, *Dirac-Born-Infeld Action from Dirichlet Sigma Model*, *Mod. Phys. Lett.* **A4** (1989) 2767.

[19] D. Baumann, A. Dymarsky, I. R. Klebanov, and L. McAllister, *Towards an Explicit Model of D-brane Inflation*, *JCAP* **0801** (2008) 024, [arXiv:0706.0360].

[20] D. Baumann *et. al.*, *On D3-brane Potentials in Compactifications with Fluxes and Wrapped D-branes*, *JHEP* **11** (2006) 031, [hep-th/0607050].

[21] J. Garriga and V. F. Mukhanov, *Perturbations in K-inflation*, *Phys. Lett.* **B458** (1999) 219–225, [hep-th/9904176].

[22] X. Chen, M. Huang, S. Kachru, and G. Shiu, *Observational Signatures and Non-Gaussianities of General Single Field Inflation*, hep-th/0605045.

[23] H. Firouzjahi and S. H. H. Tye, *Brane Inflation and Cosmic String Tension in Superstring Theory*, *JCAP* **0503** (2005) 009, [hep-th/0501099].

[24] U. Seljak and A. Slosar, *B Polarization of Cosmic Microwave Background as a Tracer of Strings*, *Phys. Rev.* **D74** (2006) 063523, [astro-ph/0604143].

[25] S. E. Shandera and S. H. H. Tye, *Observing Brane Inflation*, *JCAP* **0605** (2006) 007, [hep-th/0601099].

[26] M. Alishahiha, E. Silverstein, and D. Tong, *DBI in the Sky*, *Phys. Rev.* **D70** (2004) 123505, [hep-th/0404084].

[27] D. Baumann and L. McAllister, *A Microscopic Limit on Gravitational Waves from D-brane Inflation*, hep-th/0610285.

[28] X. Chen, *Inflation from Warped Space*, *JHEP* **08** (2005) 045, [hep-th/0501184].

[29] X. Chen, *Running non-Gaussianities in DBI inflation*, *Phys. Rev.* **D72** (2005) 123518, [astro-ph/0507053].

[30] E. Komatsu and D. N. Spergel, *Acoustic Signatures in the Primary Microwave Background Bispectrum*, *Phys. Rev.* **D63** (2001) 063002, [astro-ph/0005036].

[31] J. M. Maldacena, *Non-Gaussian Features of Primordial Fluctuations in Single Field Inflationary Models*, *JHEP* **05** (2003) 013, [astro-ph/0210603].

[32] A. P. S. Yadav, E. Komatsu, and B. D. Wandelt, *Fast Estimator of Primordial Non-Gaussianity from Temperature and Polarization Anisotropies in the Cosmic Microwave Background*, *Astrophys. J.* **664** (2007) 680–686, [astro-ph/0701921].

[33] E. Sefusatti and E. Komatsu, *The Bispectrum of Galaxies from High-redshift Galaxy Surveys: Primordial Non-Gaussianity and Non-linear Galaxy Bias*, *Phys. Rev.* **D76** (2007) 083004, [arXiv:0705.0343].

[34] R. Bean, S. E. Shandera, S. H. H. Tye, and J. Xu, *Comparing Brane Inflation to WMAP*, *JCAP* **0705** (2007) 004, [hep-th/0702107].

[35] G. Shiu and B. Underwood, *Observing the Geometry of Warped Compactification via Cosmic Inflation*, hep-th/0610151.

[36] S. Kecskemeti, J. Maiden, G. Shiu, and B. Underwood, *DBI Inflation in the Tip Region of a Warped Throat*, *JHEP* **09** (2006) 076, [hep-th/0605189].

[37] X. Chen, S. Sarangi, S. H. H. Tye, and J. Xu, *Is Brane Inflation Eternal?*, *JCAP* **0611** (2006) 015, [hep-th/0608082].

[38] D. N. Spergel *et. al.*, *Wilkinson Microwave Anisotropy Probe (WMAP) three year results: Implications for cosmology*, astro-ph/0603449.

[39] G. Hinshaw *et. al.*, *Three-year Wilkinson Microwave Anisotropy Probe (WMAP) Observations: TempErature Analysis*, astro-ph/0603451.

[40] N. Jarosik *et. al.*, *Three-year Wilkinson Microwave Anisotropy Probe (WMAP) Observations: Beam Profiles, Data Processing, Radiometer Characterization and Systematic Error Limits*, astro-ph/0603452.

[41] L. Page *et. al.*, *Three year Wilkinson Microwave Anisotropy Probe (WMAP) Observations: Polarization Analysis*, astro-ph/0603450.

[42] M. Tegmark *et. al.*, *Cosmological Constraints from the SDSS Luminous Red Galaxies*, *Phys. Rev.* **D74** (2006) 123507, [astro-ph/0608632].

[43] P. Astier *et. al.*, *The supernova legacy survey: Measurement of ω_m, ω_λ and w from the first year data set*, *Astron. Astrophys.* **447** (2006) 31–48, [astro-ph/0510447].

[44] A. Lewis and S. Bridle, *Cosmological Parameters from CMB and Other Data: a Monte- Carlo Approach*, *Phys. Rev.* **D66** (2002) 103511, [astro-ph/0205436].

[45] D. H. Lyth, *What Would We Learn by Detecting a Gravitational Wave Signal in the Cosmic Microwave Background Anisotropy?*, *Phys. Rev. Lett.* **78** (1997) 1861–1863, [hep-ph/9606387].

[46] M. Huang and G. Shiu, *The Inflationary Trispectrum for Models with Large Non-Gaussianities*, hep-th/0610235.

[47] G. Hailu and S. H. H. Tye, *Structures in the Gauge/Gravity Duality Cascade*, hep-th/0611353.

[48] L. Leblond and S. Shandera, *Cosmology of the Tachyon in Brane Inflation*, hep-th/0610321.

[49] X. Chen, R. Easther, and E. A. Lim, *Large Non-Gaussianities in Single Field Inflation*, astro-ph/0611645.

[50] S. Kachru, J. Pearson, and H. L. Verlinde, *Brane/flux Annihilation and the String Dual of a Non- supersymmetric Field Theory*, *JHEP* **06** (2002) 021, [hep-th/0112197].

[51] X. Chen and S. H. H. Tye, *Heating in Brane Inflation and Hidden Dark Matter*, *JCAP* **0606** (2006) 011, [hep-th/0602136].

[52] X. Chen, *Cosmological Rescaling through Warped Space*, *Phys. Rev.* **D71** (2005) 026008, [hep-th/0406198].

[53] S. Thomas and J. Ward, *IR Inflation from Multiple Branes*, *Phys. Rev.* **D76** (2007) 023509, [hep-th/0702229].

[54] R. Bean, X. Chen, H. Peiris, and J. Xu, *Comparing Infrared Dirac-Born-Infeld Brane Inflation to Observations*, *Phys. Rev.* **D77** (2008) 023527, [arXiv:0710.1812].

[55] P. Creminelli, L. Senatore, M. Zaldarriaga, and M. Tegmark, *Limits on f_{NL} Parameters from WMAP 3yr Data*, *JCAP* **0703** (2007) 005, [astro-ph/0610600].

[56] J. E. Lidsey and I. Huston, *Gravitational Wave Constraints on Dirac-Born-Infeld Inflation*, *JCAP* **0707** (2007) 002, [arXiv:0705.0240].

[57] A. Lewis, A. Challinor, and A. Lasenby, *Efficient Computation of CMB Anisotropies in Closed FRW Models*, *Astrophys. J.* **538** (2000) 473–476, [astro-ph/9911177].

[58] H. Peiris and R. Easther, *Slow Roll Reconstruction: Constraints on Inflation from the 3 year WMAP Dataset*, *JCAP* **0610** (2006) 017, [astro-ph/0609003].

[59] M. Cortes, A. R. Liddle, and P. Mukherjee, *On What Scale Should Inflationary Observables be Constrained?*, *Phys. Rev.* **D75** (2007) 083520, [astro-ph/0702170].

[60] **SDSS** Collaboration, M. Tegmark *et. al.*, *The 3D Power Spectrum of Galaxies from the SDSS*, *Astrophys. J.* **606** (2004) 702–740, [astro-ph/0310725].

[61] **PLANCK** Collaboration, *PLANCK Blue Book*, .

[62] K. M. Smith and M. Zaldarriaga, *Algorithms for Bispectra: Forecasting, Optimal Analysis, and Simulation*, astro-ph/0612571.

[63] C. Hikage, E. Komatsu, and T. Matsubara, *Primordial Non-Gaussianity and Analytical Formula for Minkowski Functionals of the Cosmic Microwave Background and Large-scale Structure*, *Astrophys. J.* **653** (2006) 11–26, [astro-ph/0607284].

[64] R. Bean, X. Chen, G. Hailu, S. H. H. Tye, and J. Xu, *Duality Cascade in Brane Inflation*, *JCAP* **0803** (2008) 026, [arXiv:0802.0491].

[65] M. J. Strassler, *The Duality Cascade*, hep-th/0505153.

[66] A. R. Brown, S. Sarangi, B. Shlaer, and A. Weltman, *A Wrinkle in Coleman - De Luccia*, *Phys. Rev. Lett.* **99** (2007) 161601, [arXiv:0706.0485].

[67] H. V. Peiris *et. al.*, *First year Wilkinson Microwave Anisotropy Probe (WMAP) Observations: Implications for Inflation*, *Astrophys. J. Suppl.* **148** (2003) 213, [astro-ph/0302225].

[68] L. Covi, J. Hamann, A. Melchiorri, A. Slosar, and I. Sorbera, *Inflation and WMAP Three Year Data: Features Have a Future!*, *Phys. Rev.* **D74** (2006) 083509, [astro-ph/0606452].

[69] J. Hamann, L. Covi, A. Melchiorri, and A. Slosar, *New Constraints on Oscillations in the Primordial Spectrum of Inflationary Perturbations*, *Phys. Rev.* **D76** (2007) 023503, [astro-ph/0701380].

[70] D. Seery and J. E. Lidsey, *Primordial Non-Gaussianities in Single Field Inflation*, *JCAP* **0506** (2005) 003, [astro-ph/0503692].

[71] X. Chen, R. Easther, and E. A. Lim, *Generation and Characterization of Large Non-Gaussianities in Single Field Inflation*, *JCAP* **0804** (2008) 010, [arXiv:0801.3295].

[72] P. J. Steinhardt, *The Very Early Universe*. Cambridge University Press, 1983.

[73] A. D. Linde, *Nonsingular Regenerating Inflationary Universe*, *Cambridge University preprint, 1982* (1982).

[74] A. Vilenkin, *The Birth of Inflationary Universes*, *Phys. Rev.* **D27** (1983) 2848.

[75] A. D. Linde, *Eternally Existing Selfreproducing Chaotic Inflationary Universe*, *Phys. Lett.* **B175** (1986) 395–400.

[76] N. Iizuka and S. P. Trivedi, *An Inflationary Model in String Theory*, *Phys. Rev.* **D70** (2004) 043519, [hep-th/0403203].

[77] O. DeWolfe, S. Kachru, and H. L. Verlinde, *The Giant Inflaton*, *JHEP* **05** (2004) 017, [hep-th/0403123].

[78] S. H. H. Tye, J. Xu, and Y. Zhang, *Multi-field Inflation with a Random Potential*, *JCAP* **0904** (2009) 018, [arXiv:0812.1944].

[79] S. H. H. Tye and J. Xu, *A Meandering Inflaton*, *Phys. Lett.* **B683** (2010) 326–330, [arXiv:0910.0849].

[80] S. H. H. Tye, *A New View of the Cosmic Landscape*, hep-th/0611148.

[81] S. H. H. Tye, *A Renormalization Group Approach to the Cosmological Constant Problem*, arXiv:0708.4374.

[82] S. Sarangi, G. Shiu, and B. Shlaer, *Rapid Tunneling and Percolation in the Landscape*, *Int. J. Mod. Phys.* **A24** (2009) 741–788, [arXiv:0708.4375].

[83] **WMAP** Collaboration, M. R. Nolta *et. al.*, *Five-Year Wilkinson Microwave Anisotropy Probe (WMAP) Observations: Angular Power Spectra*, *Astrophys. J. Suppl.* **180** (2009) 296–305, [arXiv:0803.0593].

[84] R. Nagata and J. Yokoyama, *Band-power Reconstruction of the Primordial Fluctuation Spectrum by the Maximum Likelihood Reconstruction Method*, *Phys. Rev.* **D79** (2009) 043010, [arXiv:0812.4585].

[85] G. Nicholson and C. R. Contaldi, *Reconstruction of the Primordial Power Spectrum using Temperature and Polarisation Data from Multiple Experiments*, *JCAP* **0907** (2009) 011, [arXiv:0903.1106].

[86] D. S. Salopek and J. R. Bond, *Nonlinear Evolution of Long Wavelength Metric Fluctuations in Inflationary Models*, *Phys. Rev.* **D42** (1990) 3936–3962.

[87] A. A. Starobinsky, *Spectrum of Adiabatic Perturbations in the Universe when There are Singularities in the Inflation Potential*, *JETP Lett.* **55** (1992) 489–494.

[88] L. Knox, *Determination of Inflationary Observables by Cosmic Microwave Background Anisotropy Experiments*, *Phys. Rev.* **D52** (1995) 4307–4318, [astro-ph/9504054].

[89] **PLANCK** Collaboration, F. R. Bouchet, *The Planck satellite: Status & Perspectives*, *Mod. Phys. Lett.* **A22** (2007) 1857–1863.

[90] A. H. Guth and S. Y. Pi, *Fluctuations in the New Inflationary Universe*, *Phys. Rev. Lett.* **49** (1982) 1110–1113.

[91] Q. Huang and S. H. H. Tye, *The Cosmological Constant Problem and Inflation in the String Landscape*, *Int. J. Mod. Phys.* **A24** (2009) 1925–1962, [arXiv:0803.0663].

[92] D. Baumann, A. Dymarsky, S. Kachru, I. R. Klebanov, and L. McAllister, *Holographic Systematics of D-brane Inflation*, *JHEP* **03** (2009) 093, [arXiv:0808.2811].